12
B.S.

AFGL-TR-77-0157
ENVIRONMENTAL RESEARCH PAPERS, NO. 605
HAES REPORT NO. 50

AD A046474

Rocketborne Measurement of an Infrared Enhancement Associated With a Bright Auroral Breakup

K. D. BAKER
DORAN J. BAKER
JAMES C. ULWICK
A. T. STAIR, Jr.

5 July 1977

AD No. ____
DDC FILE COPY

This research was funded under Contract F19628-74-C-0130 and sponsored by DNA under subtask K43AAXHX604, entitled "E&F Region Ionization and Chemical Specie Measurements"

Approved for public release; distribution unlimited.

DDC
RECEIVED
NOV 14 1977
B

OPTICAL PHYSICS DIVISION PROJECT 7670
AIR FORCE GEOPHYSICS LABORATORY
HANSCOM AFB, MASSACHUSETTS 01731

AIR FORCE SYSTEMS COMMAND, USAF

This report has been reviewed by the ESD Information Office (OI) and is releasable to the National Technical Information Service (NTIS).

This technical report has been reviewed and is approved for publication.

FOR THE COMMANDER

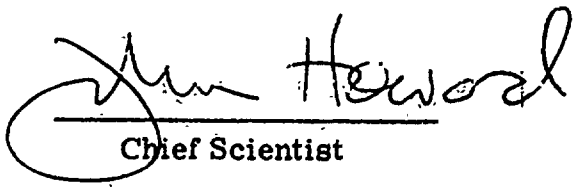

Chief Scientist

Qualified requestors may obtain additional copies from the Defense Documentation Center. All others should apply to the National Technical Information Service.

(18) DNA

(19) HAES-50

Unclassified
SECURITY CLASSIFICATION OF THIS PAGE (When Data Entered)

REPORT DOCUMENTATION PAGE

READ INSTRUCTIONS BEFORE COMPLETING FORM

(14) 1. REPORT NUMBER: AFGL-TR-77-0157

2. GOVT ACCESSION NO.

3. RECIPIENT'S CATALOG NUMBER

(6) 4. TITLE (and Subtitle): ROCKETBORNE MEASUREMENT OF AN INFRARED ENHANCEMENT ASSOCIATED WITH A BRIGHT AURORAL BREAKUP.

5. TYPE OF REPORT & PERIOD COVERED: Scientific. Interim.

6. PERFORMING ORG. REPORT NUMBER: ERP No. 605

(10) 7. AUTHOR(s): K. D. Baker, James C. Ulwick, Doran J. Baker, A. T. Stair, Jr.

8. CONTRACT OR GRANT NUMBER(s): HAES Rpt No. 50

9. PERFORMING ORGANIZATION NAME AND ADDRESS: Air Force Geophysics Laboratory (OPR), Hanscom AFB, Massachusetts 01731

10. PROGRAM ELEMENT, PROJECT, TASK AREA & WORK UNIT NUMBERS: 62101F; 7670 1004 (16) (17) 10

11. CONTROLLING OFFICE NAME AND ADDRESS: Air Force Geophysics Laboratory (OPR), Hanscom AFB, Massachusetts 01731

12. REPORT DATE: 5 July 1977 (11)

13. NUMBER OF PAGES: 101 (12) 93 p.

14. MONITORING AGENCY NAME & ADDRESS (if different from Controlling Office)

15. SECURITY CLASS. (of this report): Unclassified

15a. DECLASSIFICATION/DOWNGRADING SCHEDULE

(9) Environmental research papers, Nov 75 - Dec 76

16. DISTRIBUTION STATEMENT (of this Report)

Approved for public release; distribution unlimited.

DDC REPRODUCED NOV 14 1977 RECEIVED

17. DISTRIBUTION STATEMENT (of the abstract entered in Block 20, if different from Report)

18. SUPPLEMENTARY NOTES

*Utah State University, Logan, Utah.

Work performed on the report was funded under contract F19628-74-C-0130 and sponsored by DNA subtask K43AAXHX604 entitled "E&F region Ionization & Chemical specie measurements.

19. KEY WORDS (Continue on reverse side if necessary and identify by block number)

Infrared atmospheric emissions
Autoral emissions
Infrared excitation
Auroral processes
Rocket measurements

20. ABSTRACT (Continue on reverse side if necessary and identify by block number)

A Paiute-Tomahawk sounding rocket containing a 1.5-5.3 μm cryogenically cooled spectrometer was flown into a very bright (IBC III+) auroral breakup from Poker Flat, Alaska. The main emission features at 2.8, 4.3, and 5.3 μm were all found to be enhanced due to the large energy input to the atmosphere associated with the aurora. The most prominent enhancement occurred in the 4.3 μm region.

ABSTRACT METHOD

DD FORM 1 JAN 73 1473 EDITION OF 1 NOV 65 IS OBSOLETE

AIR FORCE (1) OCTOBER 26, 1977--706

Unclassified
SECURITY CLASSIFICATION OF THIS PAGE (When Data Entered)

409578

1B

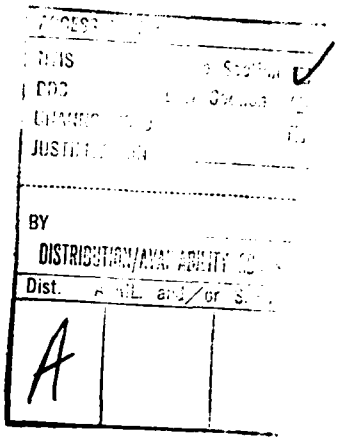

Preface

The High Altitude Effects Simulation (HAES) Program sponsored by the Defense Nuclear Agency since the early 1970 time period, comprises several groupings of separate, but interrelated technical activities, for example, ICECAP (Infrared Chemistry Experiments – Coordinated Auroral Program). Each of the latter have the common objective of providing information ascertained as essential for the development and validation of predictive computer codes designed for use with high priority DoD radar, communications, and optical defensive systems.

Since the inception of the HAES Program, significant achievements and results have been described in reports published by DNA, participating service laboratories, and supportive organizations. In order to provide greater visibility for such information and enhance its timely applications, significant reports published since early calendar 1974 shall be identified with an assigned HAES serial number and the appropriate activity acronym (for example, ICECAP) as part of the report title. A complete and current bibliography of all HAES reports issued prior to and subsequent to HAES Report No. 1 dated 5 February 1974 entitled, "Rocket Launch of an SWIR Spectrometer into an Aurora (ICECAP 72)," AFCRL Environmental Research Paper No. 466, is maintained and available on request at DASIAC, DoD Nuclear Information and Analysis Center, 816 State Street, Santa Barbara, California 93102, Telephone: (805)965-0551.

This report, which is the fourth scientific report under AFGL contract F19628-74-C-0130, is the 50th report in the HAES series and covers technical activities performed during the period November 1975 through December 1976.

PRECEDING PAGE NOT FILMED
BLANK

The purpose of the work herein is to provide the results of measurements of auroral infrared spectra in the range 1.5-5.3 μm from a rocket-borne CVF spectrometer that penetrated an intense auroral breakup (IBC III^{+}). The Paiute-Tomahawk sounding rocket (A10.205-2) was launched from Poker Flat, Alaska as part of the ICECAP 73 program.

Contents

1. OBJECTIVES 11

2. INSTRUMENTATION 11

3. ROCKET FLIGHT SUMMARY 13

4. AURORAL AND GEOPHYSICAL CONDITIONS 16

   4.1 All-sky Camera Results 17
   4.2 Ground-based Photometers 17
   4.3 Magnetometer and Riometer 21
   4.4 Chatanika Radar Results 21

5. EXPERIMENTAL RESULTS 25

6. DISCUSSION OF RESULTS 38

REFERENCES 41

APPENDIX A: Calibrations 43

APPENDIX B: Circular Variable Filter Spectrometer Spectral Scans 51

DISTRIBUTION LIST 95

Illustrations

1. Liquid-Nitrogen Cooled Infrared CVF Spectrometer 13
2. Elevation of the Rocket Axis 14
3. Aspect Angles of the Rocket Axis for Ascent of Rocket 10.205-2 15
4. All-sky Camera Pictures From Ft. Yukon During Flight of 10.205-2 (Romick[4]) 18
5. All-sky Camera Pictures From Poker Flat During Flight of 10.205-2 (Kofsky[5]) 19
6. Ground-based Photometer Data (λ3914A) for Rocket Entry Position 20
7. Ft. Yukon Meridian Scanning Photometer Data Scaled From the Records for (a) Rocket Entry Position, and (b) Rocket Exit Position 22
8. College, Alaska, Riometer and Magnetometer Data Around the Flight of Rocket 10.205-2 23
9. Electron Density History From Chatanika Radar Results at 91 and 122 km in the Vicinity of the Rocket Flight 24
10. E-region Electron Density Contours Around Launch Time of Paiute-Tomahawk 10.205-2 26
11. (a) Electron Density Profiles From Chatanika Radar Results, and (b) Data From λ3914-A Forward-Viewing Rocket Photometer 27
12. Spectral Scan From CVF Spectrometer Taken at 73 km on Rocket Ascent 28
13. 73 km Spectral Scan on Logarithmic Scale 29
14. Typical Background Scans of Spectrometer Before Removal of Cold Cover 30
15. Coadded Background Scans of Spectrometer in Low Gain Range 31
16. Coadded Background Scans of Spectrometer in High Gain Range 32
17. Data Scan at 87 km With Approximate Instrumental Noise Levels Shown at (a) Low Gain Range, and (b) High Gain Range 33
18. Spectral Position of Peak of Emission Feature Near 4.3 μm (Rocket Ascent) 34
19. Altitude Profile of Peak Spectral Emission Measured at 4.3 μm for Rocket Ascent 35
20. Comparison of 4.3-μm Profile for Rocket Ascent and Descent 36
21. Magnitude of Zenith Spectral Emission Measured at λ5.3 μm and λ2.8 μm 37

A1. Output Volts vs Photon (kR) 46
A2. Inverse Spectral Radiant Responsivity vs Wavelength (μm) 47
A3. Reference Position (φ) vs Wavelength (μm) 48
A4. Relative Response R(λ) vs Cross Section Field (Degrees) 49

B1. A10.205-2, Ascent, High Gain – 71.77 km 52
B2. A10.205-2, Ascent, High Gain – 72.56 km 52

B3.	A10.205-2, Ascent, High Gain – 73.34 km	53
B4.	A10.205-2, Ascent, High Gain – 74.12 km	53
B5.	A10.205-2, Ascent, High Gain – 74.90 km	54
B6.	A10.205-2, Ascent, High Gain – 75.68 km	54
B7.	A10.205-2, Ascent, High Gain – 76.46 km	55
B8.	A10.205-2, Ascent, High Gain – 77.23 km	55
B9.	A10.205-2, Ascent, High Gain – 78.00 km	56
B10.	A10.205-2, Ascent, High Gain – 78.77 km	56
B11.	A10.205-2, Ascent, High Gain – 79.53 km	57
B12.	A10.205-2, Ascent, High Gain – 80.30 km	57
B13.	A10.205-2, Ascent, High Gain – 81.06 km	58
B14.	A10.205-2, Ascent, High Gain – 81.82 km	58
B15.	A10.205-2, Ascent, High Gain – 82.58 km	59
B16.	A10.205-2, Ascent, High Gain – 83.33 km	59
B17.	A10.205-2, Ascent, High Gain – 84.09 km	60
B18.	A10.205-2, Ascent, High Gain – 84.84 km	60
B19.	A10.205-2, Ascent, High Gain – 85.58 km	61
B20.	A10.205-2, Ascent, High Gain – 86.33 km	61
B21.	A10.205-2, Ascent, Low Gain – 86.33 km	62
B22.	A10.205-2, Ascent, Low Gain – 87.08 km	62
B23.	A10.205-2, Ascent, Low Gain – 87.82 km	63
B24.	A10.205-2, Ascent, Low Gain – 88.56 km	63
B25.	A10.205-2, Ascent, Low Gain – 89.30 km	64
B26.	A10.205-2, Ascent, Low Gain – 90.03 km	64
B27.	A10.205-2, Ascent, Low Gain – 90.76 km	65
B28.	A10.205-2, Ascent, Low Gain – 91.49 km	65
B29.	A10.205-2, Ascent, Low Gain – 92.22 km	66
B30.	A10.205-2, Ascent, Low Gain – 92.95 km	66
B31.	A10.205-2, Ascent, Low Gain – 93.67 km	67
B32.	A10.205-2, Ascent, Low Gain – 94.39 km	67
B33.	A10.205-2, Ascent, Low Gain – 95.11 km	68
B34.	A10.205-2, Ascent, Low Gain – 95.83 km	68
B35.	A10.205-2, Ascent, Low Gain – 96.55 km	69
B36.	A10.205-2, Ascent, Low Gain – 97.26 km	69
B37.	A10.205-2, Ascent, Low Gain – 97.97 km	70
B38.	A10.205-2, Ascent, High Gain – 97.97 km	70
B39.	A10.205-2, Ascent, High Gain – 98.68 km	71

B40. A10.205-2, Ascent, High Gain – 99.39 km 71
B41. A10.205-2, Ascent, High Gain – 100.09 km 72
B42. A10.205-2, Ascent, High Gain – 100.79 km 72
B43. A10.205-2, Ascent, High Gain – 101.49 km 73
B44. A10.205-2, Ascent, High Gain – 102.19 km 73
B45. A10.205-2, Ascent, High Gain – 102.88 km 74
B46. A10.205-2, Ascent, High Gain – 103.58 km 74
B47. A10.205-2, Ascent, High Gain – 104.27 km 75
B48. A10.205-2, Ascent, High Gain – 104.96 km 75
B49. A10.205-2, Ascent, High Gain – 105.64 km 76
B50. A10.205-2, Ascent, High Gain – 106.33 km 76
B51. A10.205-2, Ascent, High Gain – 107.01 km 77
B52. A10.205-2, Ascent, High Gain – 107.69 km 77
B53. A10.205-2, Ascent, High Gain – 108.37 km 78
B54. A10.205-2, Ascent, High Gain – 109.04 km 78
B55. A10.205-2, Ascent, High Gain – 109.71 km 79
B56. A10.205-2, Ascent, High Gain – 110.38 km 79
B57. A10.205-2, Ascent, High Gain – 111.05 km 80
B58. A10.205-2, Ascent, High Gain – 111.72 km 80
B59. A10.205-2, Ascent, High Gain – 112.38 km 81
B60. A10.205-2, Ascent, High Gain – 113.05 km 81
B61. A10.205-2, Ascent, High Gain – 113.71 km 82
B62. A10.205-2, Ascent, High Gain – 114.36 km 82
B63. A10.205-2, Ascent, High Gain – 115.02 km 83
B64. A10.205-2, Ascent, High Gain – 115.67 km 83
B65. A10.205-2, Ascent, High Gain – 116.32 km 84
B66. A10.205-2, Ascent, High Gain – 116.97 km 84
B67. A10.205-2, Ascent, High Gain – 117.62 km 85
B68. A10.205-2, Ascent, High Gain – 118.26 km 85
B69. A10.205-2, Ascent, High Gain – 118.90 km 86
B70. A10.205-2, Ascent, High Gain – 119.54 km 86
B71. A10.205-2, Ascent, High Gain – 120.18 km 87
B72. A10.205-2, Ascent, High Gain – 120.82 km 87
B73. A10.205-2, Ascent, High Gain – 121.45 km 88
B74. A10.205-2, Ascent, High Gain – 122.08 km 88
B75. A10.205-2, Ascent, High Gain – 122.71 km 89
B76. A10.205-2, Ascent, High Gain – 123.34 km 89

Illustrations

B77. A10.205-2, Ascent, High Gain – 123.96 km 90
B78. A10.205-2, Ascent, High Gain – 124.58 km 90
B79. A10.205-2, Ascent, High Gain – 125.20 km 91
B80. A10.205-2, Ascent, High Gain – 125.82 km 91
B81. A10.205-2, Ascent, High Gain – 126.44 km 92
B82. A10.205-2, Ascent, High Gain – 127.05 km 92
B83. A10.205-2, Ascent, High Gain – 127.66 km 93
B84. A10.205-2, Ascent, High Gain – 128.27 km 93
B85. A10.205-2, Ascent, High Gain – 129.48 km 94

Tables

1. Characteristics of Optical Instruments Aboard Paiute-Tomahawk 10.205-2 12
2. Paiute-Tomahawk 10.205.2 Trajectory Equations 14
3. Geophysical Conditions at Launch 16
4. Look Angles to Rocket Position at 100 km on Ascent and Descent 17
A1. NS-1B-5 Revised Calibration (High Gain Channels) 44
A2. Time Variations for the 4278, 5577, and 6300 A Emissions at the 100-km Rocket Entry and Exit Points as Seen From Ft. Yukon 45

Rocketborne Measurement of an Infrared Enhancement Associated With a Bright Auroral Breakup

1. OBJECTIVES

The objective of the rocket flight described herein was to measure the atmospheric emissions in the shortwave infrared region during intense auroral activity. This paper reports measurements of auroral infrared emission spectra in the range of 1.5-5.3 μm associated with an intense auroral breakup (IBC III$^+$) penetrated by a rocket payload. The rocket system was a Paiute-Tomahawk flown from the Poker Flat Research Range near Chatanika, Alaska, at 0031:42 Alaska Standard Time (UT-10 hr) on 24 March 1973.

2. INSTRUMENTATION

The primary instrument of the rocket payload of Paiute-Tomahawk USAF 10.205-2 was a spectrometer for measurements of auroral emission spectra in the shortwave infrared region (1.5-5.3 μm). As supporting measurements, the rocket payload also included a forward-viewing photometer for monitoring the auroral activity of the region penetrated by the rocket. The basic characteristics of the optical instruments are summarized in Table 1.

(Received for publication 24 June 1977)

PRECEDING PAGE NOT FILMED BLANK

Table 1. Characteristics of Optical Instruments Aboard Paiute-Tomahawk 10.205-2

Infrared Spectrometer:	
Wavelength	1.5-5.3 μm
Spectral resolution	~4 percent
Scan rate	2 Hz
Electrical bandwidth	100 Hz
Field-of-view	5^{o} (full angle)
Orientation	0^{o} (along forward vehicle axis)
Minimum detectable signal	~1 MR/μm at 4.3 μm
Inverse responsivity	14.5 MR/(μm V) at 4.3 μm (high gain)
Photometer:	
Wavelength	3914 A
Spectral bandwidth	13 A
Electrical bandwidth	100 Hz
Field-of-view	5^{o} (full angle)
Orientation	0^{o} (coaligned with spectrometer)
Minimum detectable signal	0.5 kR
Maximum signal	190 kR

The infrared spectrometer[1] used a circular-variable filter to scan from 1.5 to 5.3 μm at a rate of twice per second (see Figure 1). The spinning filter, an idium antimonide detector, and associated optics were housed in a dewar cooled to 77^{o}K by a reservoir of liquid nitrogen. The calibration curves for the spectrometer are included in Appendix A.[2,3] The instrument had a 5^{o} full angle field of view directed along the forward vehicle axis. An interference filter/photomultiplier photometer operating at 3914 A was coaligned with the spectrometer to

1. Stair, A.T. Jr., Wheeler, N.B., Baker, D.J., and Wyatt, C.L. (1973) Cryogenic IR spectrometers for rocketborne measurements, IEEE/NEREM 1973 Record, Part 3: Infrared, The Institute of Electrical and Electronic Engineers, Boston, Massachusetts.
2. Wyatt, C.L., and Kemp, J.C. (1973) Calibration of SWIR Spectrometer Model NS-1B-5, prepared for AFGL Contract No. F19628-73-C-0048, Utah State University, Logan.
3. Wyatt, C.L. (1974) Revised Calibration of SWIR Spectrometers Model NS-1B-5 and Model NS-1B-6, prepared for AFGL Contract No. F19628-73-C-0048, Utah State University, Logan.

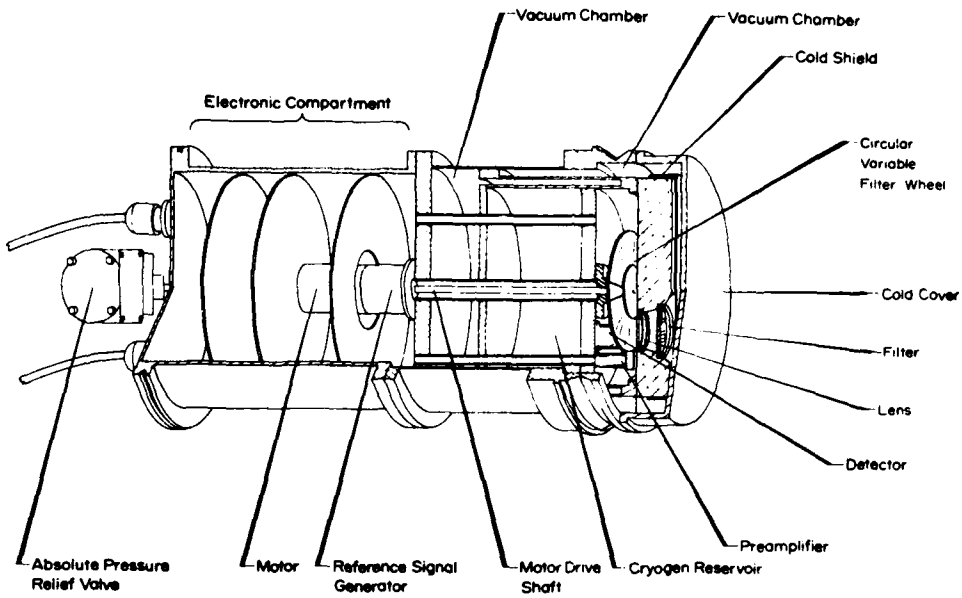

Figure 1. Liquid-Nitrogen Cooled Infrared CVF Spectrometer

monitor the auroral activity and provide a means of calculating the energy deposition rate from the measured emission profile. Calibration curves for the photometer are also included in Appendix A. These instruments were uncovered at about 70 km by the ejection of a split clamshell nose cone. The payload remained attached to the rocket motor. The rocket was spin stabilized only, but the aspect was known precisely from the output of an onboard gyro aspect system.

3. ROCKET FLIGHT SUMMARY

Paiute-Tomahawk 10.205-2 was launched at 0031:42 Alaskan Standard Time on 24 March 1973, from the Poker Flat Research Range, north of Fairbanks, Alaska. The rocket flew to a peak altitude of 211 km at T + 234 sec. The flight azimuth was 0° true. The rocket trajector equations used for data analysis are given in Table 2. The rocket nose cone was ejected at T + 56 sec at an altitude of 71 km, exposing the optical instruments at that time.

The rocket roll rate was approximately 6 Hz and the rocket axis had a precessional motion on a cone of about 16° (half angle) with a period of 33 sec. The elevation of the rocket axis is shown as a function of time in Figure 2 for the duration of the flight. As can be seen, the angle to the vertical of the optical axes of the

Table 2. Paiute-Tomahawk 10.205-2 Trajectory Equations

Parameter	Equation*	Coefficients
Altitude, Z	$Z = At^2 + Bt + C$	A = -0.00456 km/sec^2 B = 2.1100 km/sec C = -32.65 km
Ground Range East Component, X	$X = Dt + E$	D = 0.1888859 km/sec E = 2.9953884 km
Ground Range North Component, Y	$Y = Ft + G$	F = 0.1718641 km/sec G = -0.6411241 km

*These equations are valid for Z > 40 km.

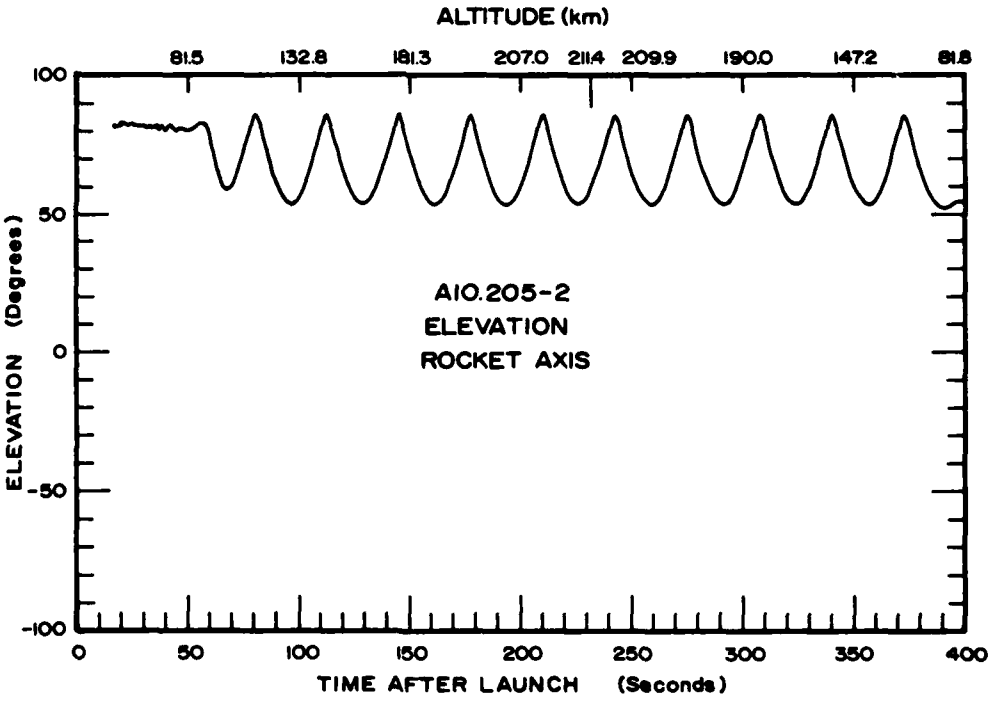

Figure 2. Elevation of the Rocket Axis

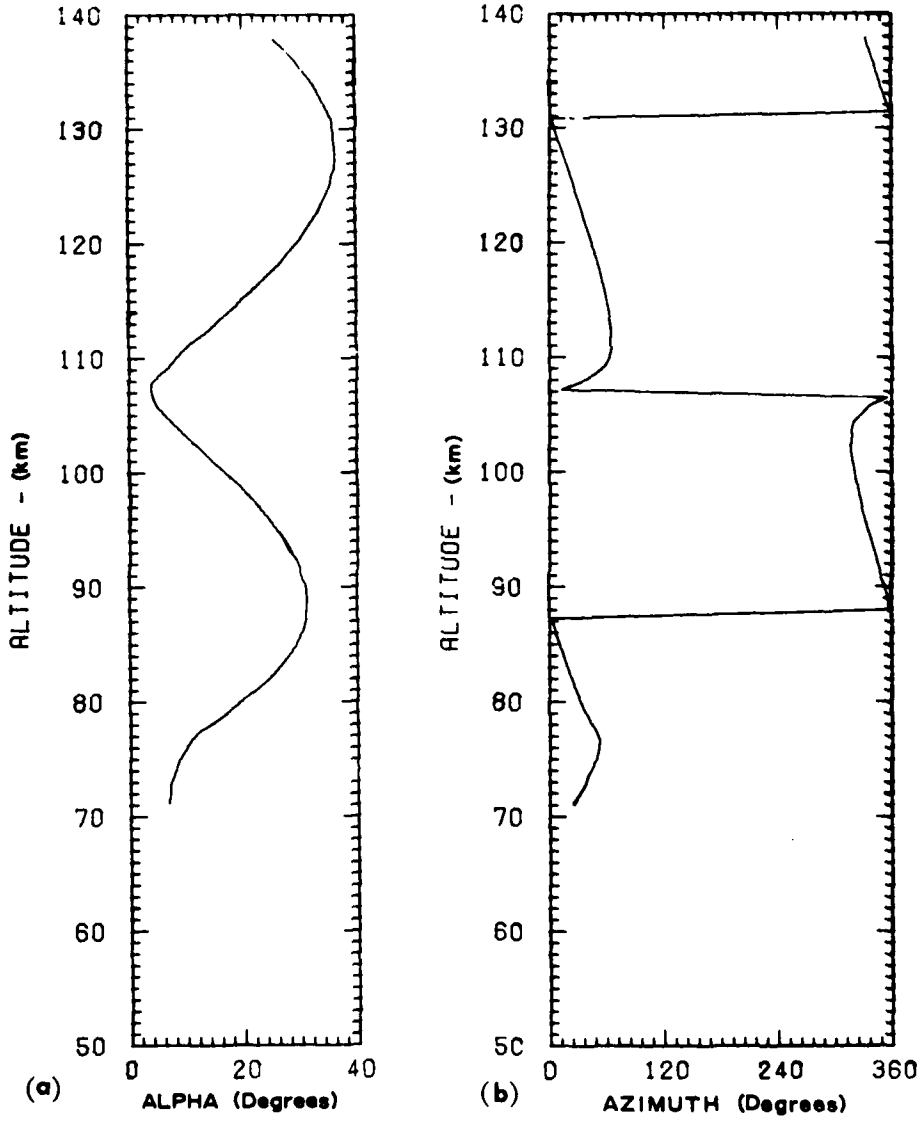

Figure 3. Aspect Angles of the Rocket Axis for Ascent of Rocket 10.205-2. (a) angle from vertical α; and (b) azimuth from true north

instruments goes through a range of from 4^{o} to 36^{o}. In studying the data to follow, this viewing aspect should be kept in mind. Figure 3(a) shows an altitude plot of this angle from the vertical as a function of altitude for the ascent portion of the rocket flight from tip off (71 km) to 138 km. The corresponding plot of the azimuth of the rocket axis is shown in Figure 3(b).

4. AURORAL AND GEOPHYSICAL CONDITIONS

Paiute-Tomahawk 10.205-2 was launched during an auroral substorm and the rocket traversed the initial bright region of the auroral expansion phase in the midnight sector. The extreme brightness of the aurora (>500 kR of λ 5577 A), the negative bay of greater than 1000 γ's, the extreme electron density (4×10^{6} cm^{-3}), and large auroral absorption (14 dB at 30 MHz) in concert indicate that the rocket penetrated a highly disturbed, highly dosed, active region during the auroral break-up expansion. Due to partially obscured skies at Poker Flat and Ester Dome and the rapid time fluctuations of the event, detailed triangulation analysis of ground-based data were not possible but still give a general picture of the magnitude of the energy deposition of the region traversed by the rocket. The general geophysical conditions associated with the launch are summarized in Table 3, and a brief summary of the ground-based measurements coverage is given below.

Table 3. Geophysical Conditions at Launch

General condition	Expansion phase of auroral substorm (intense breakup)
Maximum auroral brightness penetrated (λ 5577 A)	500 kR
Estimated energy deposition rate at time of penetration	400 $ergs/cm^2$ sec
Estimated energy deposited in region for 5 min before rocket penetration	1.5×10^{4} $ergs/cm^2$
Maximum N_e penetrated	4×10^{6} $electrons/cm^3$
30 MHz riometer absorption	14 dB
Local magnetic bay	-1000 γ

4.1 All-sky Camera Results

During the rocket flight, the general optical conditions at the three prime observing sites were: clear at Ft Yukon, thin overcast at Poker Flat, and thick overcast at Ester Dome. The all-sky camera pictures from Ft. Yukon and Poker Flat (Chatanika) are shown in Figure 4,[4] and Figure 5.[5] The times from rocket liftoff are shown on the figures. The approximate rocket position at 100 km on rocket ascent and descent is given in Table 4.

Table 4. Look Angles to Rocket Position at 100 km on Ascent and Descent

Site	Ascent		Descent	
	El (deg)	Az (deg)	El (deg)	Az (deg)
Ester Dome	59	47	36	47
Poker Flat (Chatanika)	78	54	45	49
Ft. Yukon	29	211	44	197

As can be seen from Figures 4 and 5, the rocket was launched into a dynamic, explosive auroral display and penetrated a very bright auroral form on rocket ascent. The spatial region where the rocket subsequently penetrated on descent also experienced very bright aurora. However, the conditions had subsided to moderately bright aurora by the time the rocket descented to 100 km.

4.2 Ground-based Photometers

Meridian scanning photometers were operated during the rocket measurements program at Ft. Yukon and Ester Dome along the geomagnetic meridian ($\sim 29^{\circ}$ Az),[4] and at Poker Flat along the rocket flight azimuth (49°). Fixed photometers

---

4. Romick, C.J. (1974) Report on the Geophysical Description and Available Data Associated With Rocket PF-PT-54 (PT-10.205.2), prepared for Utah State University, University of Alaska, Fairbanks.

5. Kofsky, I.L., Meriwether, J.W., Schroeder, J.W., and Sluder, R.B. (1975) Data Reduction and Auroral Characterizations for ICECAP, HAES Report No. 4, DNA Report No. 3511F, Contract No. DNA 001-73-C-0027, Photometrics, Inc., Lexington, Massachusetts.

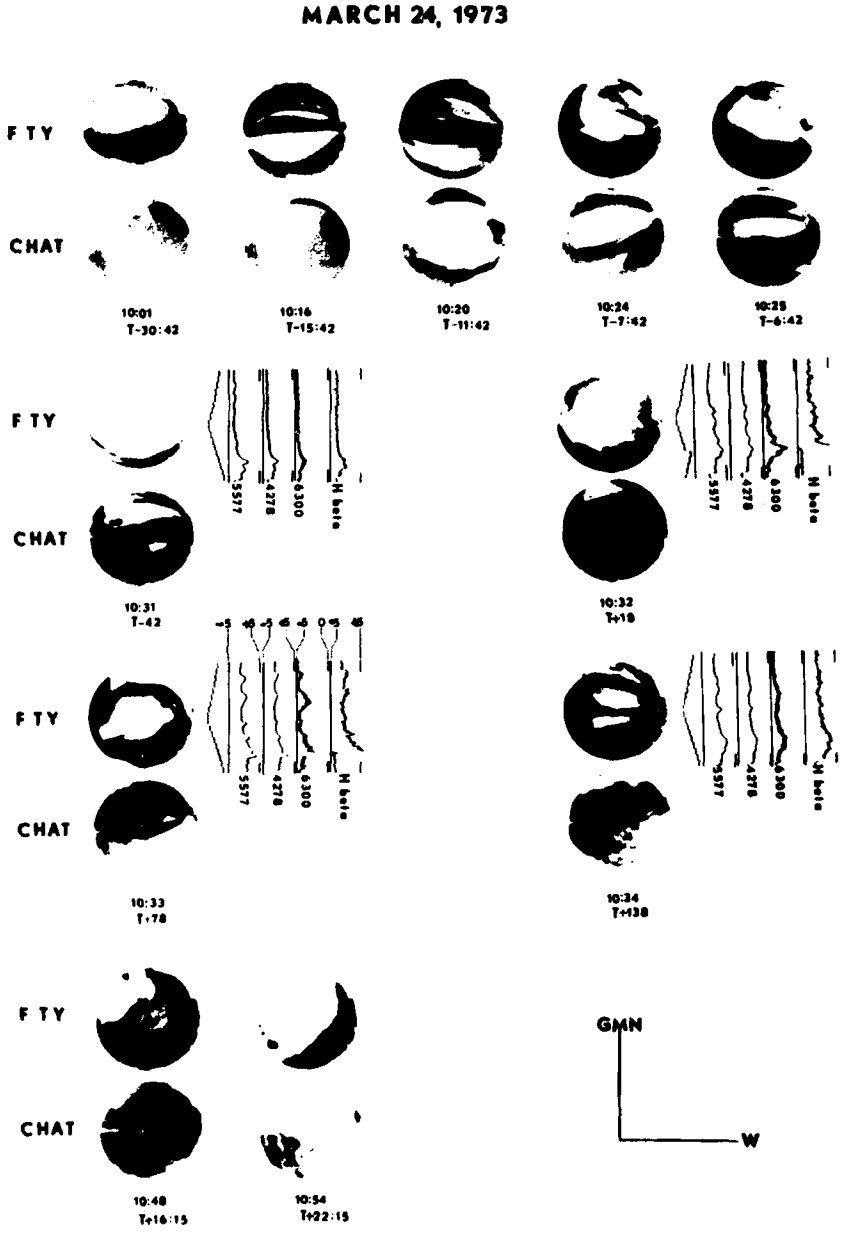

Figure 4. All-sky Camera Pictures From Poker Flat During Flight of 10.205-2 (Romick[4])

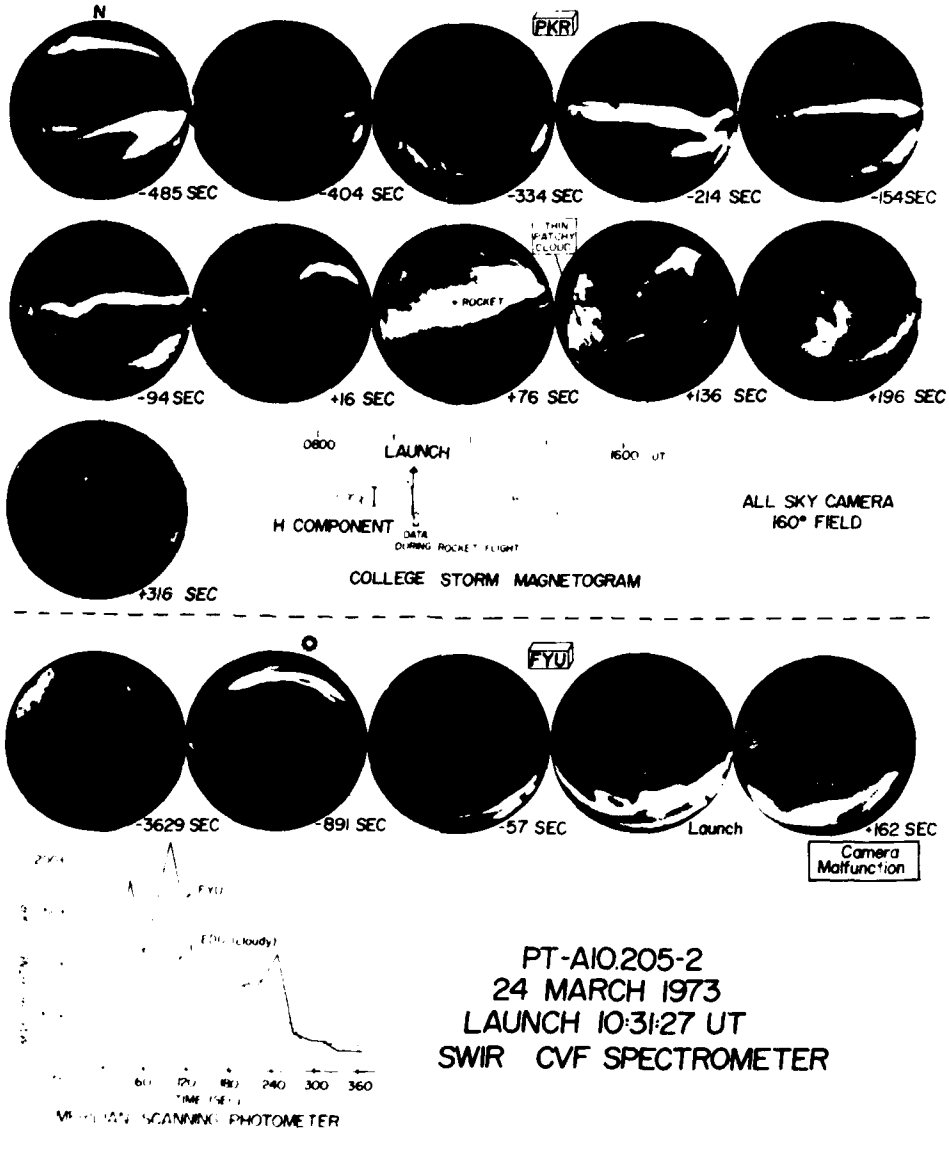

Figure 5. All-sky Camera Pictures From Poker Flat During Flight of 10.205-2 (Kofsky[5])

were pointed at the rocket auroral entry position at Poker Flat (USU) and Chatanika.[6] Overcast conditions from Ester Dome prevented the acquisition of any quantitative photometric data from that site. The thin clouds over Poker Flat allowed photometric measurements, but reduced intensities by a factor that was estimated to be less than 2. Ft. Yukon operated with clear skies during the mission.

The time history of the auroral intensity of the region penetrated by the rocket on ascent is best portrayed by the results of the fixed position, λ3914 A photometer shown in Figure 6. This photometer had a 5° (full angle) field of view centered on a position along the flight azimuth at an angle of 78°. From this vantage point, the rocket position would be within the photometer field of view at rocket flight times from about T + 60 sec (78 km) to T + 120 sec (155 km). More importantly, though, the instrument provides a continuous monitor of auroral activity and particle energy deposition in the auroral region penetrated by the rocket (85-125 km) for a period

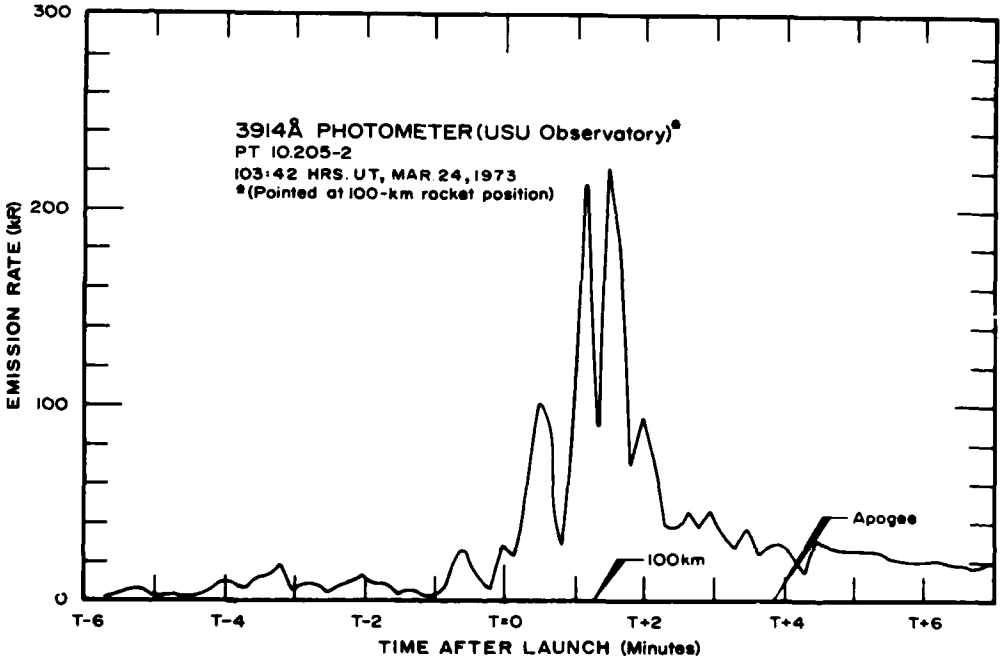

Figure 6. Ground-based Photometer Data (λ3914 A) for Rocket Entry Position. The rocket time at 100 km on ascent and apogee are indicated.

6. Sears, R.D. (1973) Ionospheric Irregularities: Alaska Photometric Measurements, DNA Report No. 3235F, Contract No. DNA 001-73-C-0110, Lockheed Palo Alto Research Laboratory, Palo Alto, California.

of minutes before the launch up until the rocket penetration. The data shown in Figure 6 run from a period of 6 min before launch up through rocket apogee. The first of the large double peaks with a magnitude of 210 kR occurred at T + 68 sec, at which time the rocket was at an altitude of 90 km. Based on the data of Figure 6, it is estimated that a total of about 1.5×10^4 ergs/cm^2 was deposited in the region penetrated by the rocket in the 5 min prior to penetration.

The photometer data from Ft. Yukon for 100-km rocket entry and exit points are given in Table A2 in the Appendix for λ5577, λ4278, and λ6300 A for the period of rocket flight and the preceding 280 sec.[4] Figure 7 shows these data at λ5577 and λ4278 A for the rocket entry and exit positions. The λ5577 A emission rate exceeded 100 kR from shortly after rocket liftoff until the rocket reached an altitude of about 165 km (T + 130 sec). In interpreting the results from Ft. Yukon, two factors are important: (1) in observing the auroral form the viewing aspect is considerably different from those of the instruments at Poker Flat and those onboard the rocket, and (2) due to the relatively low elevation angles, appreciable corrections must be made for optical extinction. The λ5577 A intensities at the rocket entry point should be multiplied by a factor of about 2 to correct for atmospheric extinction.

4.3 Magnetometer and Riometer

The launch of Paiute-Tomahawk 10.205-2 occurred at the onset of a large negative bay in the horizontal component of the terrestrial magnetic field. The College, Alaska, magnetograms are shown in Figure 8 for the period around the launching. The launch time is indicated. The magnetic bay seen here had a magnitude of approximately 1000 gammas. Magnetometer data from other stations and a more complete description of the magnetic activity and current systems has been given by Romick.[4]

Also shown in Figure 8 is the 30-MHz auroral absorption as measured at College Station. The absorption reached levels of about 20 dB, indicating that high-energy electron fluxes penetrated low into the ionosphere. Throughout the flight of the rocket, the riometer showed absorption greater than 10 dB.

4.4 Chatanika Radar Results

The incoherent-scatter radar located near the Poker Flat Research Range (Chatanika) was operated by the Stanford Research Institute in support of the ICECAP rocket measurements program.[7] These results are particularly useful

---

7. Baron, M.B., and Chang, N.J. (1975) ICECAP 73A - Chatanika Radar Results, HAES Report No. 15, DNA Report No. 3531T, Contract No. DNA-001-74-C-0167, Stanford Research Institute, Menlo Park, California.

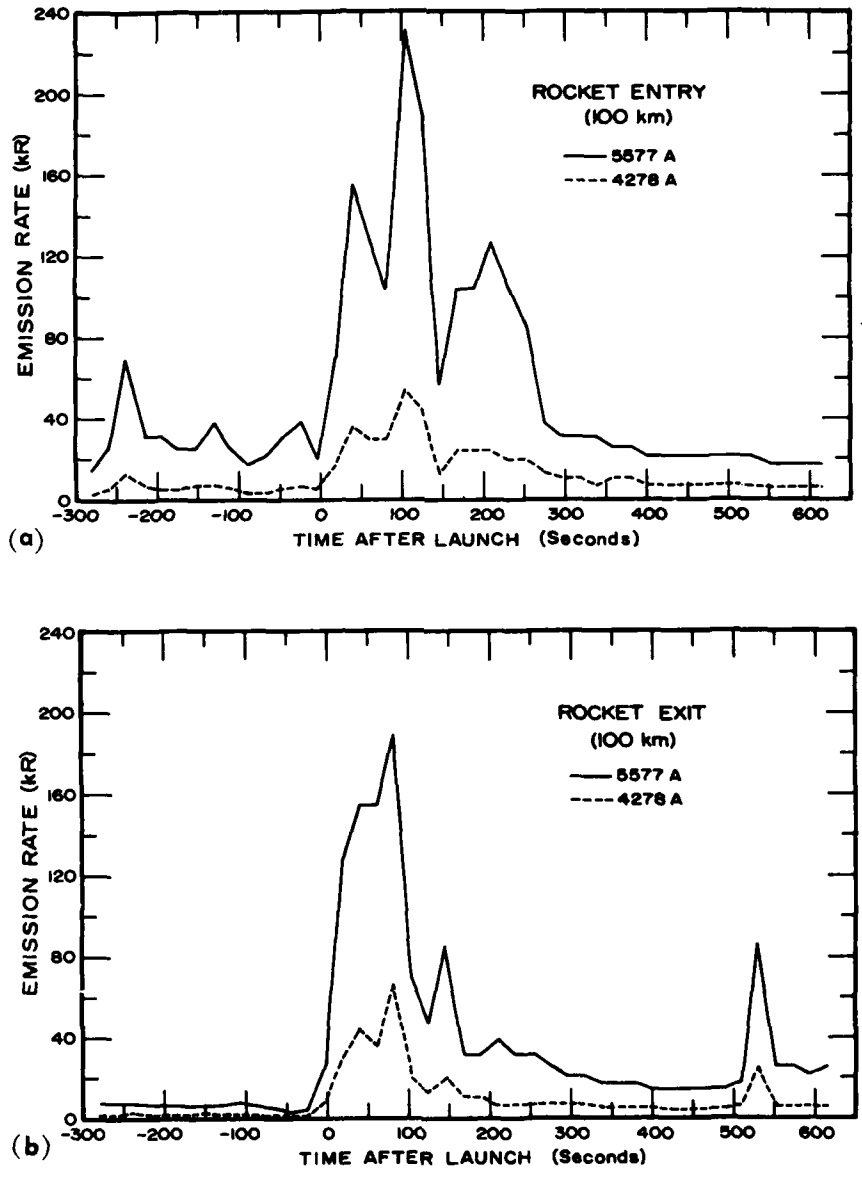

Figure 7. Ft. Yukon Meridian Scanning Photometer Data Scaled From the Records for (a) Rocket Entry Position, and (b) Rocket Exit Position

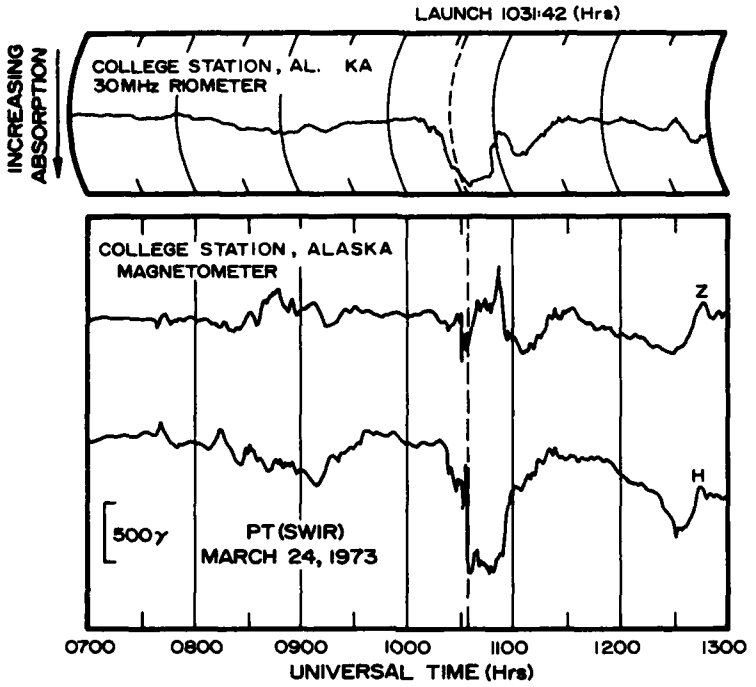

Figure 8. College, Alaska, Riometer and Magnetometer Data Around the Flight of Rocket 10.205-2. The peak absorption shortly after rocket launch is about 14 dB

in the case of the Paiute-Tomahawk 10.205-2 since no onboard measurements of electron density and related particle flux data were obtained. The radar results yield a good picture of the time history of energy deposition in the region proved by the rocket.

The radar was operated in a three-position mode to facilitate electric field and related measurements until shortly before rocket launch (T - 6 min) at which time the radar was fixed on the predicted rocket entry point (El 78.9°, Az 38.7°) to document the energy deposition in that region prior to and during rocket penetration. Figure 9 shows the electron densities (30-sec integration time) measured at 91 and 122 km for the period from 1025 to 1100 hr.[7] The electron densities exceeded 10^6 cm^{-3} at 90 km for a good part of the time that the rocket was on the upleg trajectory. These high electron densities at 90 km indicate that the influx of particles of relatively high energy deposited most of their energy below 100 km. These data are consistent with the increased riometer absorption as seen on Figure 8.

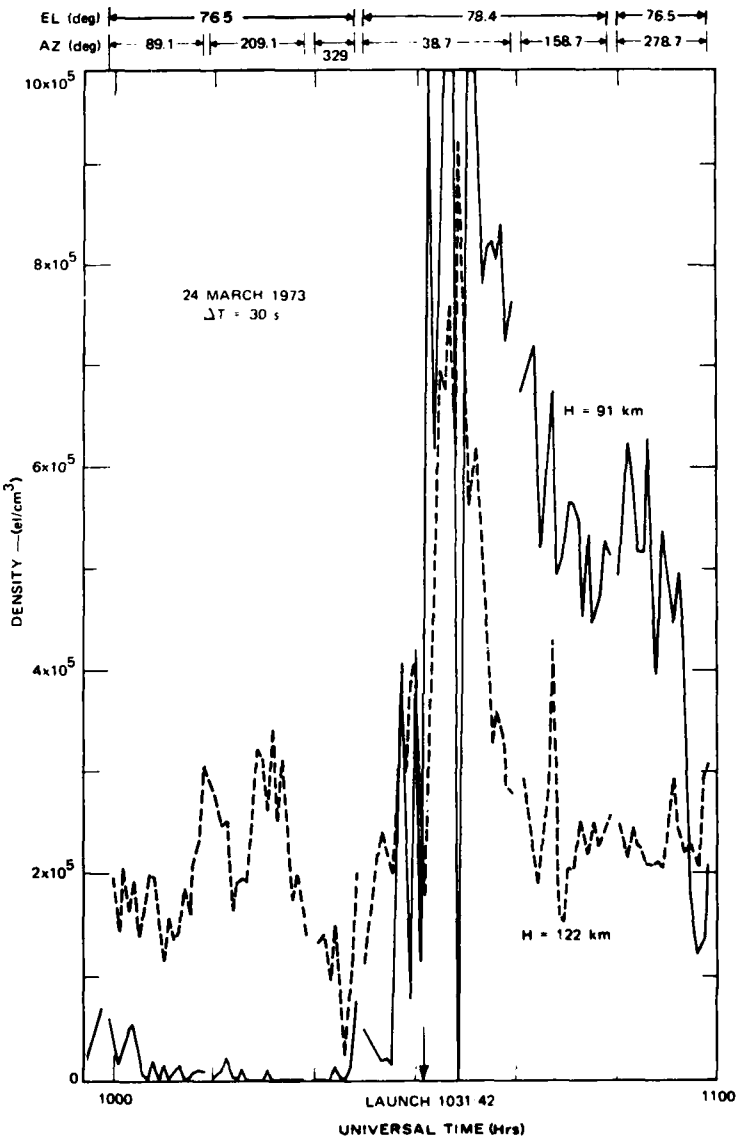

Figure 9. Electron Density History From Chatanika Radar Results at 91 and 122 km in the Vicinity of the Rocket Flight. The radar antenna azimuth and elevation are shown at the top

The radar electron density data are shown as contours in Figure 10.[7] These contours were made using a data integration time of 5 sec. An intense region of ionization occurred between 1033:05 (T + 83 sec) and 1033:25 (T + 103 sec) hr UT from 80 to 100 km. The peak at 1033: 15 hr of 7×10^6 cm^{-3} corresponds to an instantaneous energy deposition of about 1800 ergs cm^{-2} sec^{-1}.

The electron density data are plotted as height profiles in Figure 11(a) at reduced integration times (courtesy M. Baron, SRI). Figure 11(a) gives the electron density profiles at T + 51 sec (63 km rocket altitude) and a composite of data taken at T + 63 sec (rocket altitude 82 km) and T + 87 sec (116 km). This composite was made because the echo from the rocket body contaminates the measurements at the time the rocket passes the altitude of interest. The profiles before and after rocket passage are very similar; it is therefore felt that the composite of Figure 11(a) gives a valid representation of the electron density distribution penetrated by the rocket. Baron and Chang[7] detail much more information accumulated during this mission, including electric fields, ion and electron temperatures, currents, auroral clutter maps, conductivities, ion and neutral wind velocities, and energy deposition.

5. EXPERIMENTAL RESULTS

The rocket penetrated a very bright auroral region on rocket ascent. The results of the forward-viewing λ3914-A photometer shown in Figure 11(b) verify that this indeed occurred. The maximum possible output of the photometer corresponded to about 200 kR so the instrument was in saturation from about 80 to 97 km. This strong emission peaked somewhere in the vicinity of 90 km at an emission rate in excess of 200 kR. The corresponding emission rate on rocket descent was about 40 kR.

A typical scan of the infrared spectrometer is shown in Figure 12. This scan was obtained at about 72 km shortly after the spectrometer was uncovered. The spectrometer calibration (see Appendix A) was used to convert the telemetry voltage of this high gain channel to a spectral irradiance in megarayleighs per micrometer. Three prominent emission features are evident at 2.8, 4.3, and 5.3 μm. The 2.8- and 5.3-μm emissions are attributed to NO whereas the 4.3 is identified primarily with CO_2. (See the discussion in the following section.)

The 4.3-μm feature has a width at half-amplitude of about 0.16 μm which is about the resolution element of the spectrometer at that wavelength and also happens to be about the expected width of CO_2 band features. The NO features are not well measured since the NO overtone occurs near the change in filter segments at about 2.8 μm and the detector-filter combination, which cuts off at about 5.3 μm, does not include all of the fundamental band.

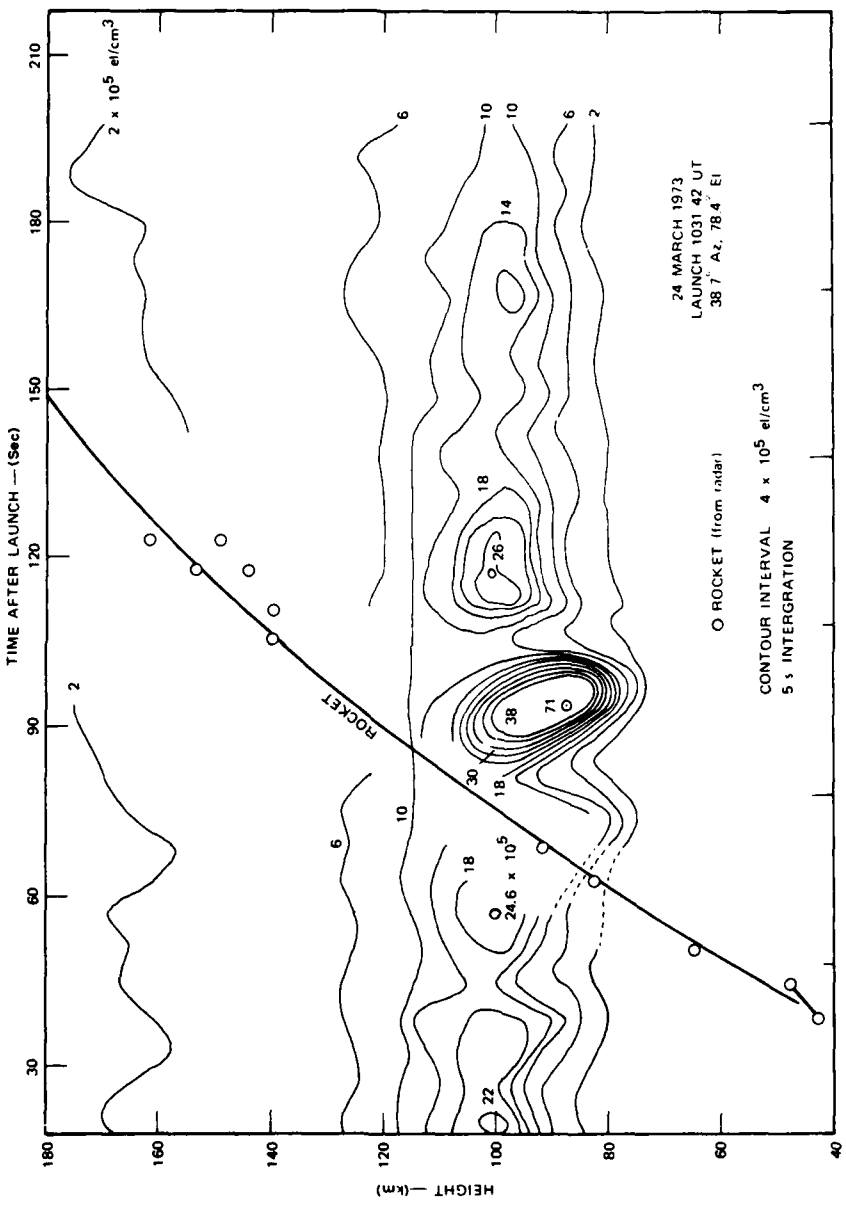

Figure 10. E-region Electron Density Contours Around Launch Time of Paiute-Tomahawk 10.205-2

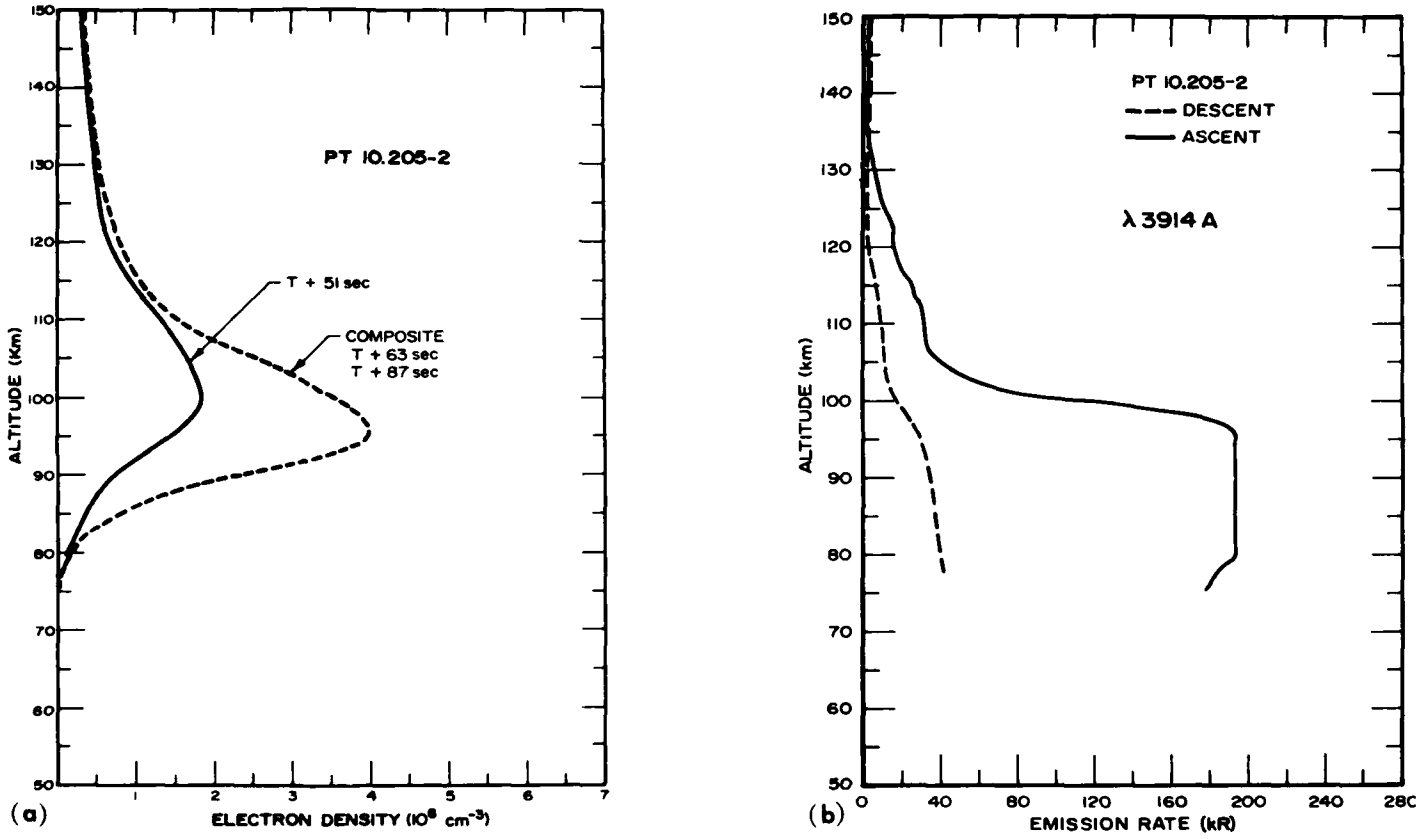

Figure 11. (a) Electron Density Profiles From Chatanika Radar Results, and (b) Data From λ3914 A Forward-Viewing Rocket Photometer

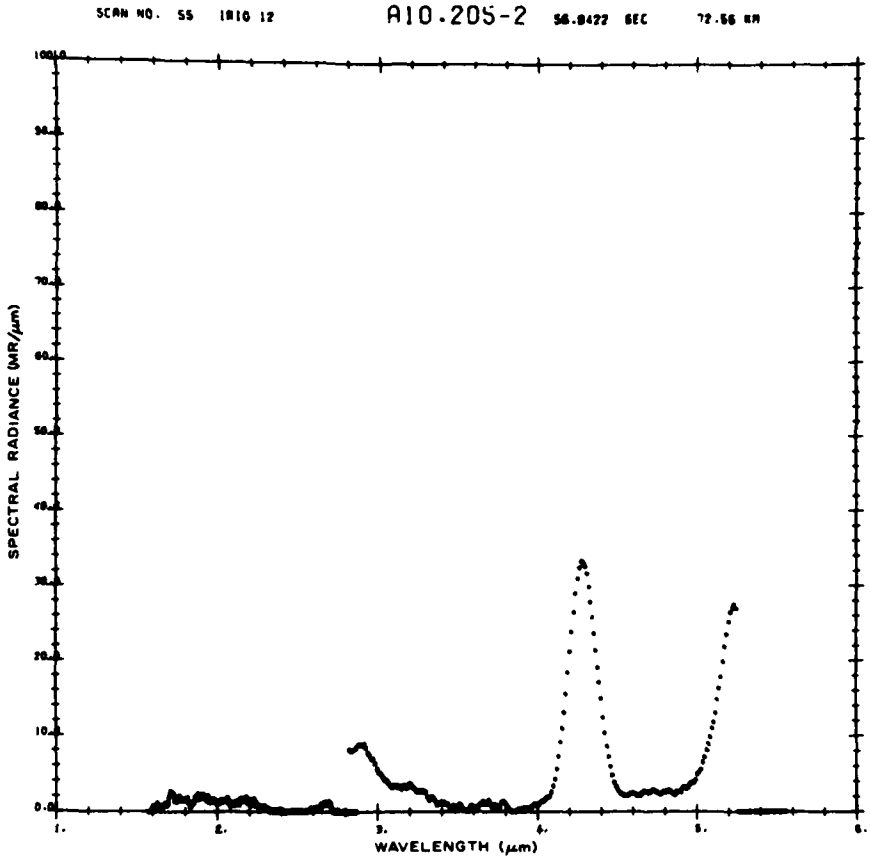

Figure 12. Spectral Scan From CVF Spectrometer Taken at 73 km on Rocket Ascent

The same scan as shown in Figure 12 is repeated in Figure 13 on a logarithmic scale. This format will be used to present the data which are included in Appendix B.

In viewing the spectral data, the quiescent level of the instrument should be taken into account. This can be accomplished by considering spectrometer scans before the instrument cold cover was removed as shown in Figure 14. These typical scans give a measure, in terms of voltage, of any offset voltages and the degree of noise fluctuations. In order to obtain a statistically more significant picture, many background scans were coadded as shown in Figure 15 for the low-gain channel and Figure 16 for the high-gain channel. In each case, the average voltage and standard deviation are shown as functions of wavelength.

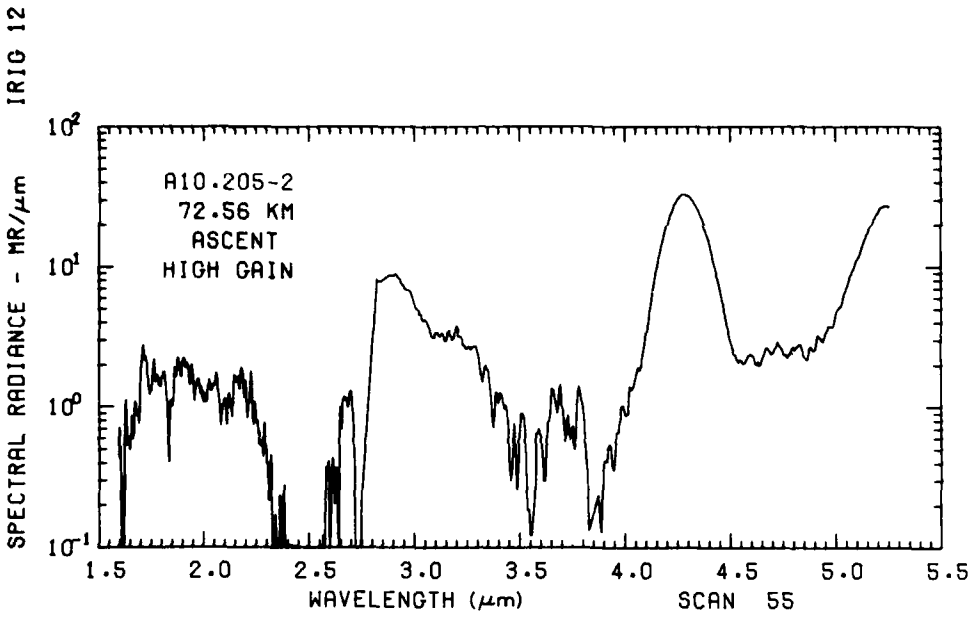

Figure 13. 73 km Spectral Scan on Logarithmic Scale

A high gain scan and also the corresponding low gain scan are shown for an altitude of about 86 km in Figure 17. The approximate noise levels of the instrument as ascertained from the data of Figures 15 and 16 are also shown.

The measured wavelength of the peak near 4.3 μm is plotted in Figure 18 for rocket ascent. The peak of this emission feature appeared to remain relatively unchanged in wavelength throughout the flight except for a slight downward trend as the rocket rises from 70 to 80 km.

The peak spectral radiances of the main feature at 4.3 μm were read from the spectral scans and are shown in Figure 19 for rocket ascent. Each point shown represents the reading from each spectral scan of the spectrometer. As the cold cover was removed, the value at about 72 km was 43 MR/μm and decreased with altitude to a minimum at about 77 km whereupon the value increased to a large peak. This large peak of about 130 MR/μm occurred at about 92 km where the auroral energy depositions were also maximum. The total measured emission rate in this band considering the spectral width to be 0.16 μm would be 21 MR. Above the peak of the emission layer, the magnitude dropped off to a value of about 5 MR/μm at 110 km. The emission diminished into the background above about 130 km.

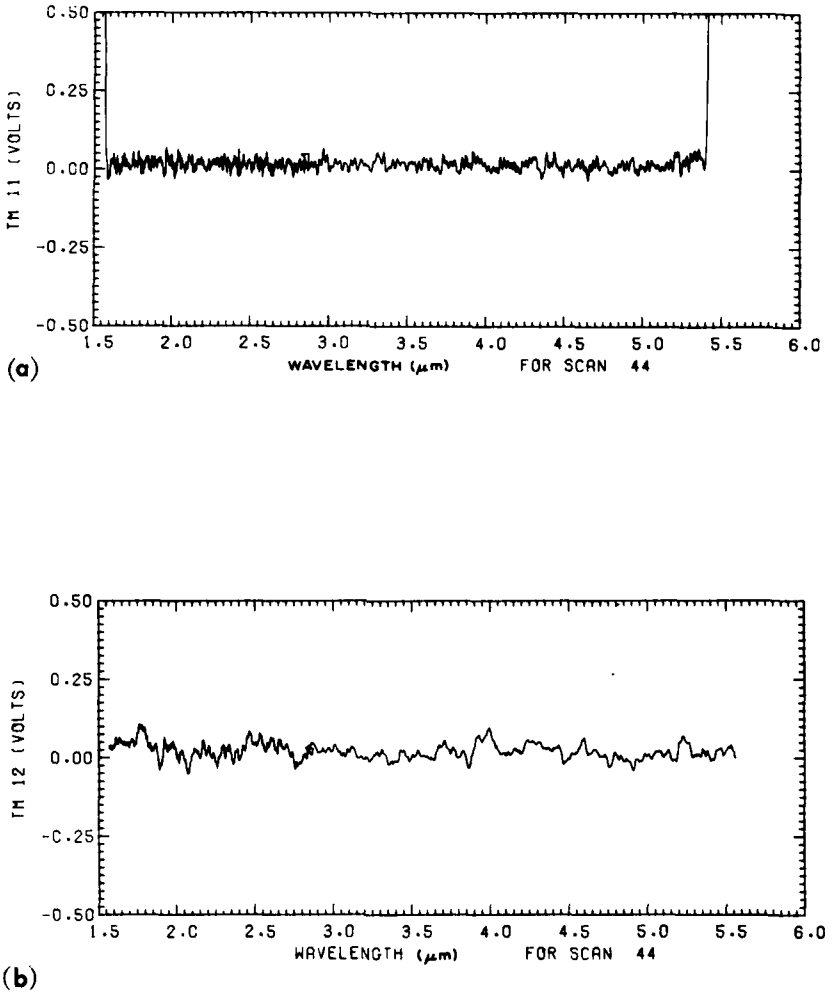

Figure 14. Typical Background Scans of Spectrometer Before Removal of Cold Cover. (a) low gain range, and (b) high gain range

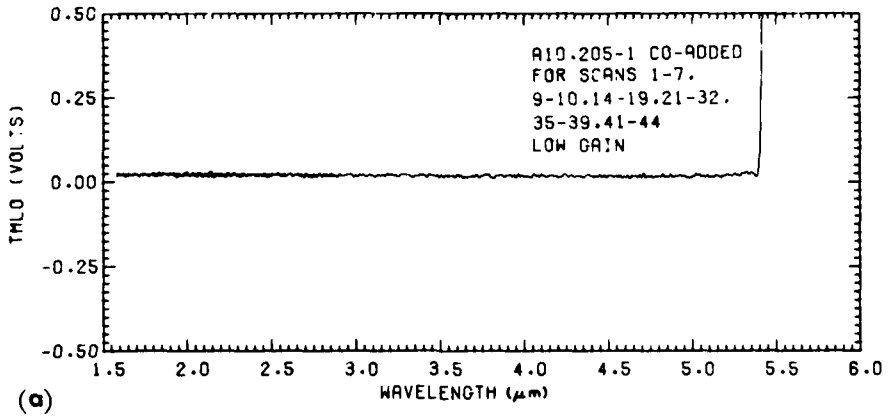

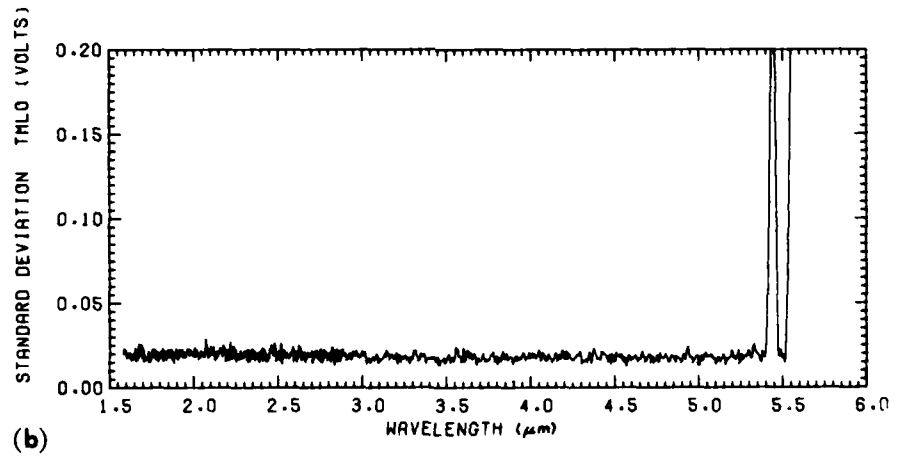

Figure 15. Coadded Background Scans of Spectrometer in Low Gain Range. (a) output voltage level, and (b) standard deviations of background fluctuations

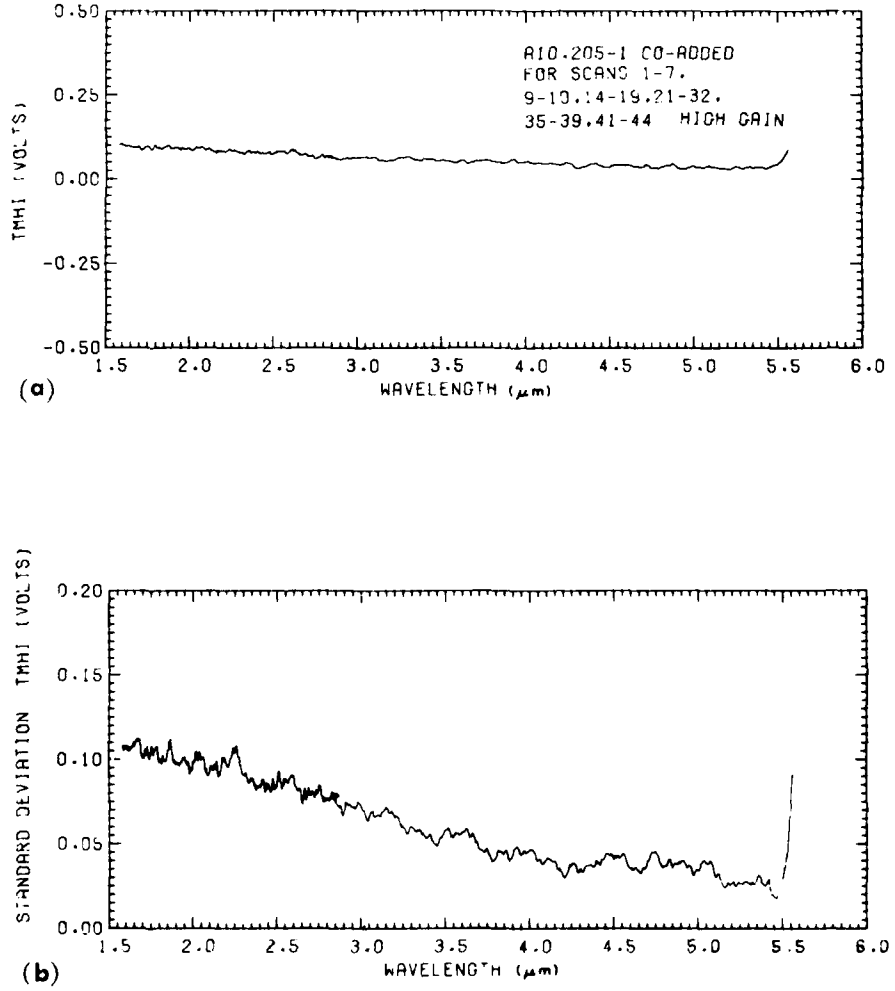

Figure 16. Coadded Background Scans of Spectrometer in High Gain Range. (a) output voltage level, and (b) standard deviations of background fluctuations

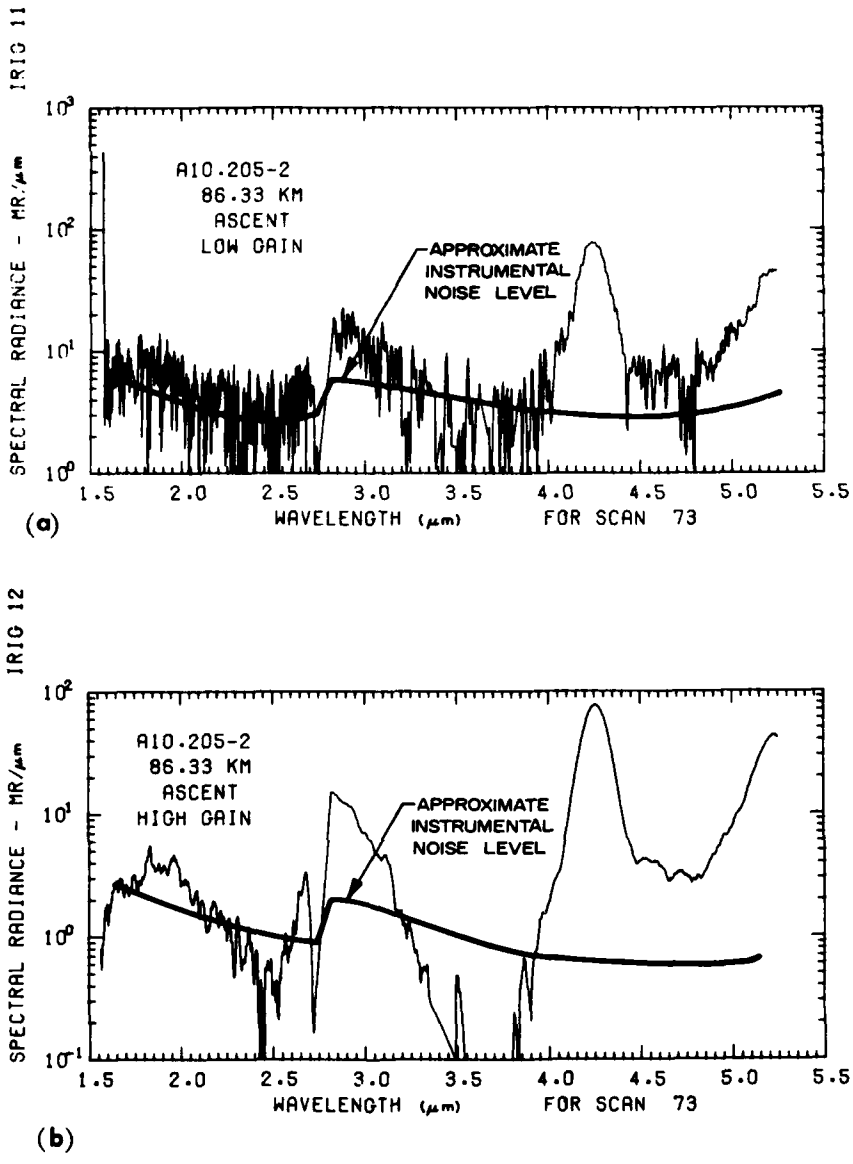

Figure 17. Data Scan at 87 km With Approximate Instrumental Noise Levels Shown at (a) low gain range, and (b) high gain range

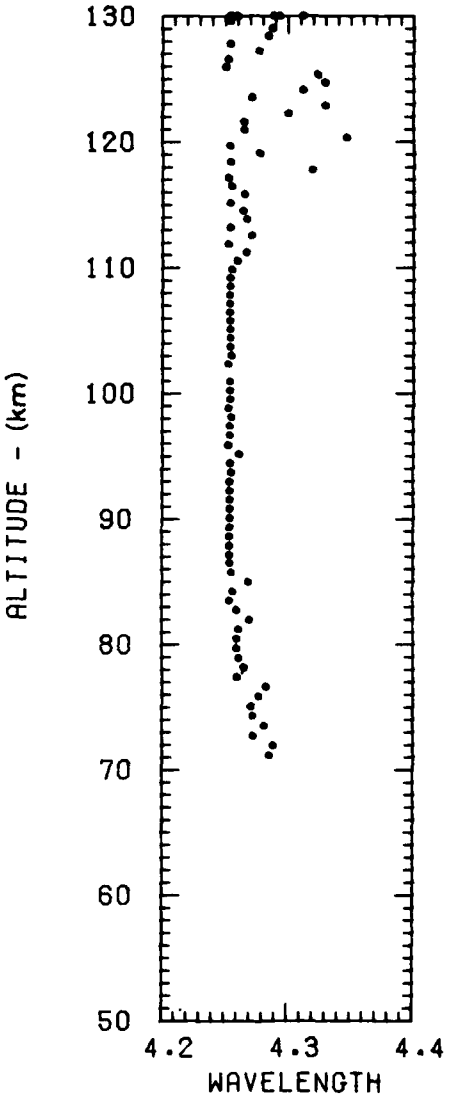

Figure 18. Spectral Position of Peak of Emission Feature Near 4.3 μm (Rocket Ascent)

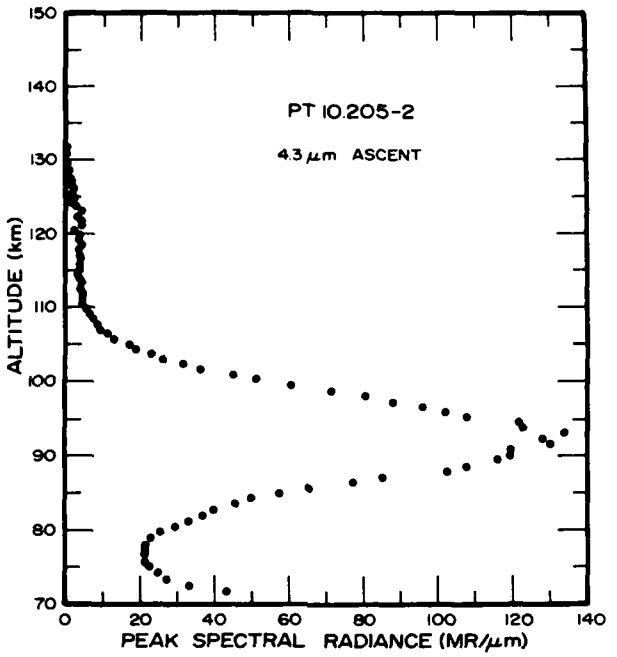

Figure 19. Altitude Profile of Peak Spectral Emission Measured at 4.3 μm for Rocket Ascent

A comparison of the 4.3-μm profile measured on rocket ascent and descent is shown in Figure 20. It is significant that although the auroral activity had significantly subsided in the region through which the probe descended (20 kR of λ3914 A at 90 km vs over 200 kR on ascent), the peak spectral radiance measured around 90 km had about the same value. Some 330 sec elapsed between the 90 km penetration on ascent and descent during which the rocket had moved a distance of 70 km horizontally to the northeast. The implications of the bright region persisting on rocket descent are that the 4.3-μm excitation/emission processes do not closely follow the instantaneous energy input due to the auroral activity, but rather lag in a manner that depends on the time history of the energy input with a decay time constant on the order of 5 min. It also appears to be significant that the emission layer is lower and broader as seen on the rocket descent compared with that observed during ascent. This could indicate a net downward diffusion of the excited species.

The values of peak spectral radiance measured at wavelengths near the location of the CVF filter junction at 2.8 μm and the high wavelength cutoff at 5.3 μm are shown in Figure 21. The data from all usable scans are shown; telemetry

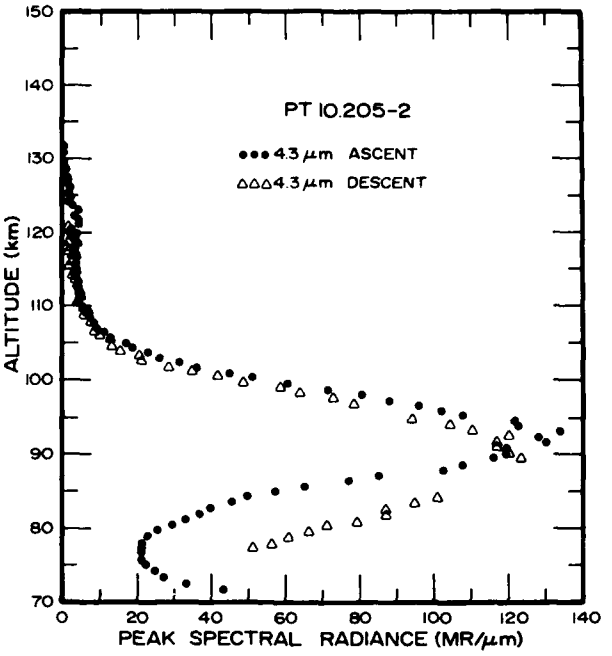

Figure 20. Comparison of 4.3-μm Profile for Rocket Ascent and Descent

dropout obliterated several scans on the descent data. A comparison of rocket ascent and descent data indicates a significant enhancement at both wavelengths associated with the much stronger auroral activity penetrated on rocket ascent. The similarity of the two ascent curves suggests that both radiations arise from the same emitting species, presumably NO. The maximum emissions at these wavelengths was observed between 80 and 90 km but did not show up as a smooth layer and had considerable structure. The increase with altitude of these optically thin emissions and the observed structure indicate that the larger emissions between 80 and 90 km are due to temporal fluctuations rather than a lower inherent altitude of these emissions compared with the slow 4.3 μm emission. It also is significant that the 2.8-μm emission was essentially absent during the rocket descent with weak auroral activity.

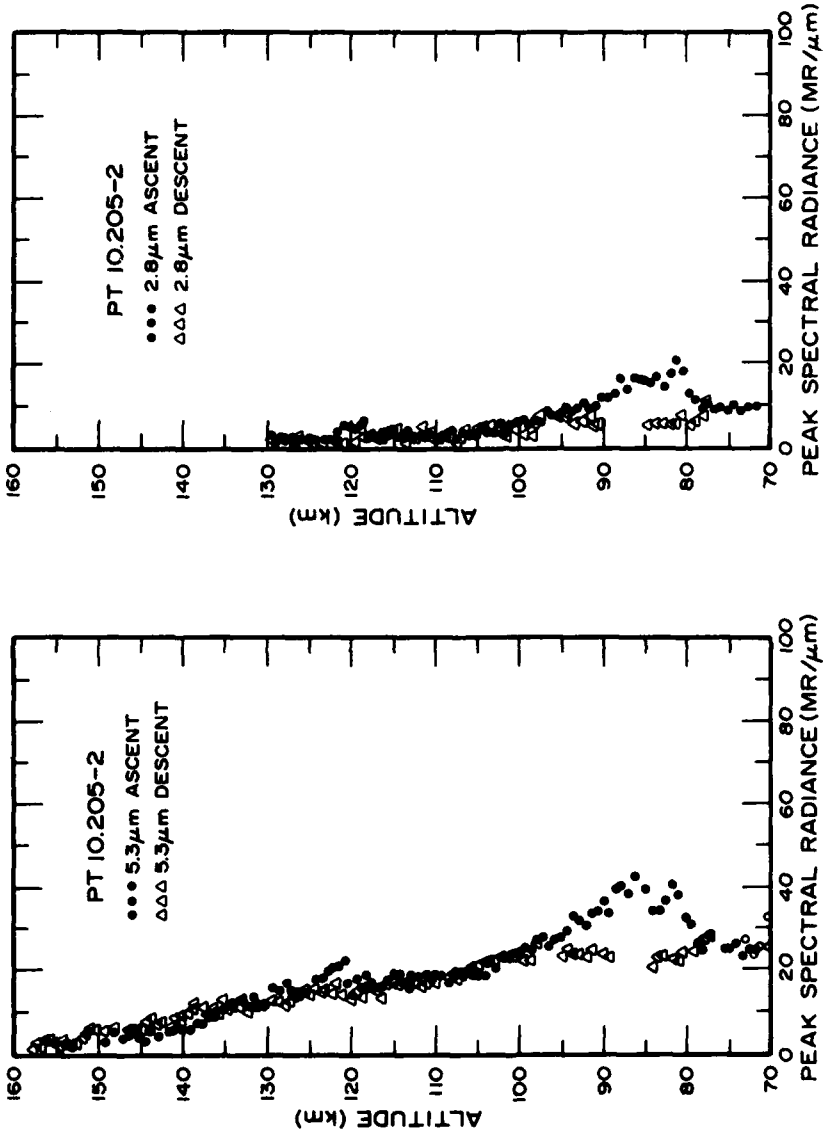

Figure 21. Magnitude of Zenith Spectral Emission Measured at $\lambda 5.3$ μm and $\lambda 2.8$ μm

6. DISCUSSION OF RESULTS

The auroral enhancements measured on rocket 10.205-2 were tentatively identified with radiation in the CO_2 (ν_3) band at 4.3 μm and the NO $\Delta v = 2$ and $\Delta v = 1$ bands at 2.8 and 5.3 μm, respectively. The rationale behind this identification is presented and a discussion of the likely excitation processes is given.

The significant features of the 4.3-μm emission layer were the strong enhancement of infrared radiation associated with this bright aurora, the layer-like shape of the measured radiation, and the relatively long time constant for the emission process. Comparison of the peak spectral radiance measured on this flight to a similar measurement during an aurorally nondisturbed time,[8, 9] shows that at an altitude of 92 km the 4.3-μm emission has been enhanced on the auroral case by a factor of about 60.

The observed increase of zenith emission below 92 km as the rocket ascended indicated that the emission region was optically thick; that is, the measured emission rate is not the integrated total emission along the optical path as is the case for optically thin emitters which allow only monotonically decreasing integrated intensity with altitude. The long persistence of the emission (as seen from ascent-descent comparisons) indicates a process for storing energy with a net radiative lifetime on the order of minutes. Both of these features are strong evidence for identifying CO_2 as the principal emitter.

The other possible candidate for 4.3-μm emission would be NO^+ in the $\Delta v = 1$ band. Emission from NO^+ would be expected to closely follow, temporally and spatially, the instantaneous energy deposition as measured by the on-board N_2^+ (λ3914 A) photometer (Figure 11) in this intense auroral case. This conclusion was based upon the knowledge that NO^+ is an optically-thin radiator in the atmosphere in the altitude range of the emission layer, and that the time constant for the concentration of NO^+ is very short compared with the observed temporal behavior of the 4.3-μm radiation. In the intense region of auroral activity on rocket ascent, the time constant for the formation or destruction of NO^+ can be approximated by $(\alpha N_e)^{-1}$, where α is the effective dissociative recombination coefficient and N_e is the electron density. Since the electron density was over 4×10^6 cm^{-3} (see

---

8. Stair, A.T., Jr., Ulwick, J.C., Baker, K.D., and Baker, D.J. (1975) Rocketborne observations of atmospheric infrared emissions in the auroral region, Atmospheres of Earth and the Planets, editor B. M. McCormac, D. Reidel Publishing Co., p. 335-346.

9. Wheeler, N.B., Stair, A.T., Jr., Frodsham, G., and Baker, D.J. (1976) Rocketborne spectral measurement of atmospheric infrared emission during a quiet condition in the auroral zone (1976), USAF Rep. No. AFGL-TR-76-0252, Environmental Research Papers, No. 582, AFGL, Hanscom AFB, Massachusetts.

Figure 10) the time constant is about 1 sec. In addition, the spectral shape of the NO^+ band would be much broader than the observed band which is on the order of or smaller than the 0.16 μm resolution element. These features of the observed 4.3-μm feature appear to preclude the possibility of a significant contribution of the 4.3-μm emission from NO^+.

The excitation mechanism for exciting CO_2 to account for the observed 4.3-μm emission involves an indirect process, since the cross section × concentration for direct excitation of CO_2 by electron bombardment is insignificant compared with the observed intensities. The proposed process to explain the observations involves vibrational excitation of N_2 by auroral electrons. The excited N_2 molecules form a reservoir of vibrational energy that can be transferred to CO_2 upon collision, since the energy spacings of the CO_2 and N_2 vibrational levels happen to coincide. This resonant v-v energy transfer is, thereby, an efficient process for exciting the CO_2 which can then radiate at 4.3 μm. This mechanism is complicated by repeated absorptions and reemissions in the CO_2, since the atmosphere is optically thick to the CO_2 radiation in the altitude range of maximum emission. It is also expected that repeated transfers of vibrational energy back and forth between N_2 and CO_2 by the reversible process $N_2^{\ddagger} + CO \rightleftarrows N_2 + CO_2$ (001) take place. Kumer[10] has shown by a more detailed analysis that the general features of the observed profiles can be explained by such a process and he derives an efficiency of $\sim$15 quanta per ion pair for the production of N_2 vibrational quanta.

The observed profiles at 2.8 and 5.3 μm are believed to be due to NO emission that is enhanced over the normal background due to the bright aurora penetrated on rocket ascent. Comparison with aurorally nondisturbed measurements[8, 9] indicates that the rocket descent data shown in Figure 21 are approximately at aurorally quiet levels. Under auroral activity, the NO is excited by nitrogen-oxygen processes[11] that energetically can excite both the $\Delta v = 1$ and $\Delta v = 2$ sequences responsible for the observed emissions at 5.3 and 2.8 μm.

A principal precursor for these excitation processes is $N(^2D)$ which is produced by a number of electron and ion reactions. From the page-full of reactions listed by Reidy et al,[11] perhaps the two most important for producing the observed NO emissions are:

---

10. Kumer, J.B. (1974) Analysis of 4.3 μm ICECAP Data, HAES Report No. 19, AFCRL-TR-74-0334, Contract No. F19628-73-C-0288, Lockheed Palo Alto Research Laboratories, Palo Alto, California.

11. Reidy, W.P., Degges, T.C., Manley, O.P., Smith, H.J., Carpenter, J.W., Stair, A.T., Jr., Ulwick, J.C., and Baker, K.D. (1974) Analysis of HAES Results: ICECAP 72, HAES Report No. 2, Final Report, DNA 3247F, Contract No. DNA 001-73-0020.

$$NO^+ + e \rightarrow N(^2D) + 0$$

$$N(^2D) + O_2 \rightarrow NO^{\ddagger} + 0 \quad .$$

These reactions will be fast compared with the 4.3-μm processes described above. The lower observed altitude of the 5.3-μm emission is believed to be caused by a temporal variation coupled with this faster response time. Comparison of the 5.3-μm profile of Figure 21 (ascent) with the 3914-A profile of Figure 11(b), shows a similar temporal increase from 75 to 80 km until the photometer saturated. The 5.3-μm structure between 80 and 90 km is strongly suggestive of auroral fluctuations, so it is suggested that the peak 5.3-μm of about 86 km is representative of an auroral brightening rather than a true layer.

The excitation mechanism (earthshine and 0 atom interchange) for NO excitation under nonauroral conditions[12] will not produce radiation at 2.8 μm, but do account for the observed background 5.3-μm emission. From the absence of the 2.8-μm emission during the less intense auroral activity, coupled with the similarity of the altitude profile under intense auroral activity, the conclusion is drawn that excited NO (Δv = 2) is responsible for the auroral enhancement at 2.8 μm.

An attempt was made to identify and measure emission from N_2O near 5.58 μm that has been observed on aircraftborne interferometer measurements.[13] The relatively small signal compared with the noise level in this region did not warrant the presentation of an altitude profile, but there was the hint of a slight increase to a value of about 3-4 MR/μm at the altitude and time of maximum auroral activity ($\sim$85 km). Compared to similar data obtained from a nonauroral background measurement,[8, 9] this would represent an increase of not more than a factor of 2 due to the intense auroral activity.

---

12. Degges, T.C. (1971) Vibrationally excited nitric oxide in the upper atmosphere, Appl. Optics 10:1856.

13. Huppi, E.R., Rogers, J.W., and Stair, A.T., Jr. (1974) Aircraft observations of the infrared emission of the atmosphere in the 700-2800 cm^{-1} region, Appl. Optics 13:1466.

References

1. Stair, A.T. Jr., Wheeler, N.B., Baker, D.J., and Wyatt, C.L. (1973) Cryogenic IR spectrometers for rocketborne measurements, IEEE/NEREM 1973 Record, Part 3: Infrared, The Institute of Electrical and Electronic Engineers, Boston, Massachusetts.

2. Wyatt, C.L., and Kemp, J.C. (1973) Calibration of SWIR Spectrometer Model NS-1B-5, prepared for AFGL Contract No. F19628-73-C-0048, Utah State University, Logan.

3. Wyatt, C.L. (1974) Revised Calibration of SWIR Spectrometers Model NS-1B-5 and Model NS-1B-6, prepared for AFGL Contract No. F19628-73-C-0048, Utah State University, Logan.

4. Romick, C.J. (1974) Report on the Geophysical Description and Available Data Associated With Rocket PF-PT-54 (PT-10.205-2), prepared for Utah State University, University of Alaska, Fairbanks.

5. Kofsky, I.L., Meriwether, J.W., Schroeder, J.W., and Sluder, R.B. (1975) Data Reduction and Auroral Characterizations for ICECAP, HAES Report No. 4, DNA Report No. 3511F, Contract No. DNA 001-73-C-0027, Photometrics, Inc., Lexington, Massachusetts.

6. Sears, R.D. (1973) Ionospheric Irregularities: Alaska Photometric Measurements, DNA Report No. 3235F, Contract No. DNA 001-73-C-0110, Lockheed Palo Alto Research Laboratory, Palo Alto, California.

7. Baron, M.B., and Chang, N.J. (1975) ICECAP 73A - Chatanika Radar Results, HAES Report No. 15, DNA Report No. 3531T, Contract No. DNA-001-74-C-0167, Stanford Research Institute, Menlo Park, California.

8. Stair, A.T., Jr., Ulwick, J.C., Baker, K.D., and Baker, D.J. (1975) Rocketborne observations of atmospheric infrared emissions in the auroral region, Atmospheres of Earth and the Planets, editor B.M. McCormac, D. Reidel Publishing Co., p. 335-346.

9. Wheeler, N.B., Stair, A.T., Jr., Frodsham, G., and Baker, D.J. (1976) Rocketborne spectral measurement of atmospheric infrared emission during a quiet condition in the auroral zone (1976), USAF Rep. No. AFGL-TR-76-0252, Environmental Research Papers, No. 582, AFGL, Hanscom AFB, Massachusetts.

10. Kumer, J.B. (1974) Analysis of 4.3 μm ICECAP Data, HAES Report No. 19, AFCRL-TR-74-0334, Contract No. F19628-73-C-0288, Lockheed Palo Alto Research Laboratories, Palo Alto, California.

11. Reidy, W.P., Degges, T.C., Manley, O.P., Smith, H.J., Carpenter, J.W., Stair, A.T., Jr., Ulwick, J.C., and Baker, K.D. (1974) Analysis of HAES Results: ICECAP 72, HAES Report No. 2, Final Report, DNA 3247F, Contract No. DNA 001-73-0020.

12. Degges, T.C. (1971) Vibrationally excited nitric oxide in the upper atmosphere, Appl. Optics 10:1856.

13. Huppi, E.R., Rogers, J.W., and Stair, A.T., Jr. (1974) Aircraft observations of the infrared emission of the atmosphere in the 700-2800 cm^{-1} region, Appl. Optics 13:1466.

Appendix A

Calibrations

Table A1. NS-1B-5 Revised Calibration (High Gain Channels)

λ	$V/E(\lambda)$	$E(\lambda)/V$	$L(\lambda)/V^1$	$MR\,\mu^{-1}/V^2$
1.5	0.45 + 9	2.22 - 9	31.10 - 8	29.3
1.75	0.70 + 9	1.43 - 9	20.00 - 8	22.0
2.0	1.00 + 9	1.00 - 9	14.00 - 8	17.6
2.25	1.35 + 9	7.41 - 10	10.40 - 8	14.7
2.50	1.60 + 9	6.25 - 10	8.77 - 8	13.8
2.75	1.80 + 9	5.56 - 10	7.80 - 8	13.5
2.75	1.10 + 9	9.10 - 10	12.80 - 8	22.1
3.0	1.00 + 9	1.00 - 9	14.00 - 8	26.4
3.25	1.10 + 9	9.10 - 10	12.80 - 8	26.1
3.50	1.45 + 9	8.90 - 10	9.68 - 8	21.3
3.75	1.80 + 9	5.56 - 10	7.80 - 8	18.4
4.00	2.15 + 9	4.65 - 10	6.53 - 8	16.4
4.25	2.55 + 9	3.92 - 10	5.50 - 8	14.7
4.50	2.78 + 9	3.60 - 10	5.05 - 8	14.3
4.75	2.80 + 9	3.57 - 10	5.01 - 8	15.0
5.00	2.50 + 9	4.00 - 10	5.61 - 8	17.6
5.25	2.05 + 9	4.88 - 10	6.84 - 8	22.6

1. $L(\lambda)/V = E(\lambda)/\Omega V$ where $\Omega = 7.127\,\mu\ 10^{-3}$.
2. $MR\,\mu^{-1}/V = 2\pi\lambda L(\lambda) \times 10^7/V$.

The sign and following digit are the power to which 10 is raised in the exponent.

Table A2. Time Variations for the 4278, 5577, and 6300 A Emissions at the 100-km Rocket Entry and Exit Points as Seen From Ft. Yukon

Time	Entry - 151°, Exit - 136°					
	5577 A		4278 A		6300 A	
	Entry	Exit	Entry	Exit	Entry	Exit
-280	14.1	7.7	2.4	1.9	1.1	0.52
-259	25.8	7.7	5.7	1.9	1.6	0.52
-238	69.9	7.7	13.0	2.4	2.7	0.52
-216	31.4	6.3	7.0	1.9	1.6	0.52
-195	31.4	6.3	5.7	1.9	1.6	1.1
-174	25.8	6.3	5.7	1.9	1.6	0.52
-152	25.8	6.3	7.0	2.4	2.1	1.1
-131	38.4	6.3	7.0	1.9	2.1	0.52
-110	25.8	7.7	5.7	1.9	2.1	0.52
-88	17.4	6.3	3.0	1.1	1.6	0.52
-67	20.9	5.0	3.7	0.8	1.6	0.52
-46	31.4	3.3	5.7	0.8	1.6	0.52
-24	38.4	4.1	6.7	1.5	2.1	0.52
-3	20.9	25.8	5.7	7.0	1.6	1.1
+18	69.9	126.9	16.1	29.5	2.7	3.2
+40	154.6	154.6	36.0	44.4	4.3	4.8
+61	126.9	154.6	29.5	36.0	3.6	4.3
+82	103.9	188.9	29.5	66.4	3.6	5.9
+104	230.9	69.9	54.1	19.5	8.0	2.7
+125	188.9	46.9	44.4	13.0	5.9	2.7
+146	57.3	85.3	13.0	19.5	3.2	3.6
+168	103.9	31.4	24.2	10.3	3.6	2.7
+189	103.9	31.4	24.2	10.3	4.3	2.1
+210	126.9	38.4	24.2	6.7	4.3	2.1
+232	103.9	31.4	19.5	6.7	4.3	2.1
+253	85.3	31.4	19.5	6.7	4.8	2.1
+274	38.4	25.8	13.0	7.0	3.2	2.1
+296	31.4	20.9	10.3	7.0	3.2	2.1
+317	31.4	20.9	10.3	7.0	3.2	1.6
+338	31.4	17.4	6.7	5.7	2.7	1.6
+360	25.8	17.4	10.3	5.7	3.2	1.6
+381	25.8	17.4	10.3	5.7	2.7	1.6
+402	20.9	14.1	7.0	5.7	2.1	1.1
+424	20.9	14.1	7.0	4.4	2.1	1.1
+445	20.9	14.1	7.0	4.4	2.1	1.1
+466	20.9	14.1	7.0	4.4	2.1	1.1
+488	20.9	14.1	7.0	4.4	1.6	1.1
+509	20.9	17.4	7.0	5.7	2.1	1.6
+530	20.9	85.3	6.7	24.2	2.1	2.7
+552	17.4	25.8	5.7	5.7	1.6	1.6
+573	17.4	25.8	5.7	5.7	1.6	1.6
+594	17.4	20.9	5.7	5.7	1.6	2.1
+616	17.4	25.8	5.7	5.7	1.6	2.1

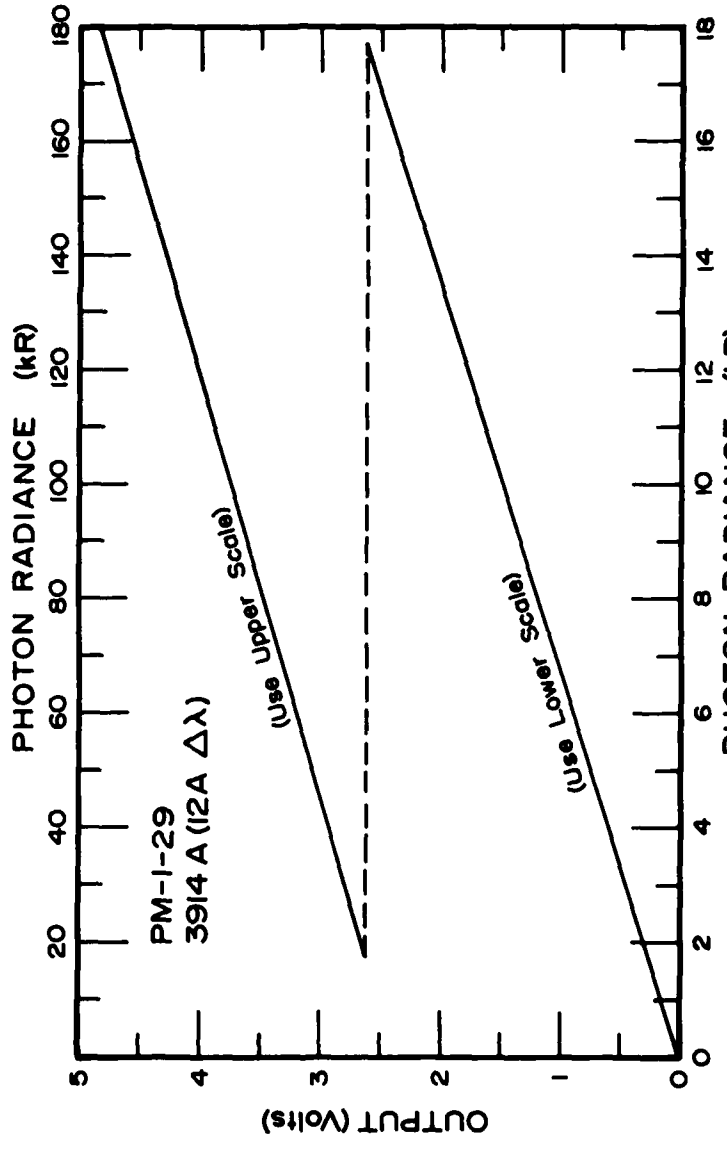

Figure A1. Output Volts vs Photon (kR)

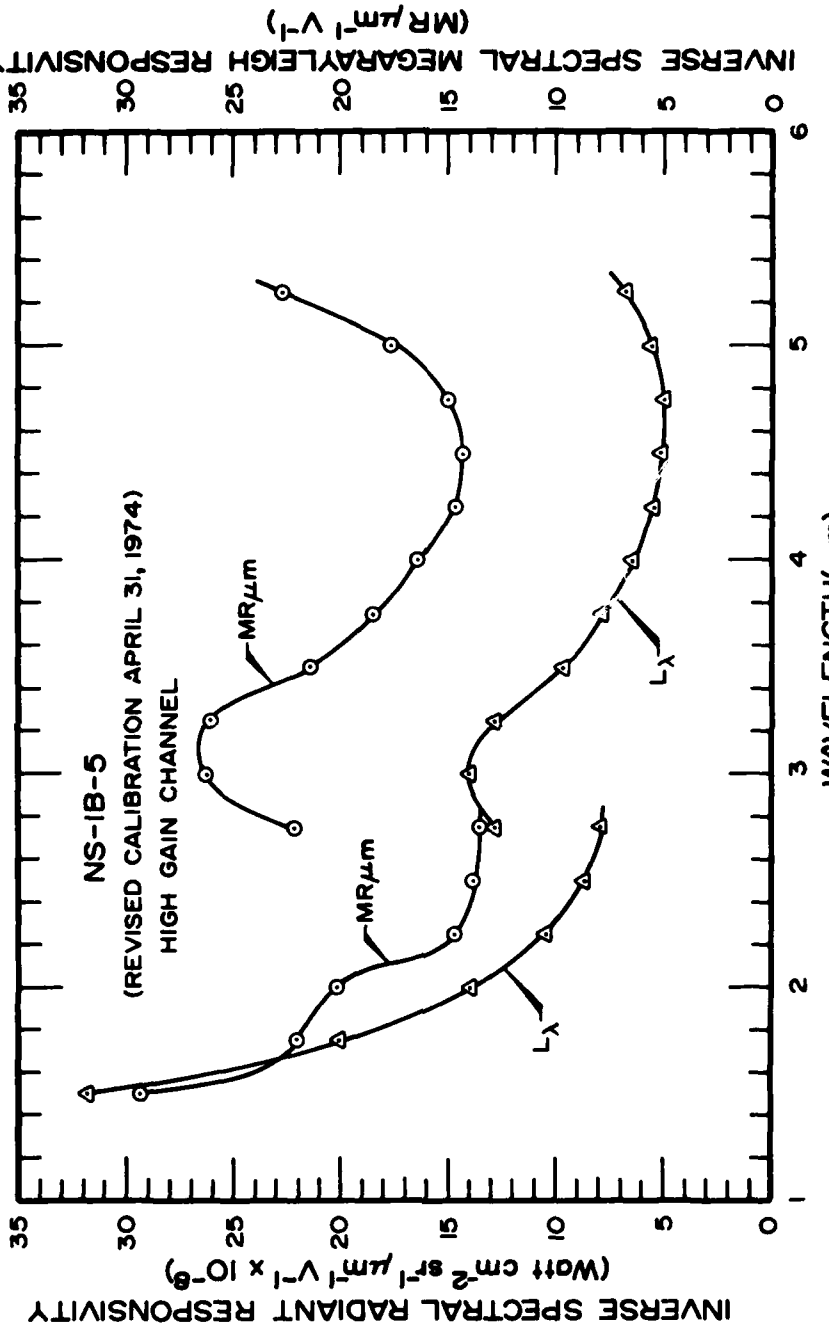

Figure A2. Inverse Spectral Radiant Responsivity vs Wavelength (μm)

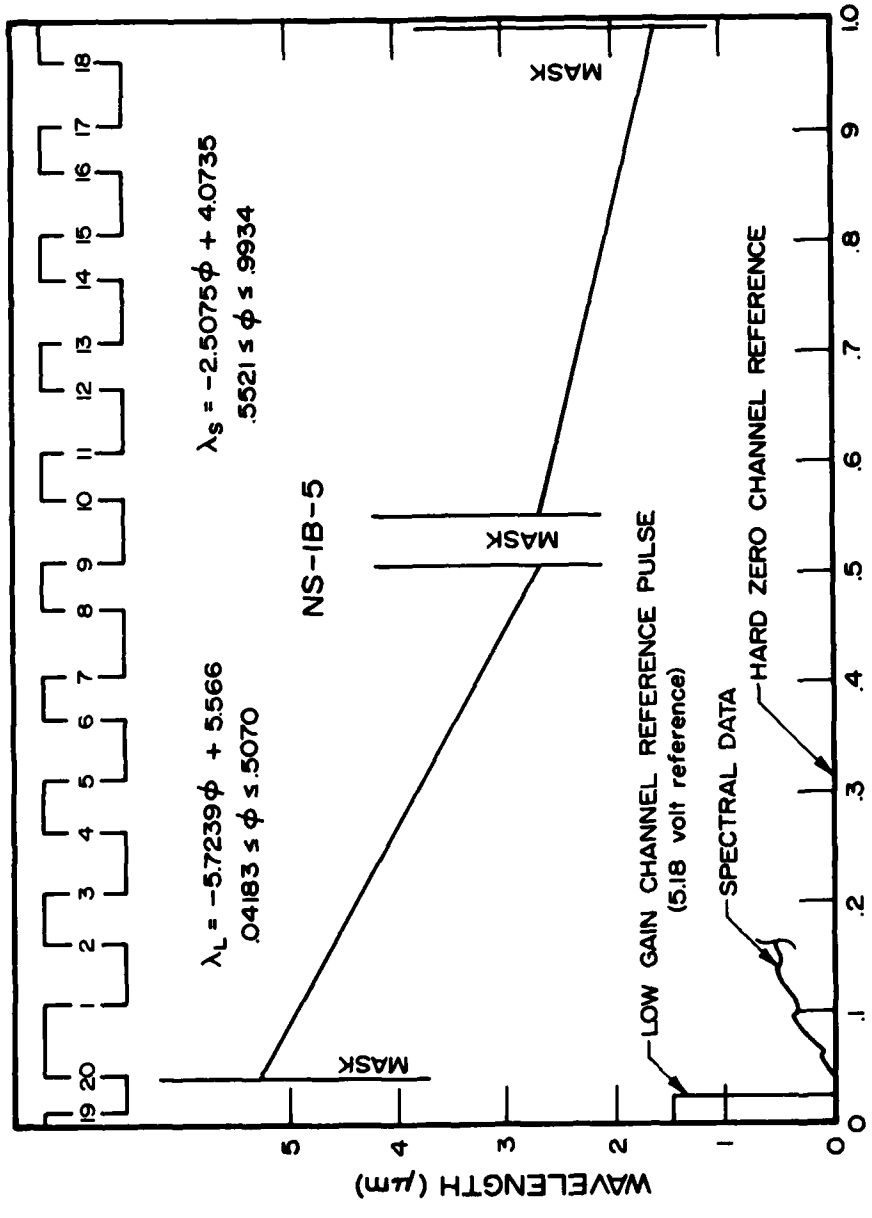

Figure A3. Reference Position (ϕ) vs Wavelength (μm)

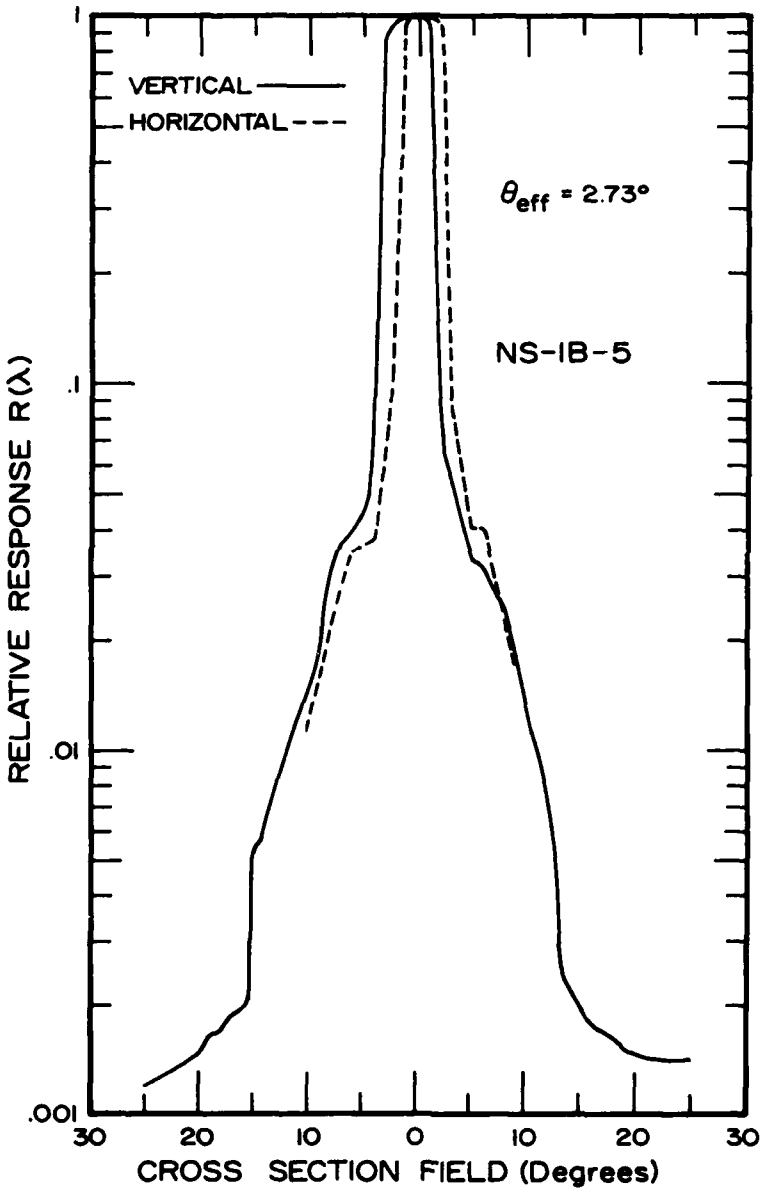

Figure A4. Relative Response R(λ) vs Cross Section Field (Degrees)

Appendix B

Circular Variable Filter Spectrometer Spectral Scans

PRECEDING PAGE NOT FILMED
BLANK

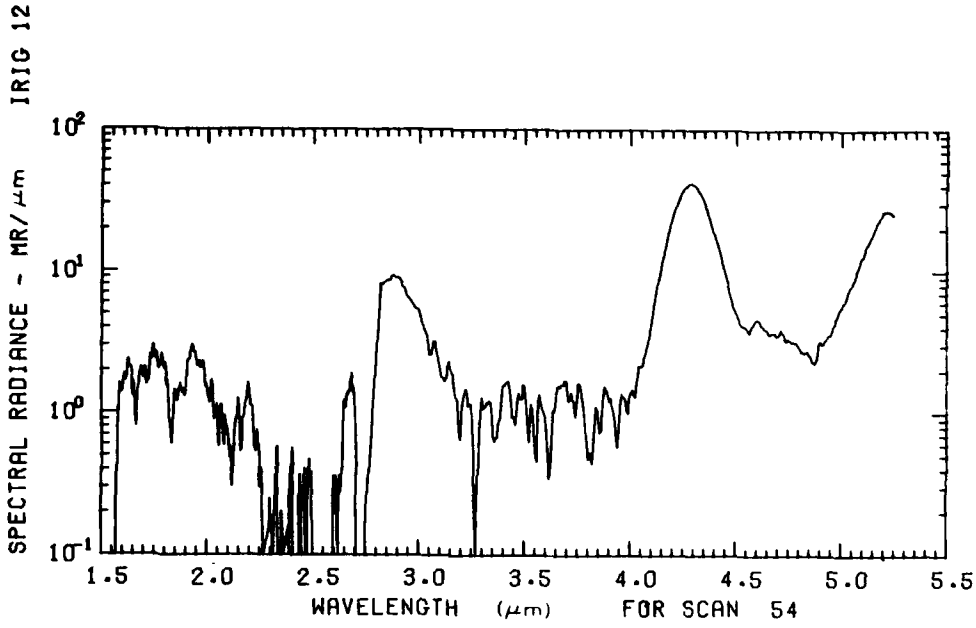

Figure B1. A10.205-2, Ascent, High Gain – 71.77 km

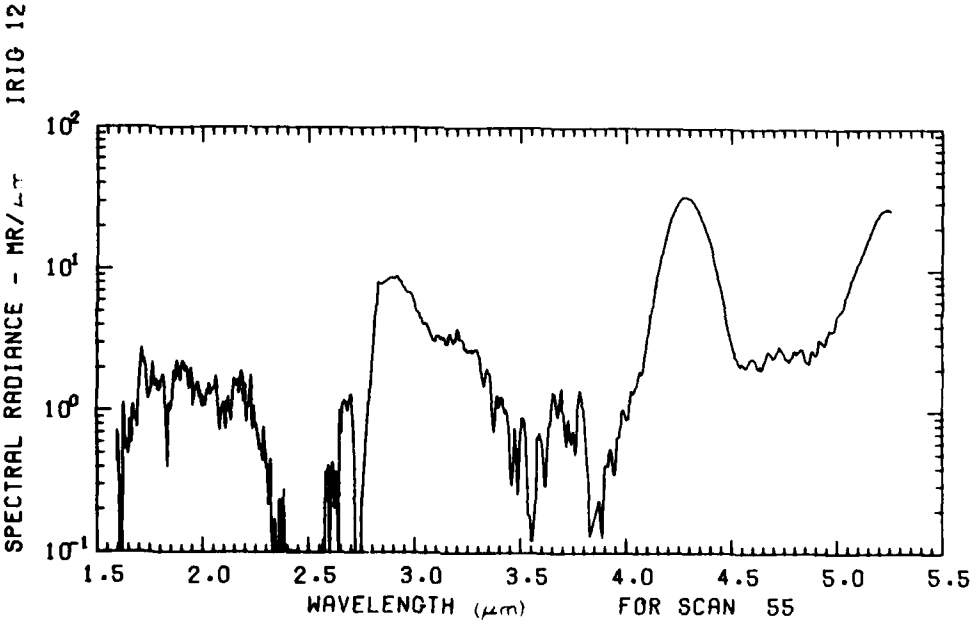

Figure B2. A10.205-2, Ascent, High Gain – 72.56 km

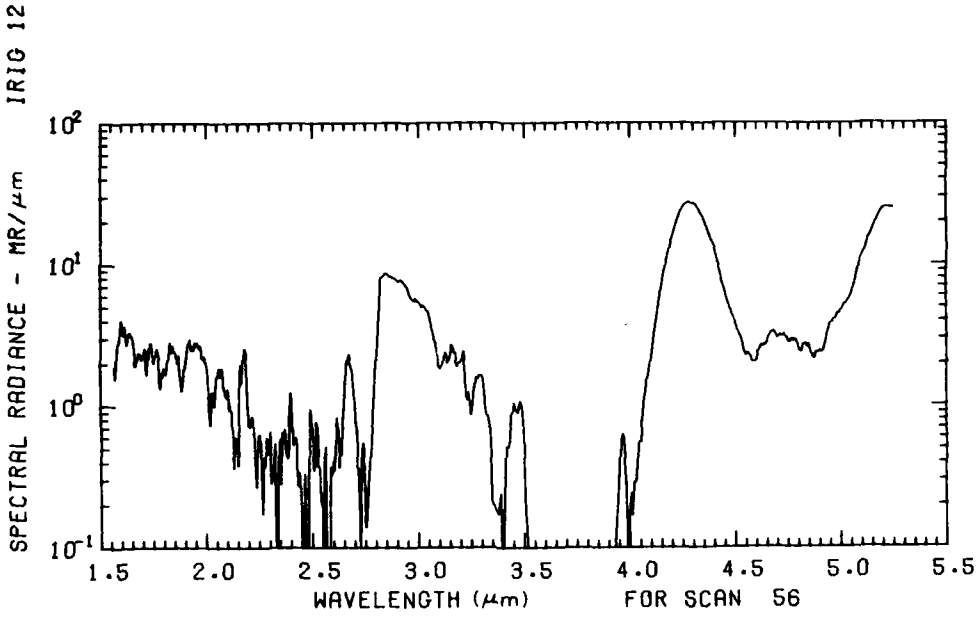

Figure B3. A10.205-2, Ascent, High Gain – 73.34 km

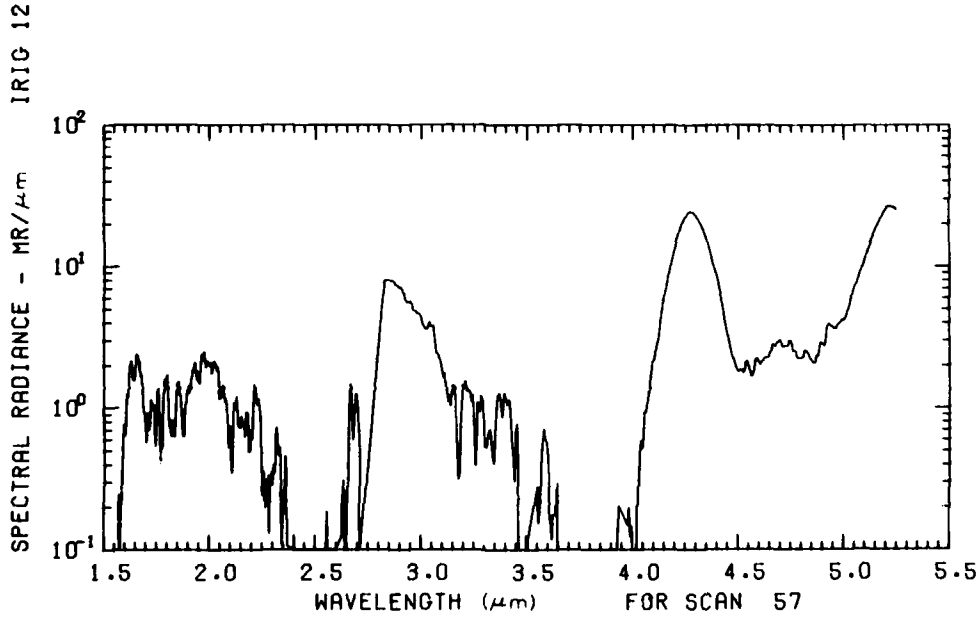

Figure B4. A10.205-2, Ascent, High Gain – 74.12 km

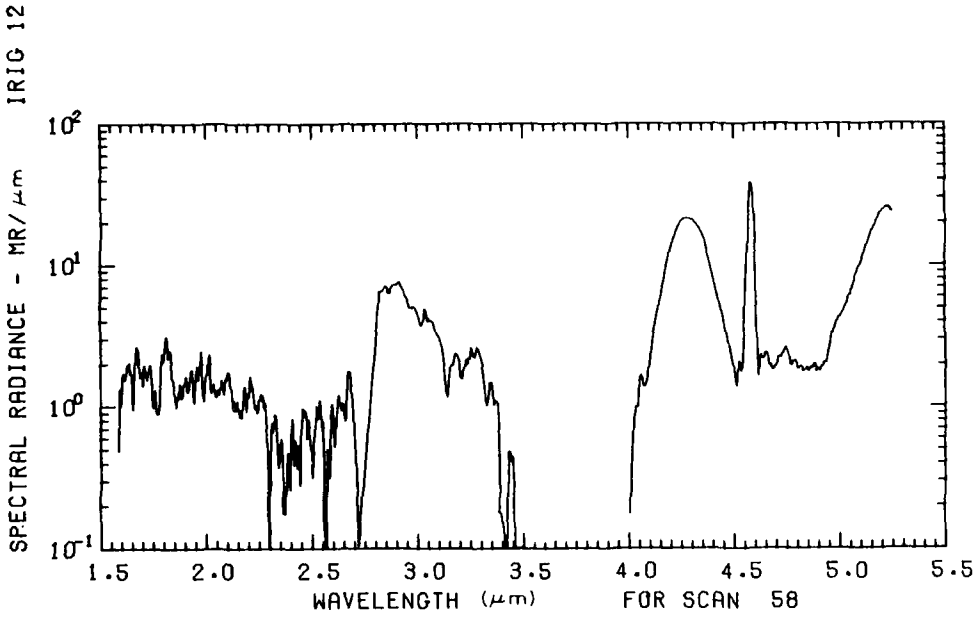

Figure B5. A10.205-2, Ascent, High Gain – 74.90 km

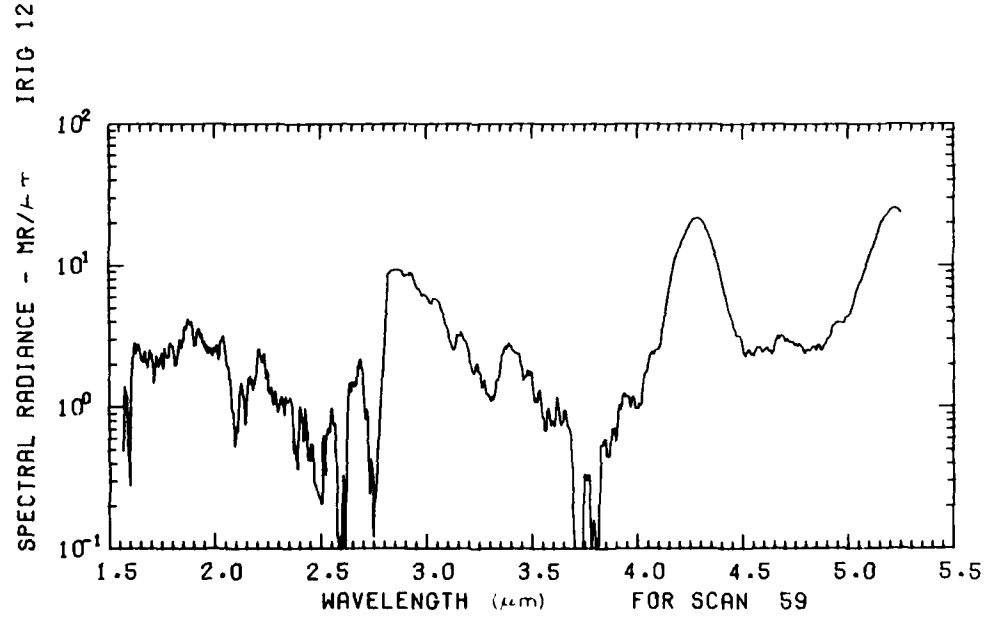

Figure B6. A10.205-2, Ascent, High Gain – 75.68 km

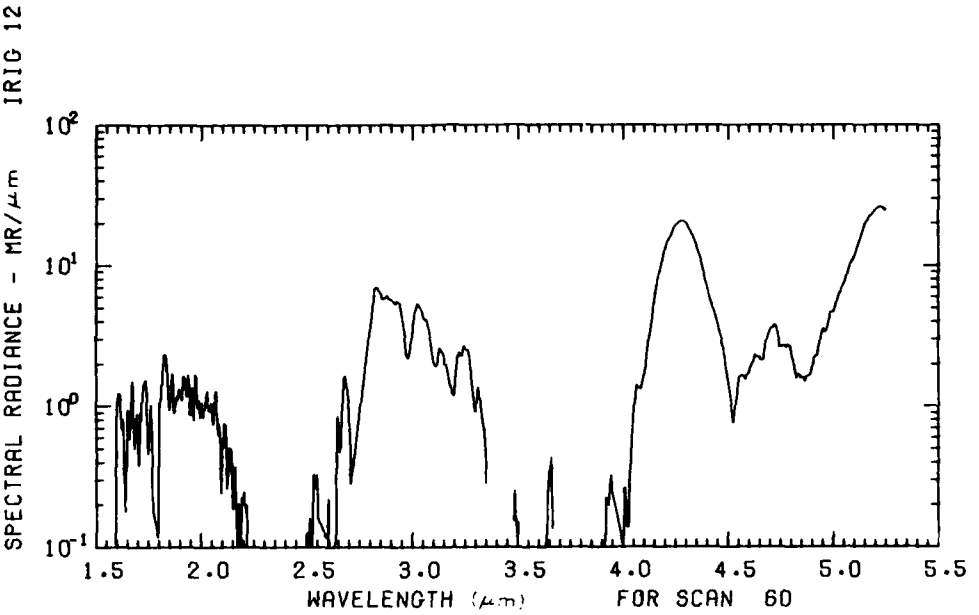

Figure B7. A10.205-2, Ascent, High Gain – 76.46 km

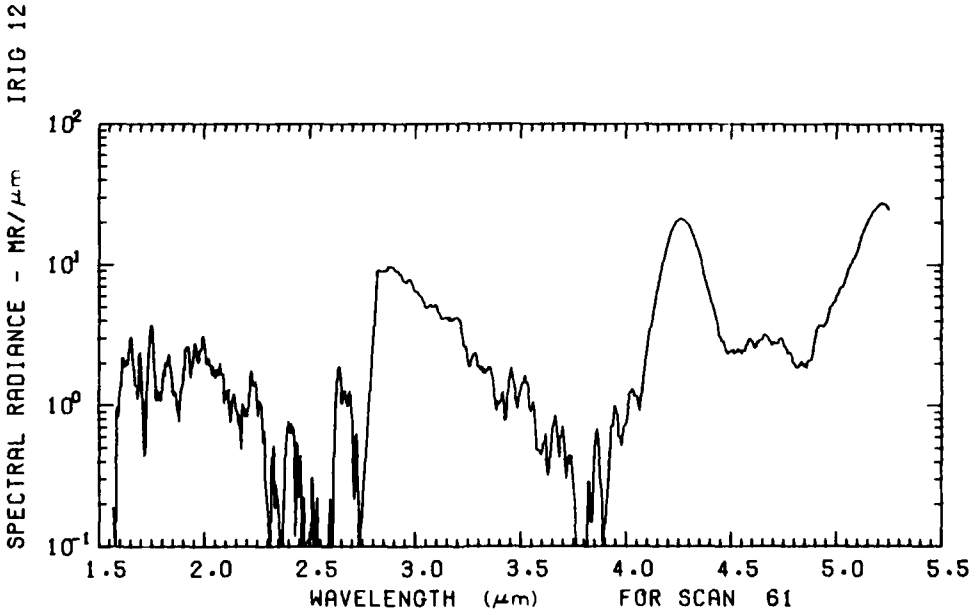

Figure B8. A10.205-2, Ascent, High Gain – 77.23 km

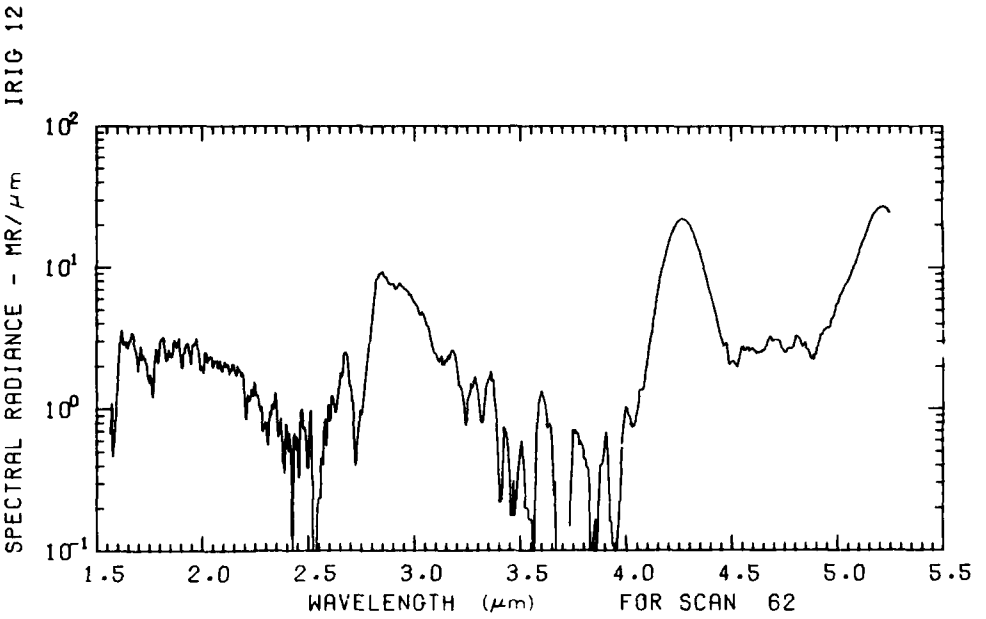

Figure B9. A10.205-2, Ascent, High Gain – 78.60 km

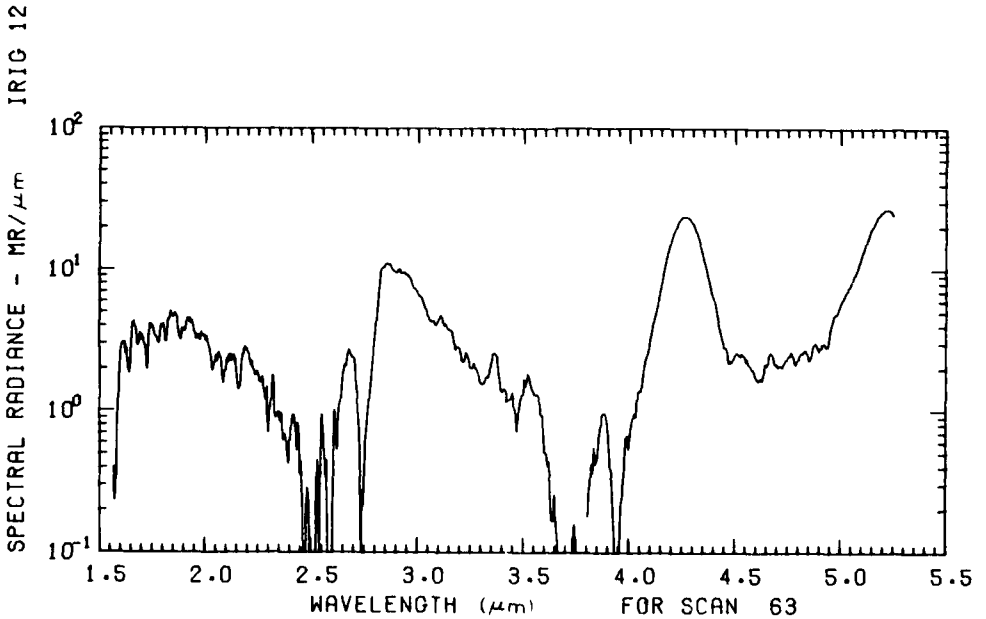

Figure B10. A10.205-2, Ascent, High Gain – 78.77 km

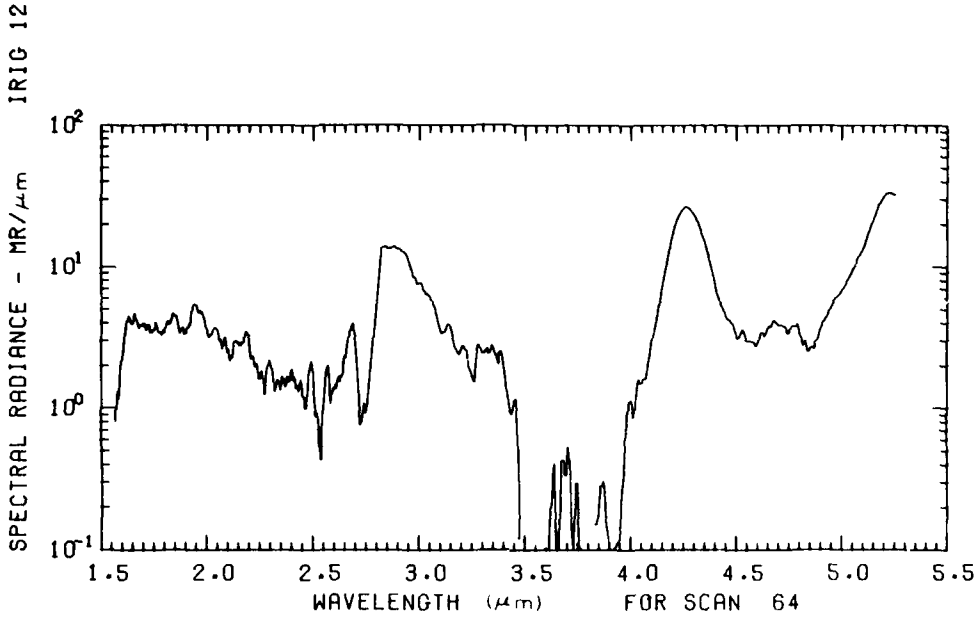

Figure B11. A10.205-2, Ascent, High Gain – 79.53 km

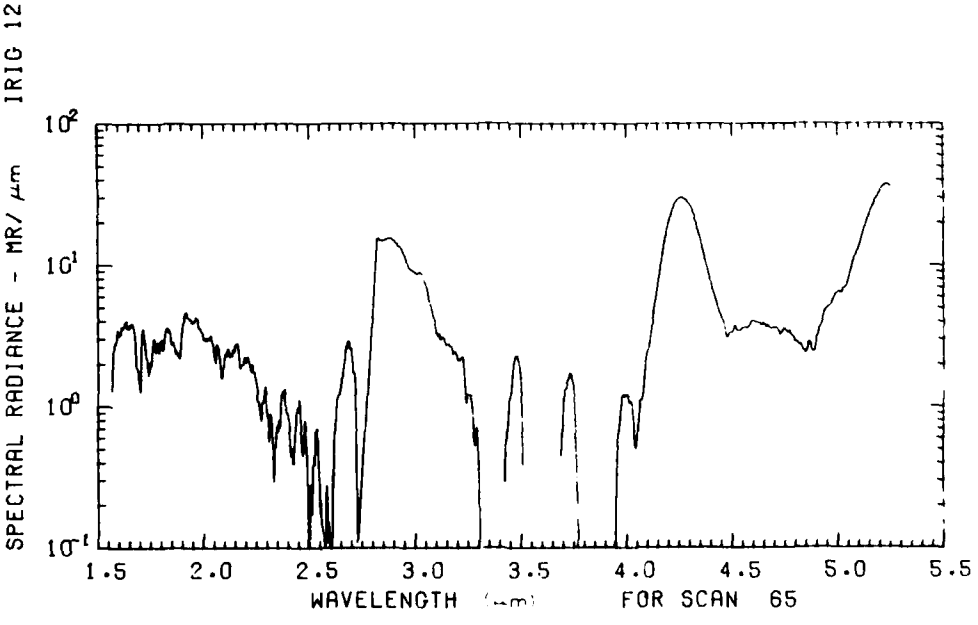

Figure B12. A10.205-2, Ascent, High Gain – 80.30 km

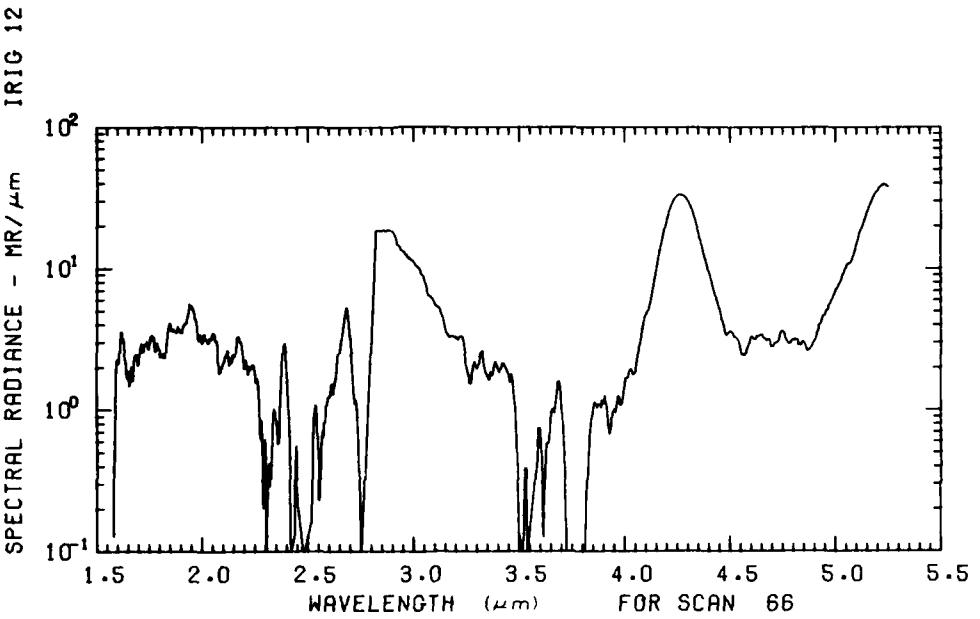

Figure B13. A10.205-2, Ascent, High Gain – 81.06 km

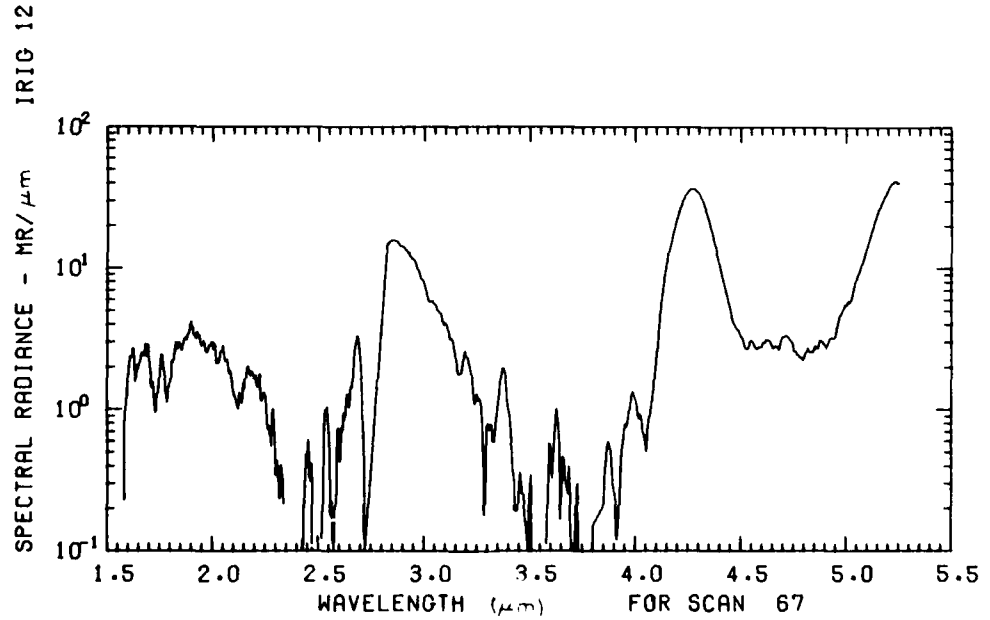

Figure B14. A10.205-2, Ascent, High Gain – 81.82 km

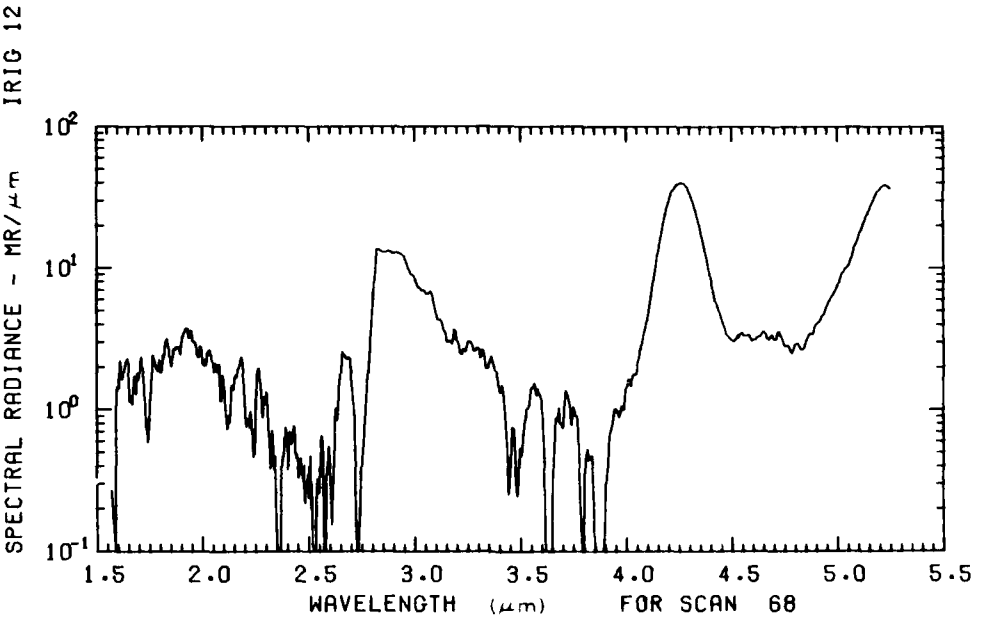

Figure B15. A10.205-2, Ascent, High Gain – 82.58 km

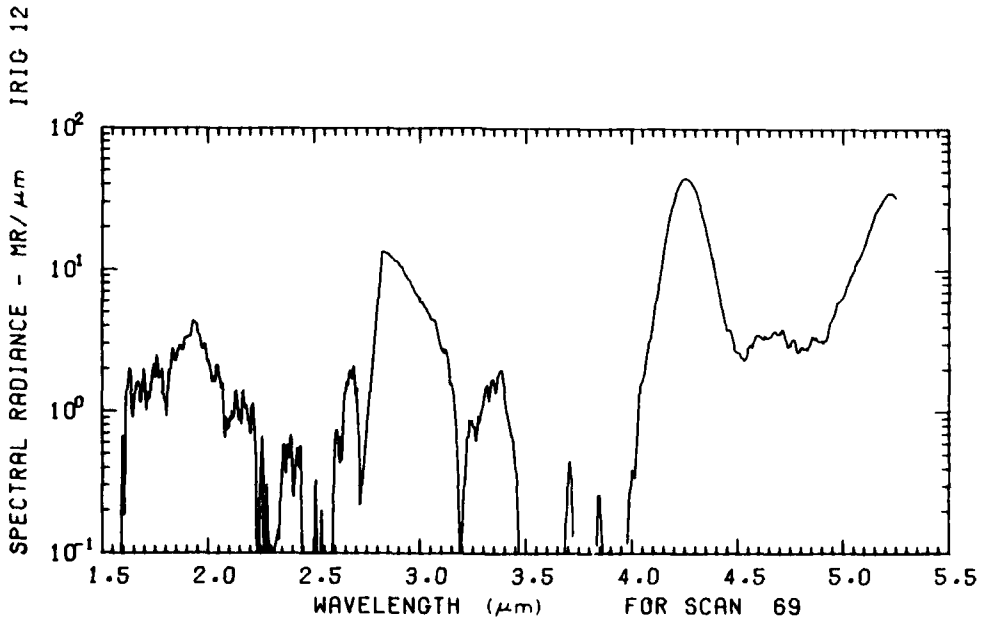

Figure B16. A10.205-2, Ascent, High Gain – 83.33 km

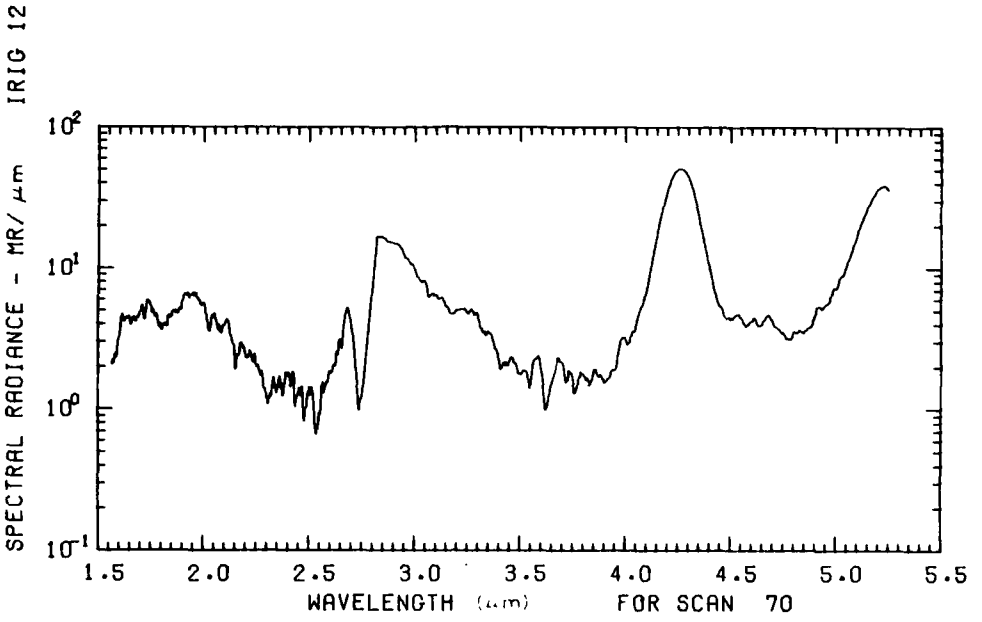

Figure B17. A10.205-2, Ascent, High Gain – 84.84 km

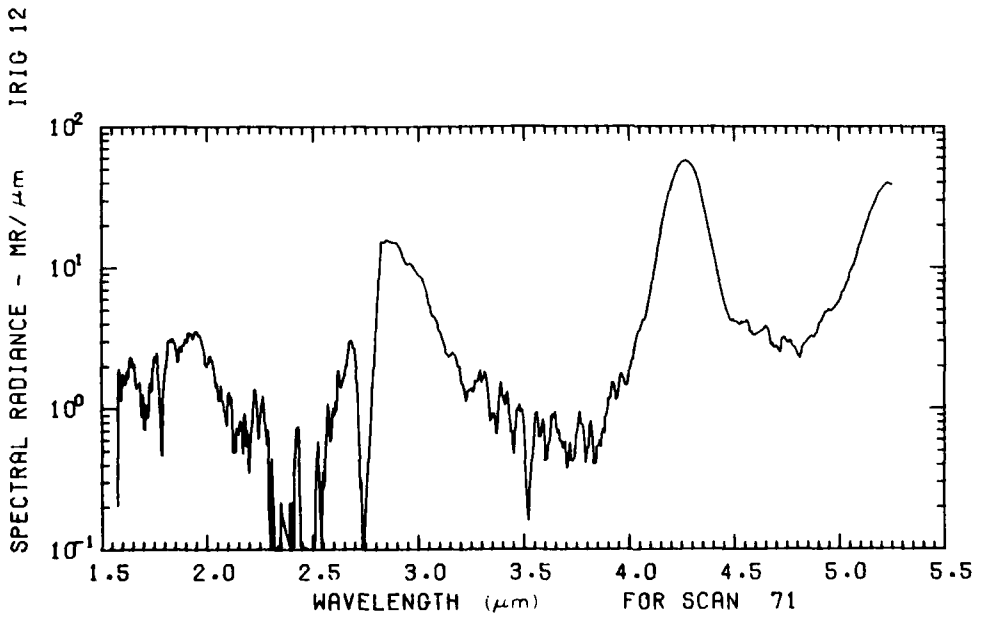

Figure B18. A10.205-2, Ascent, High Gain – 84.84 km

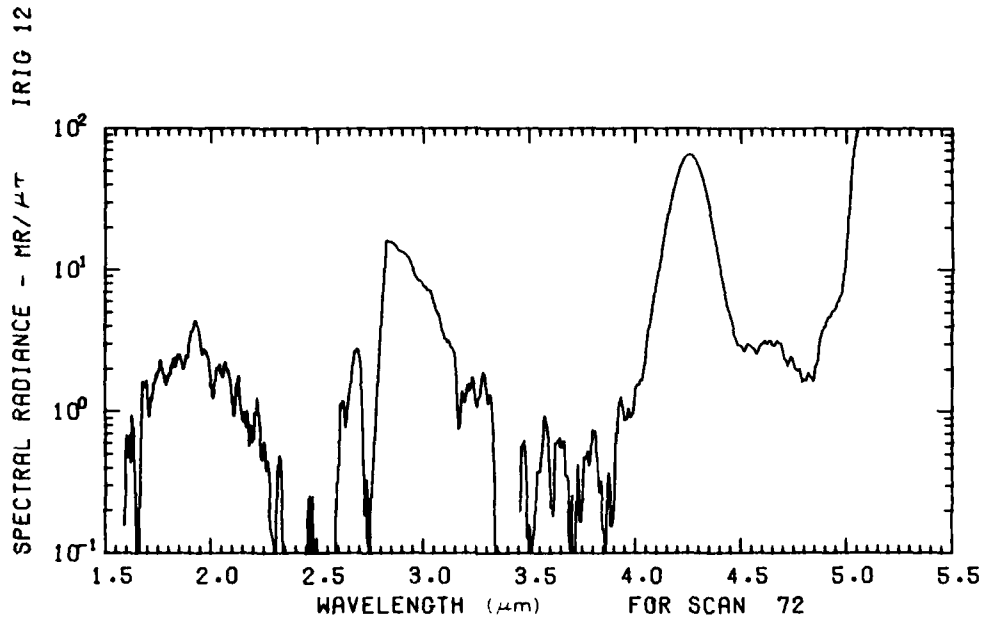

Figure B19. A10.205-2, Ascent, High Gain – 85.58 km

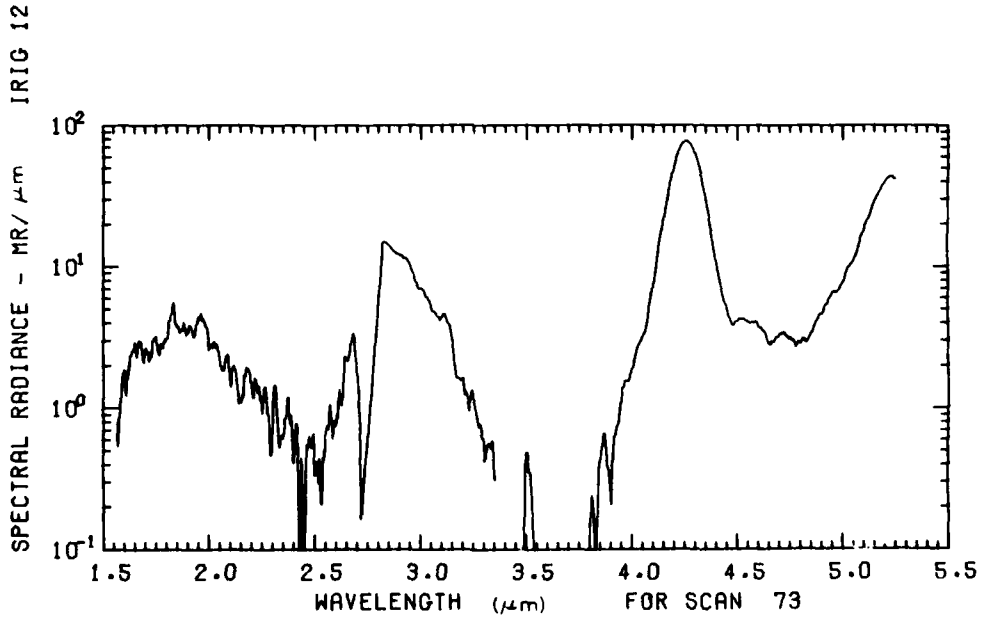

Figure B20. A10.205-2, Ascent, High Gain – 86.33 km

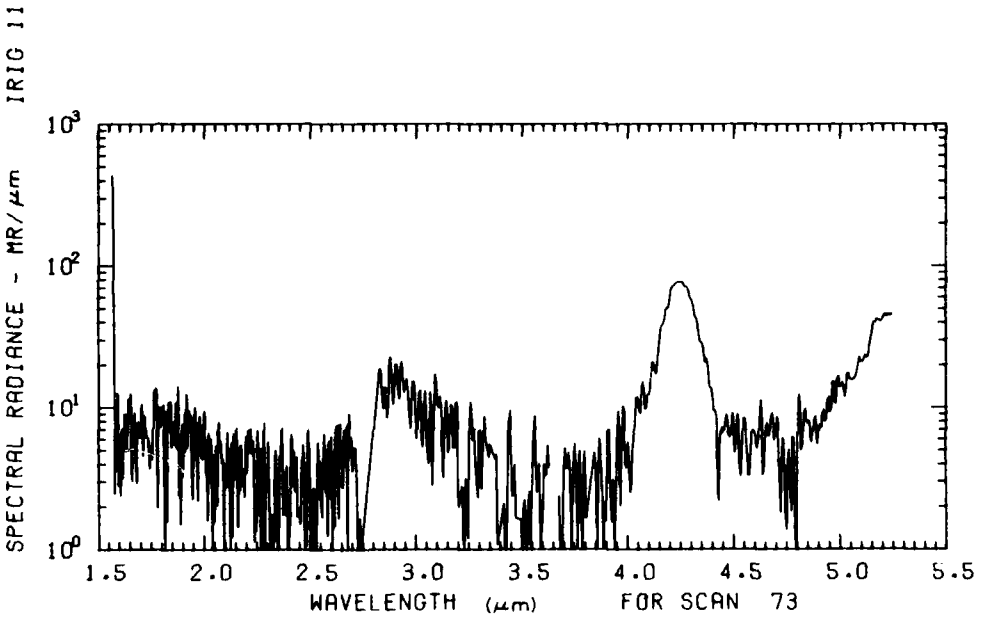

Figure B21. A10.205-2, Ascent, Low Gain – 86.33 km

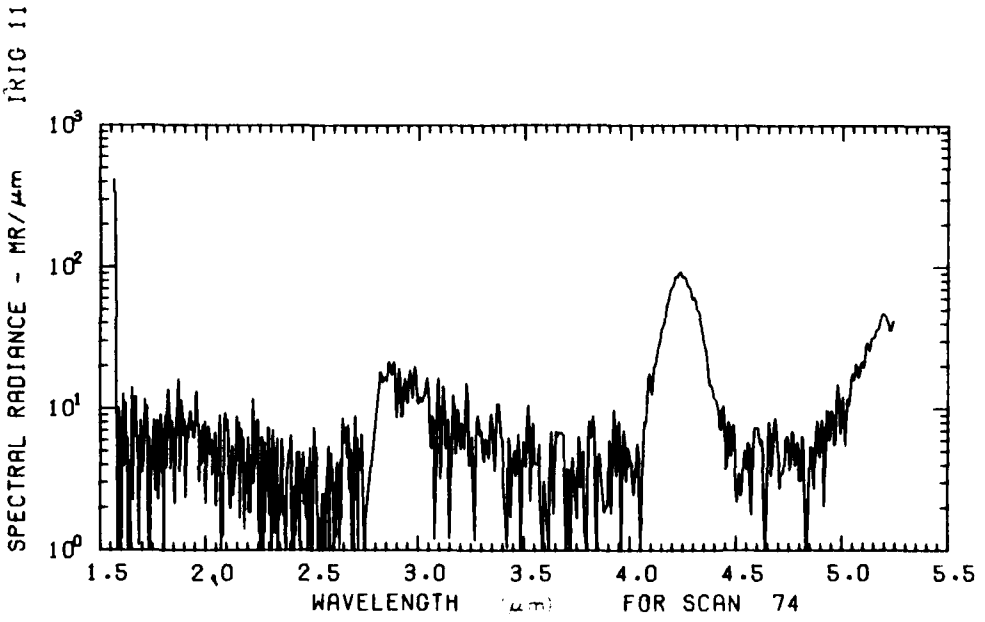

Figure B22. A10.205-2, Ascent, Low Gain – 87.08 km

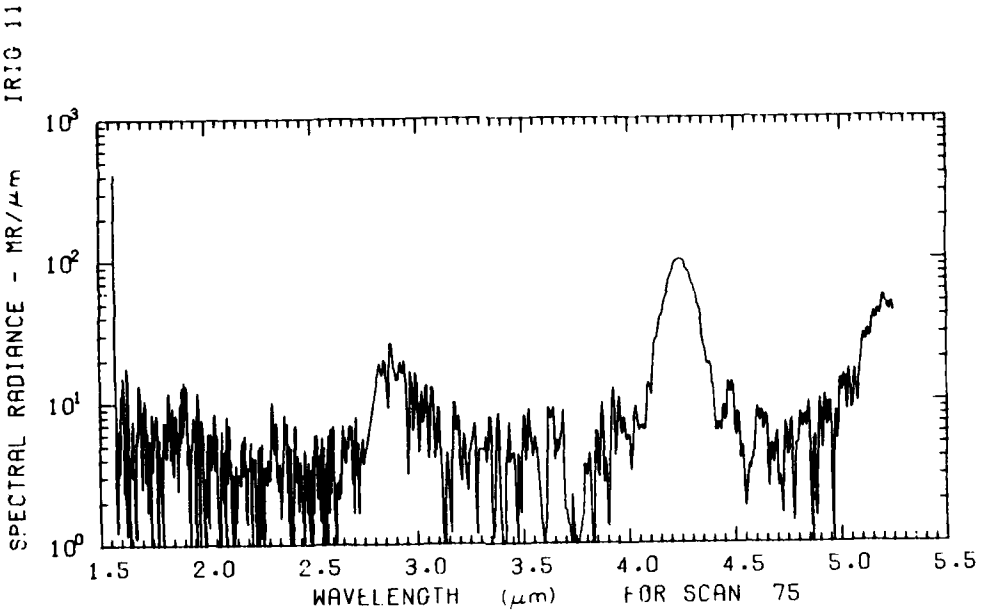

Figure B23. A10.205-2, Ascent, Low Gain – 87.82 km

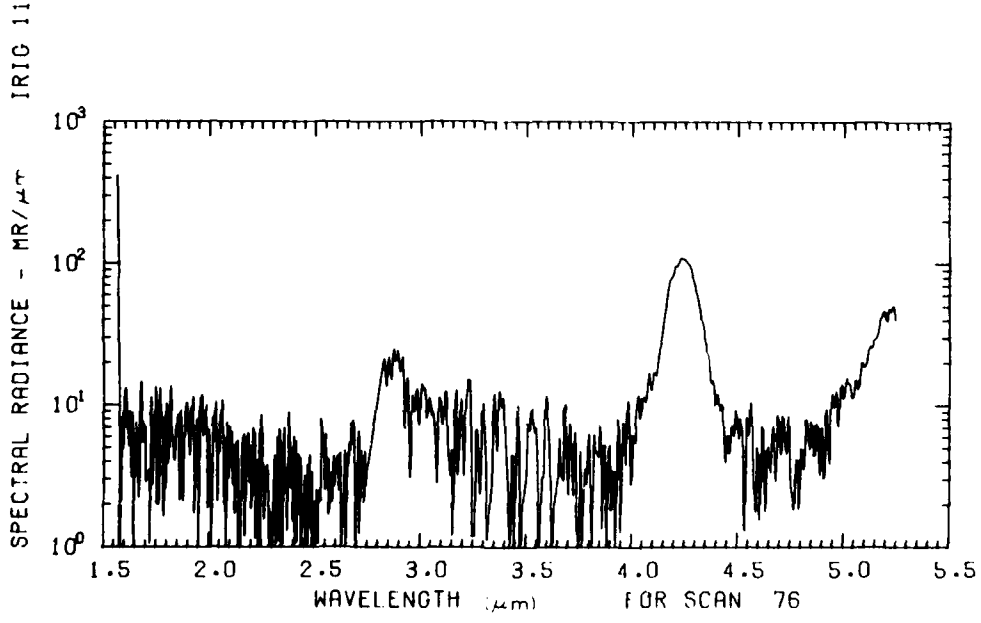

Figure B24. A10.205-2, Ascent, Low Gain – 88.56 km

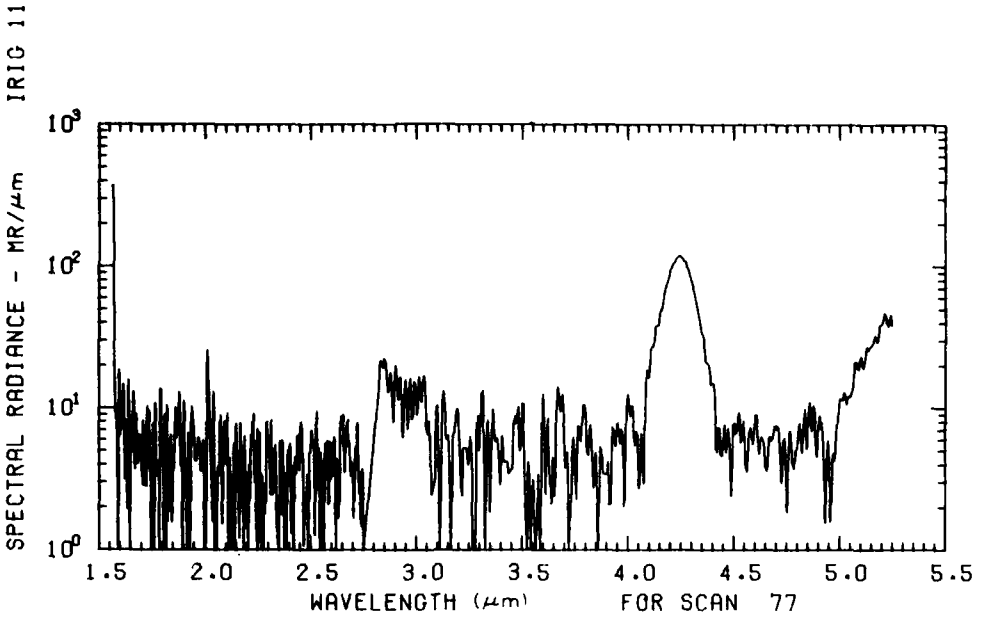

Figure B25. A10.205-2, Ascent, Low Gain – 89.30 km

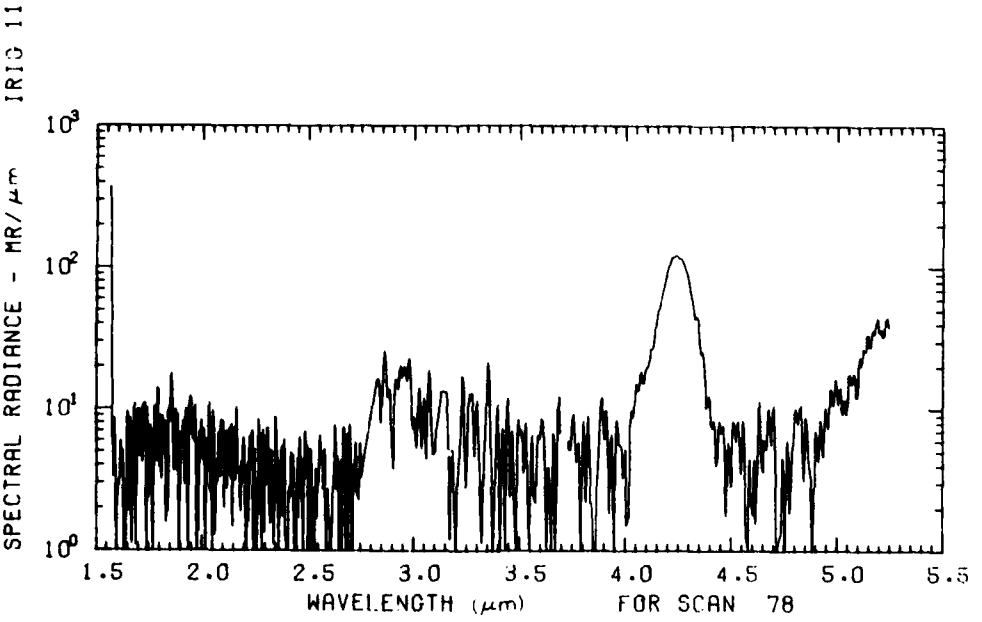

Figure B26. A10.205-2, Ascent, Low Gain – 90.03 km

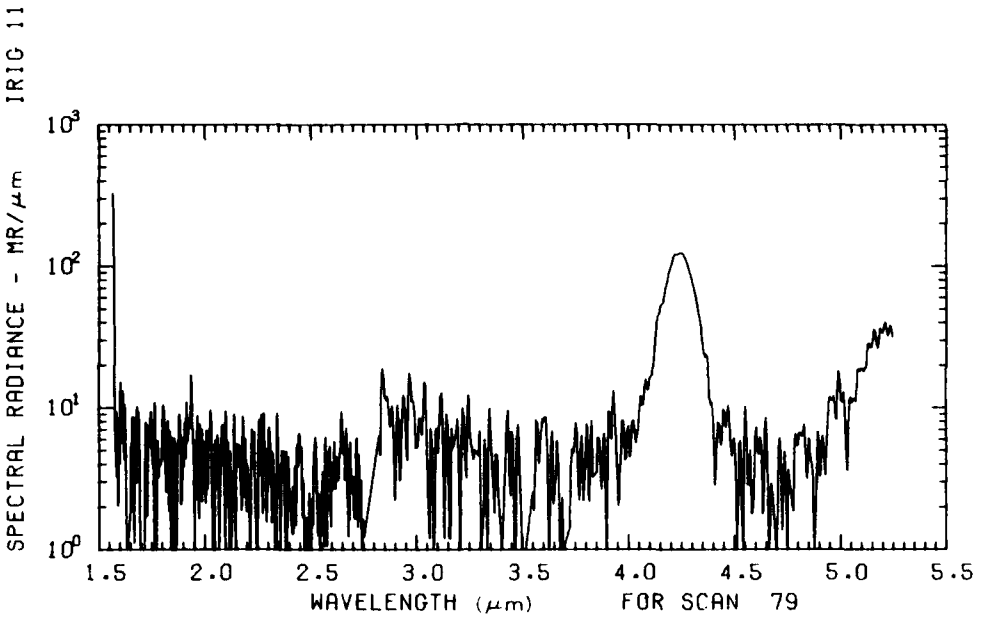

Figure B27. A10.205-2, Ascent, Low Gain – 90.76 km

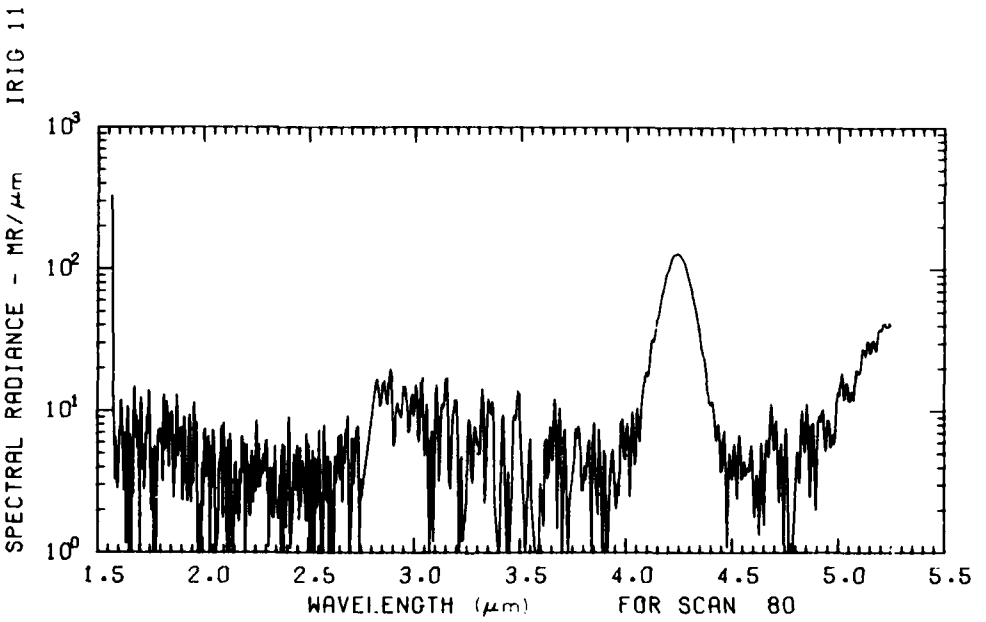

Figure B28. A10.205-2, Ascent, Low Gain – 91.49 km

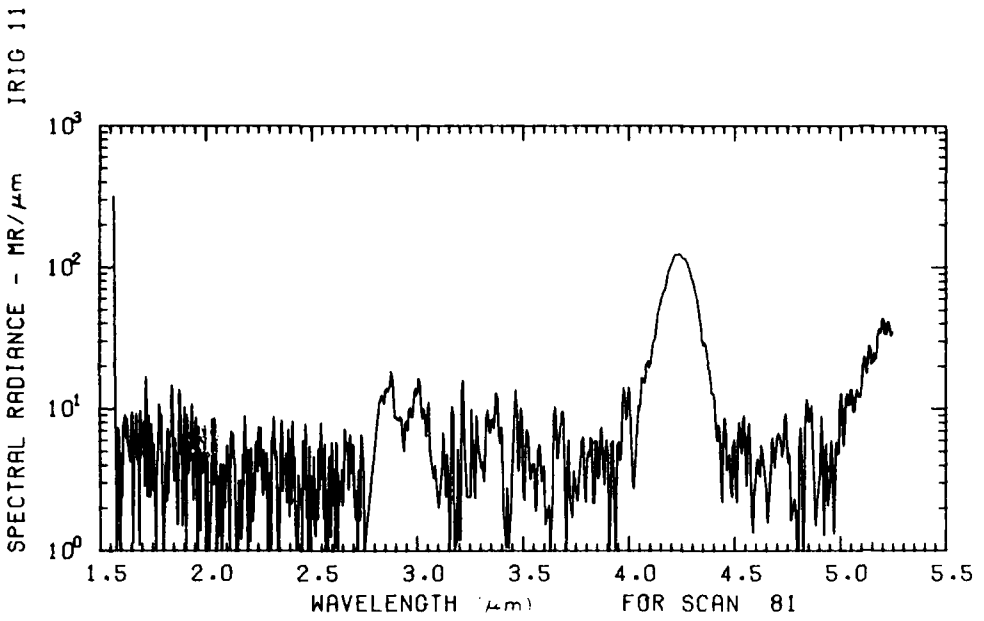

Figure B29. A10.205-2, Ascent, Low Gain – 92.22 km

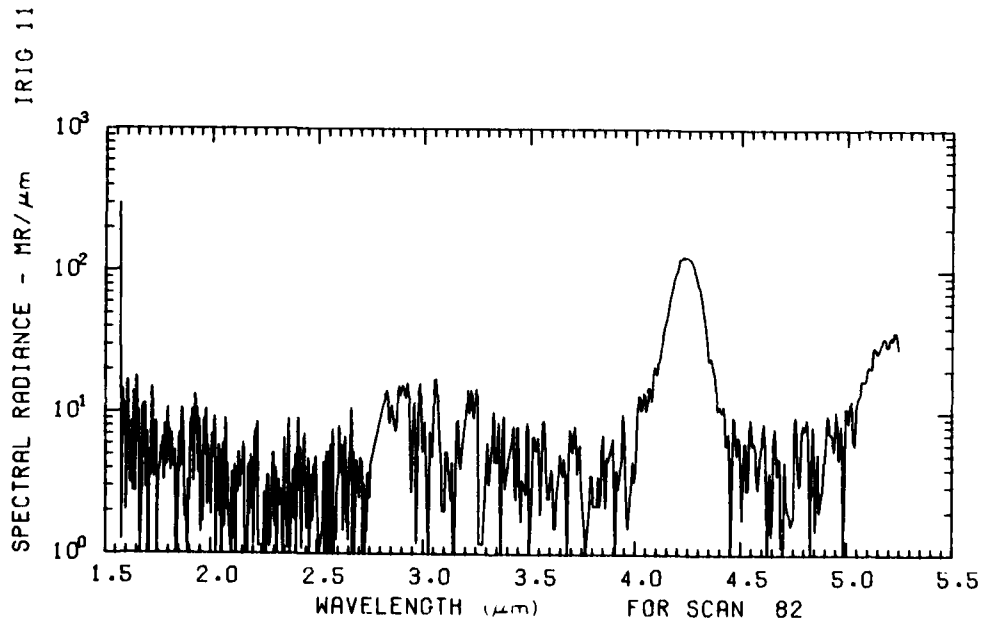

Figure B30. A10.205-2, Ascent, Low Gain – 92.95 km

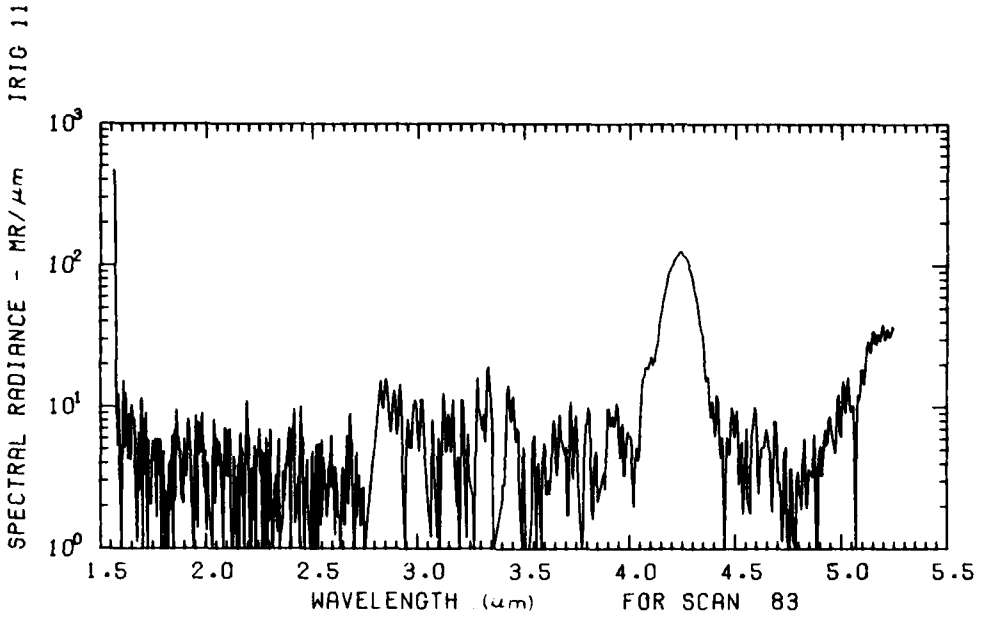

Figure B31. A10.205-2, Ascent, Low Gain – 93.67 km

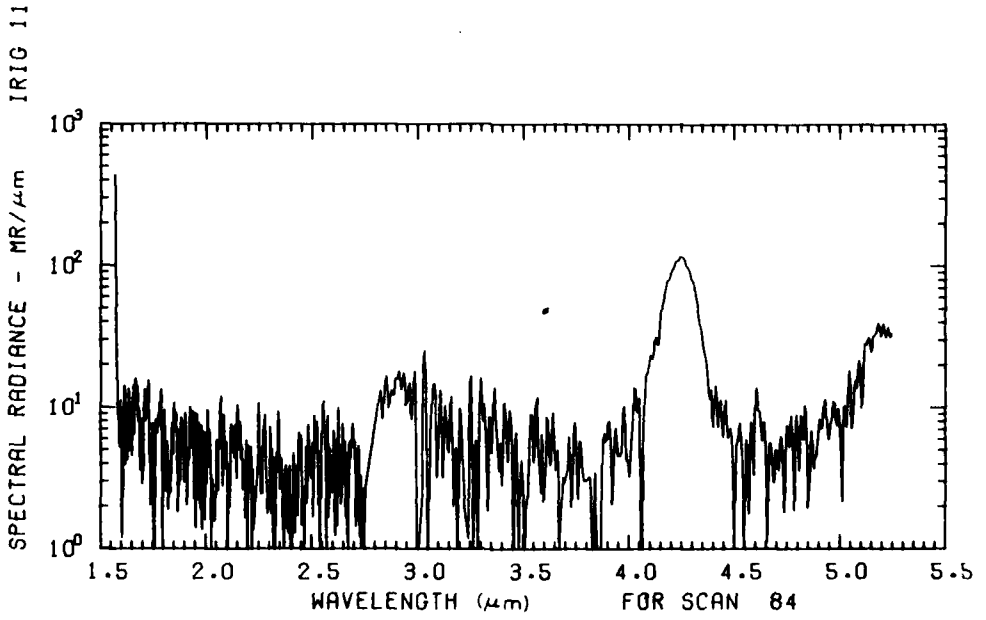

Figure B32. A10.205-2, Ascent, Low Gain – 94.39 km

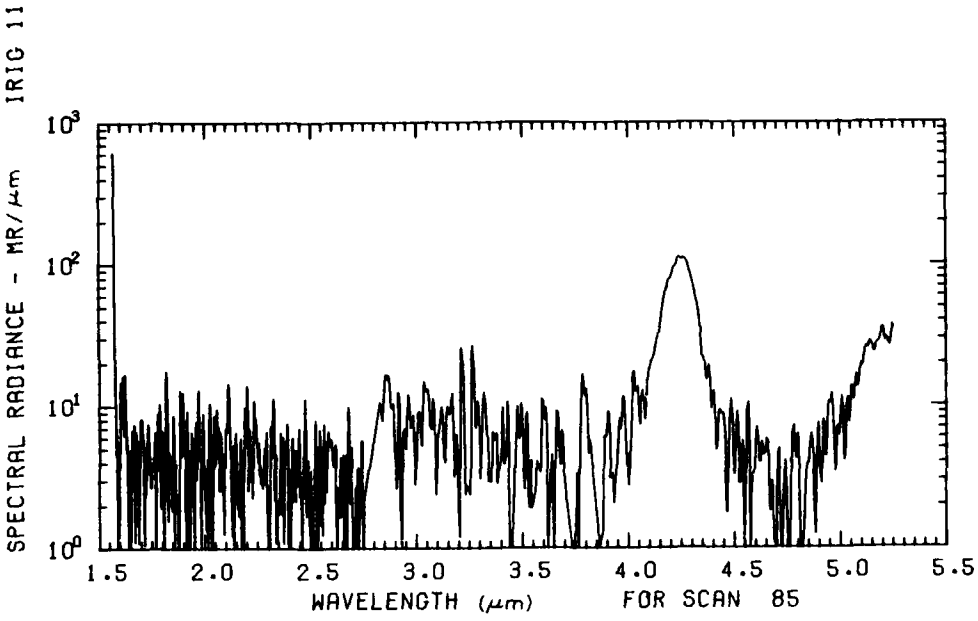

Figure B33. A10.205-2, Ascent, Low Gain – 95.11 km

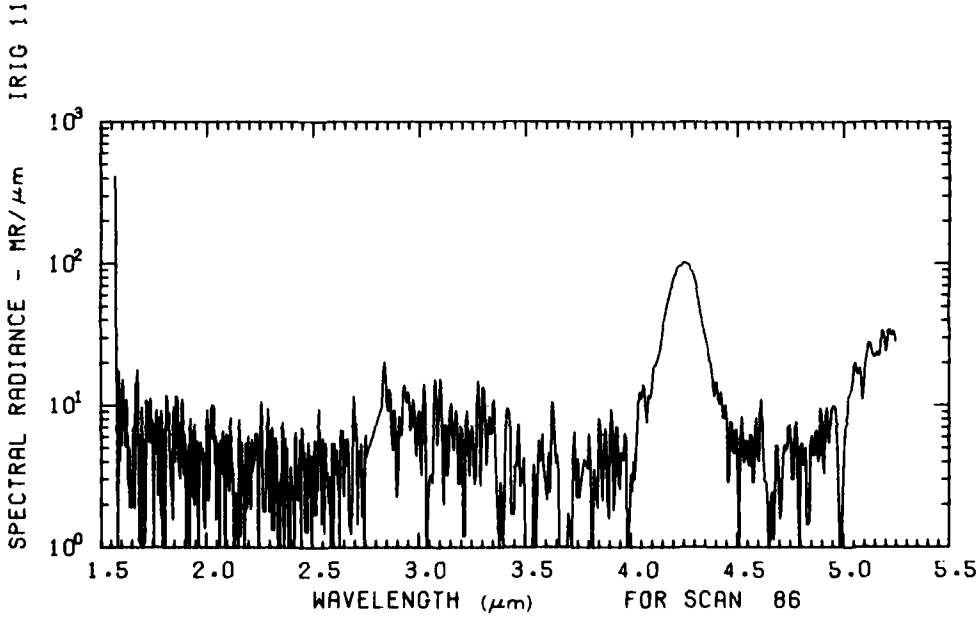

Figure B34. A10.205-2, Ascent, Low Gain – 95.83 km

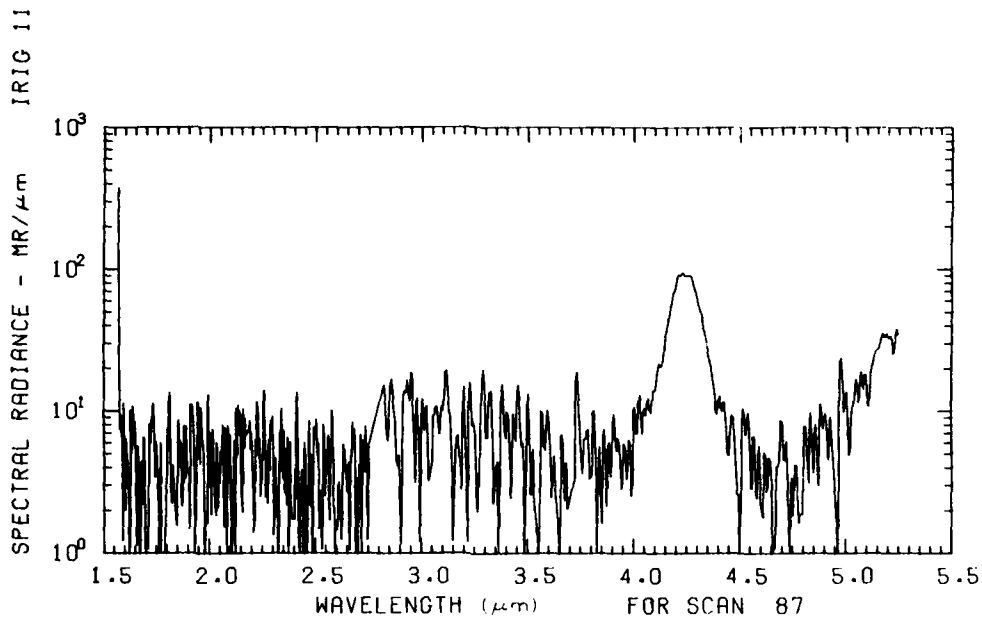

Figure B35. A10.205-2, Ascent, Low Gain – 96.55 km

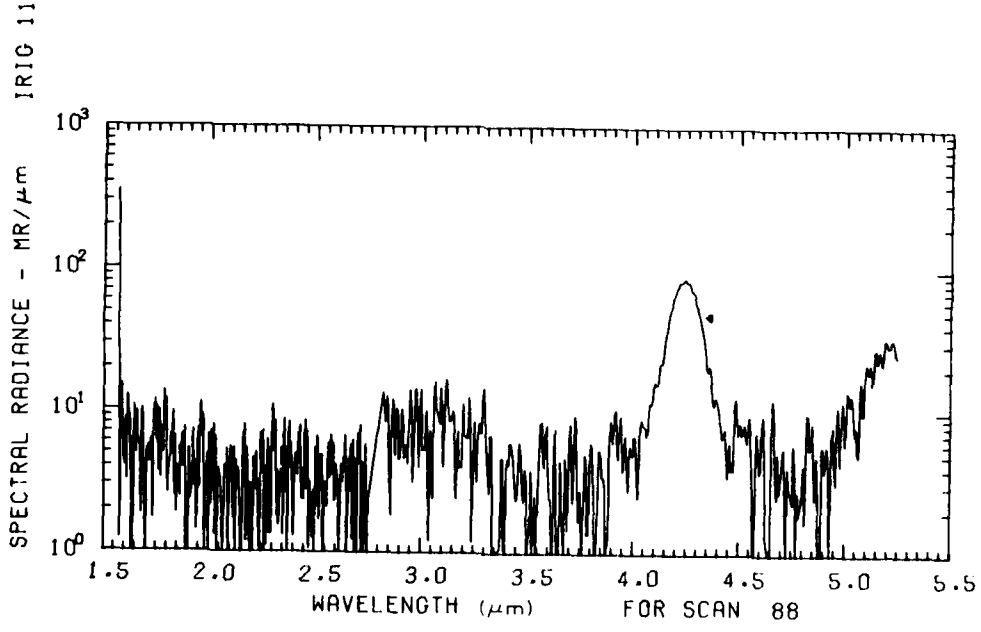

Figure 36. A10.205-2, Ascent, Low Gain – 97.26 km

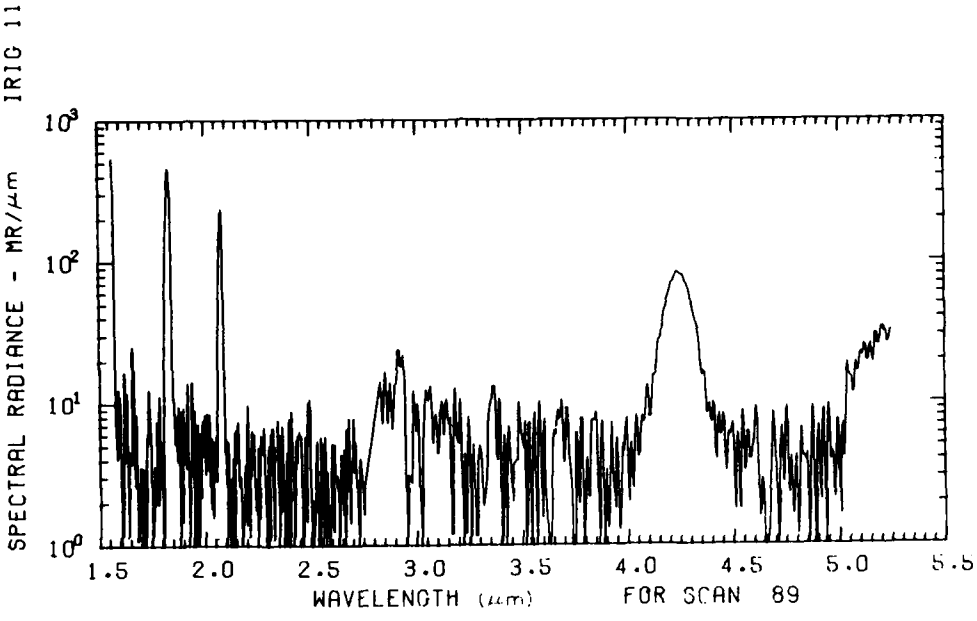

Figure B37. A10.205-2, Ascent, Low Gain – 97.97 km

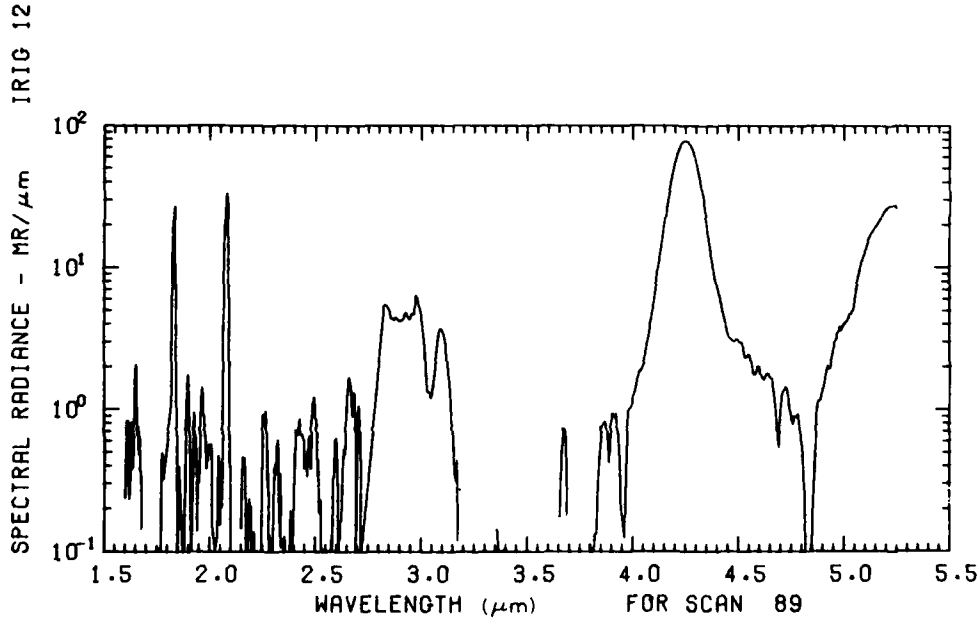

Figure B38. A10.205-2, Ascent, High Gain – 97.97 km

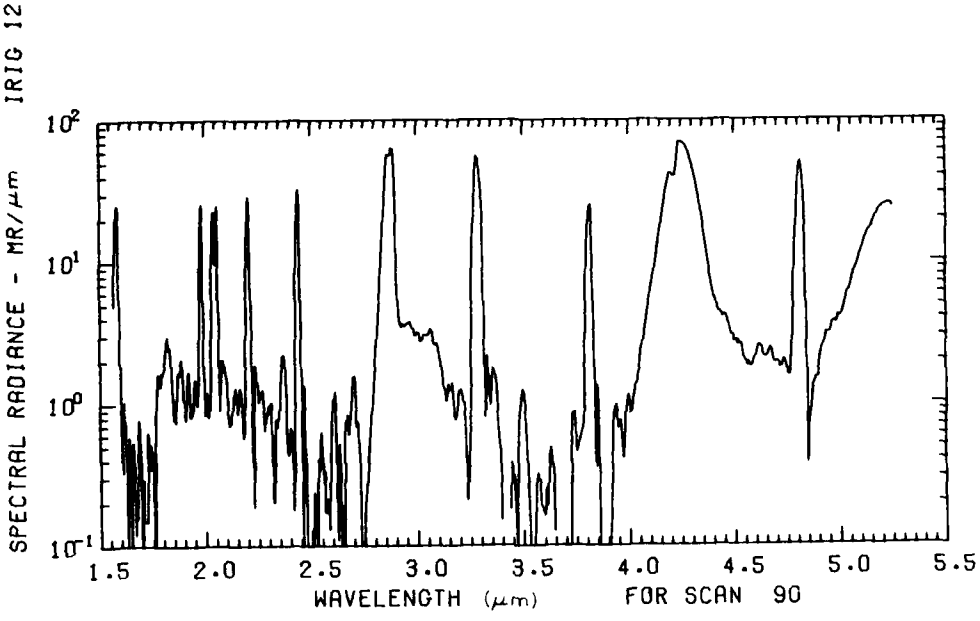

Figure B39. A10.205-2, Ascent, High Gain – 98.68 km

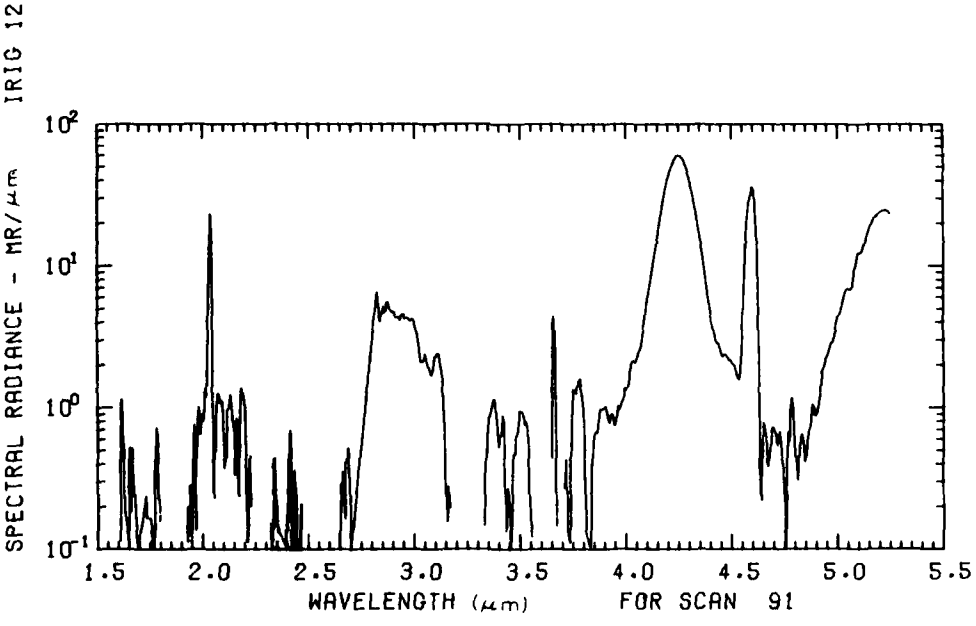

Figure B40. A10.205-2, Ascent, High Gain – 99.39 km

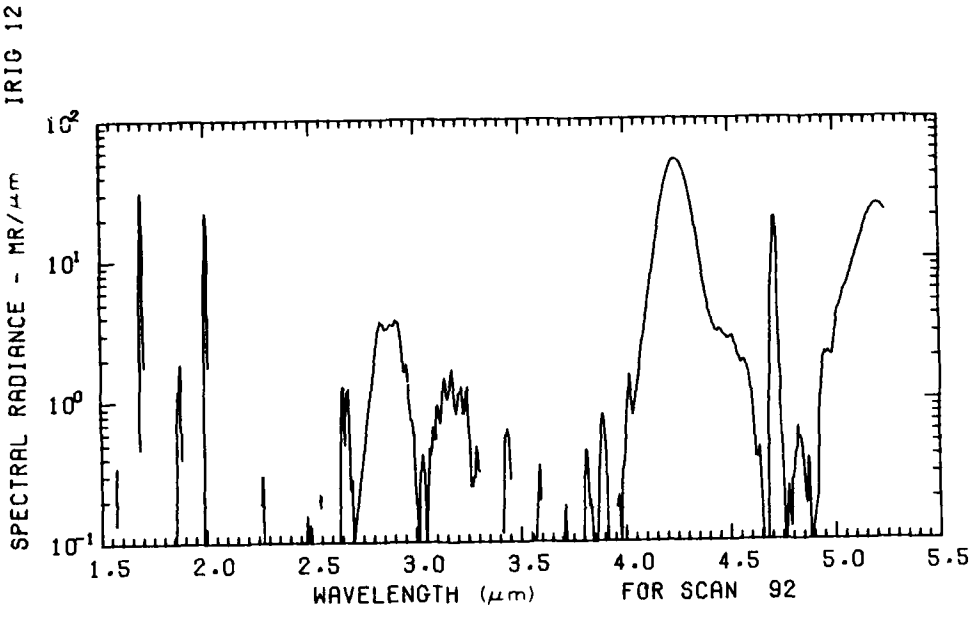

Figure B41. A10.205-2, Ascent, High Gain – 100.09 km

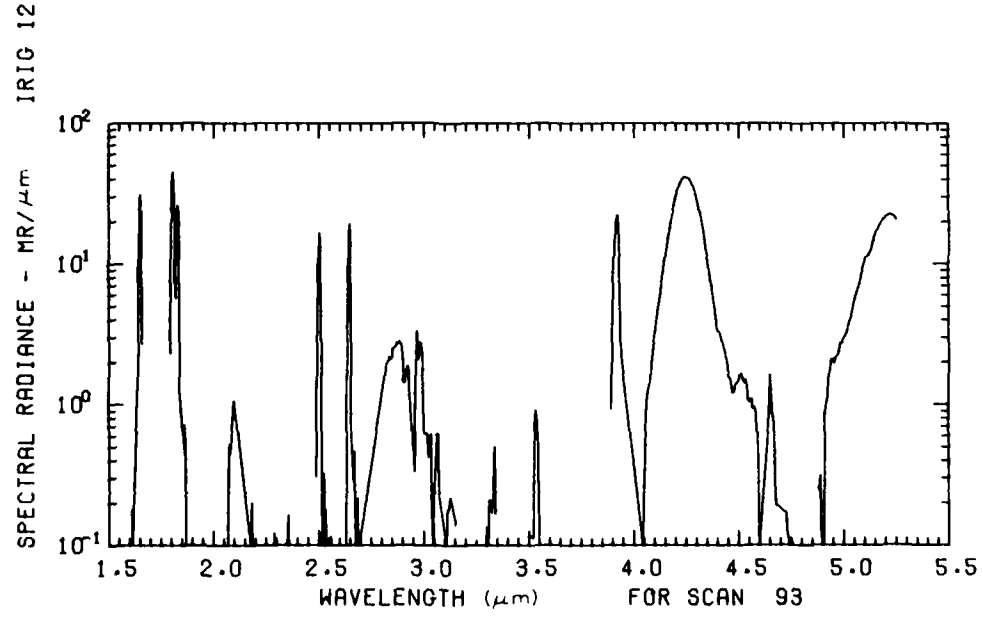

Figure B42. A10.205-2, Ascent, High Gain – 100.79 km

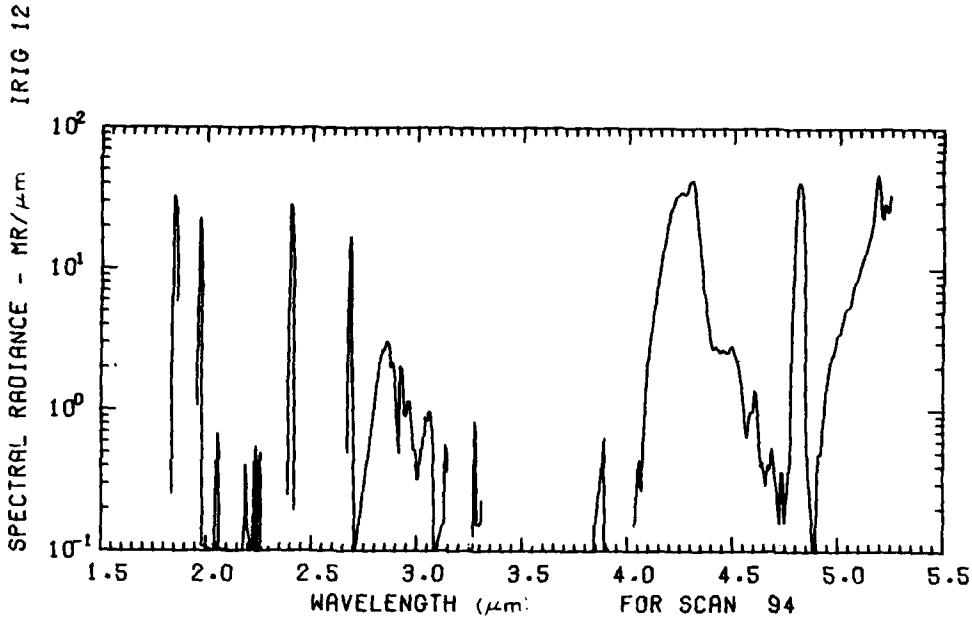

Figure B43. A10.205-2, Ascent, High Gain – 101.49 km

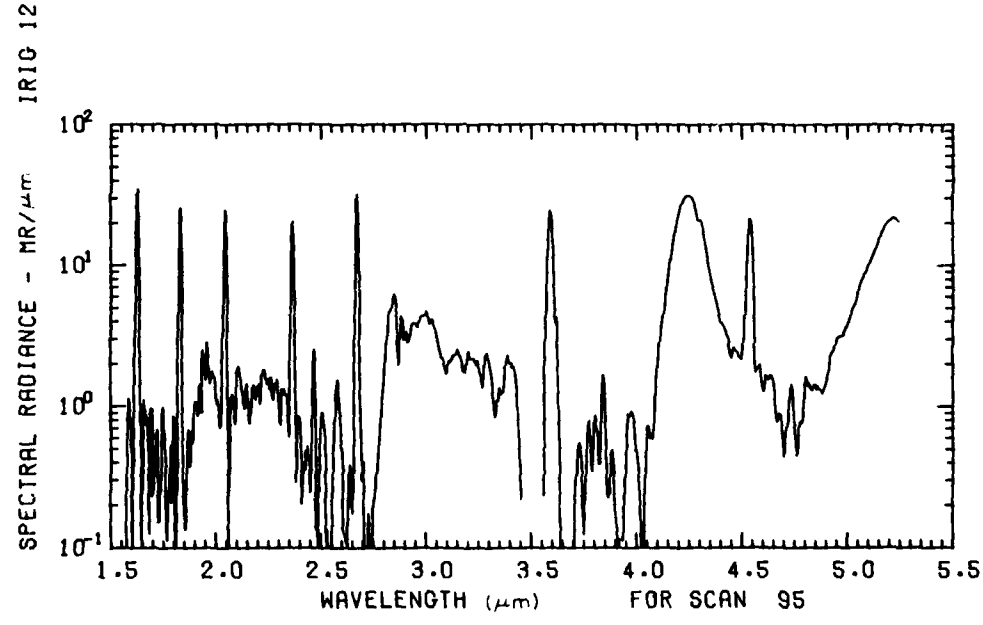

Figure B44. A10.205-2, Ascent, High Gain – 102.19 km

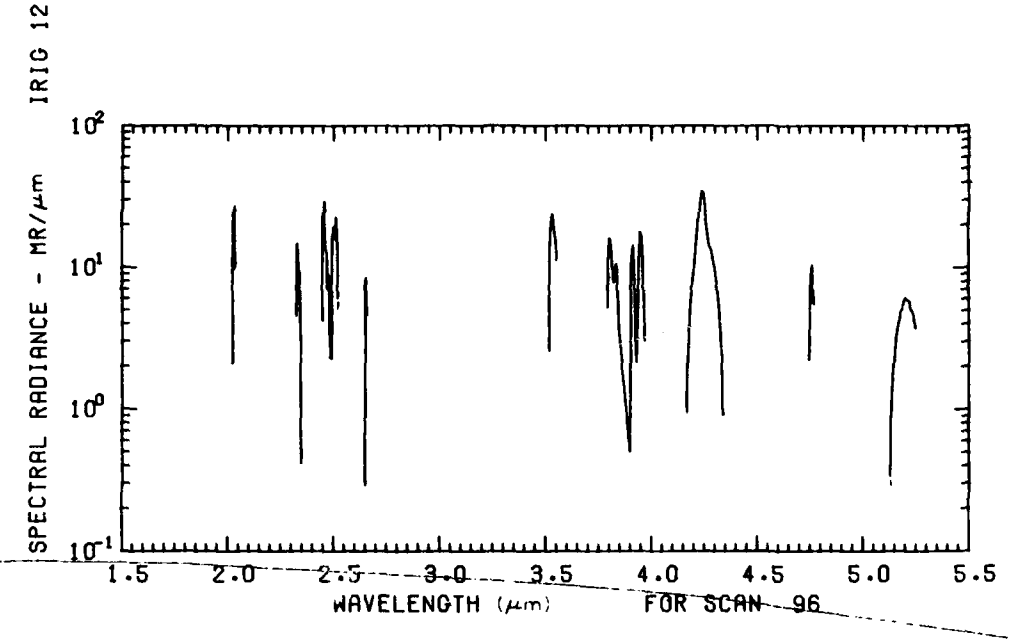

Figure B45. A10.205-2, Ascent, High Gain – 102.88 km

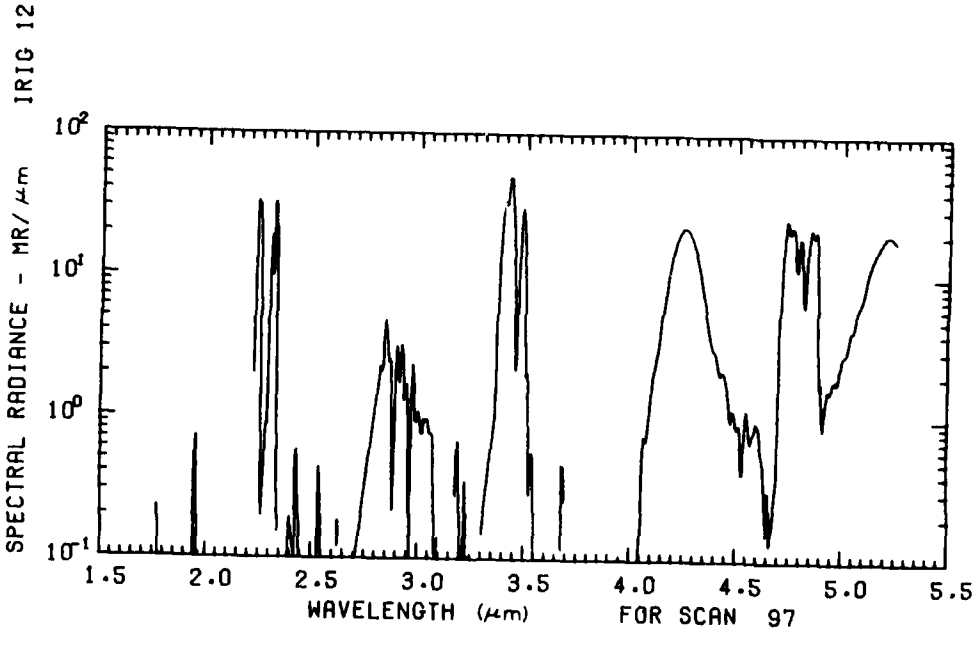

Figure B46. A10.205-2, Ascent, High Gain – 103.58 km

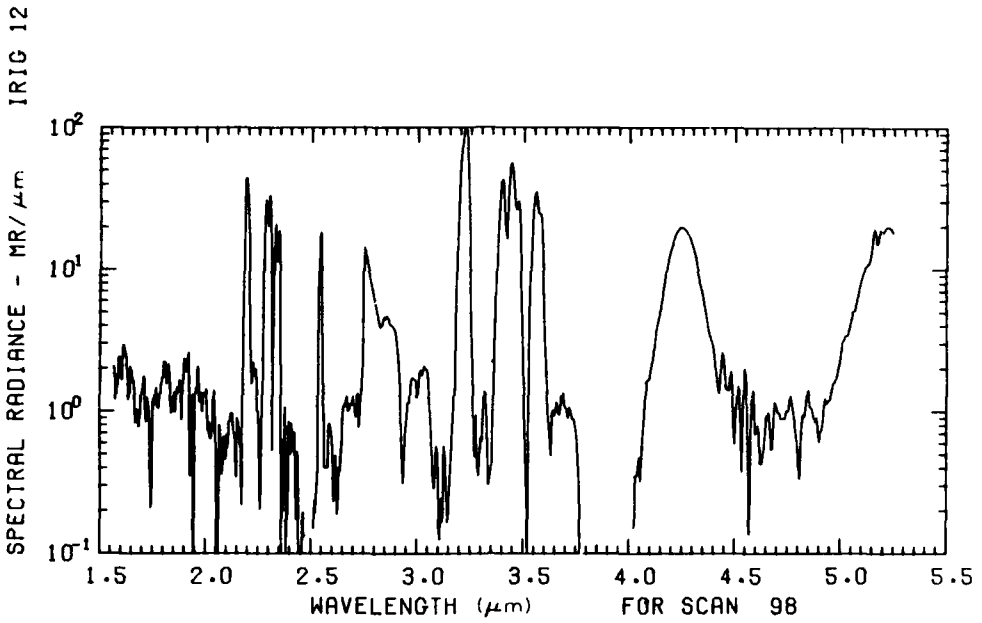

Figure B47. A10.205-2, Ascent, High Gain – 104.27 km

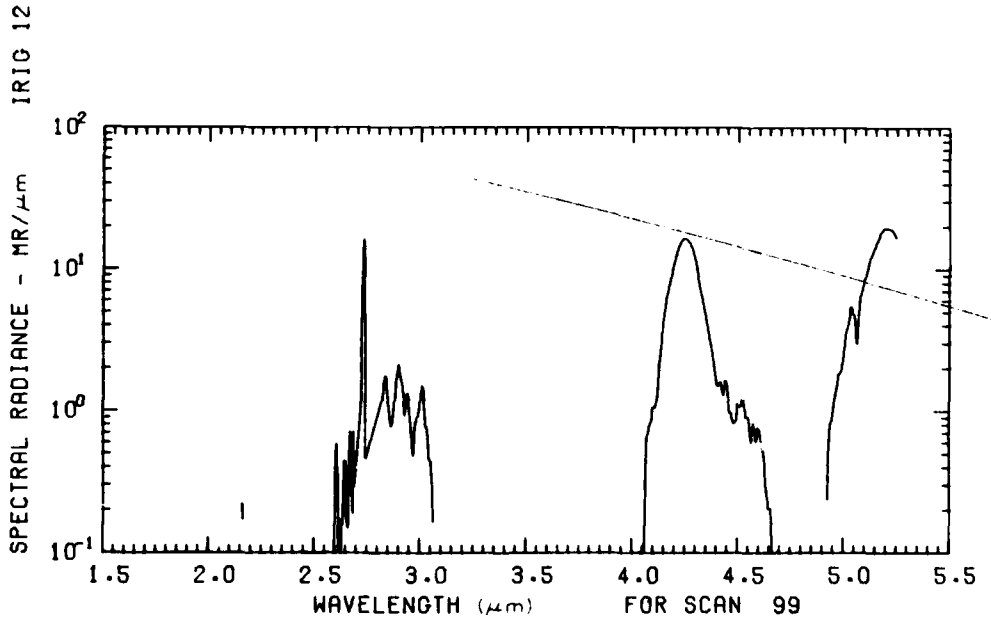

Figure B48. A10.205-2, Ascent, High Gain – 104.96 km

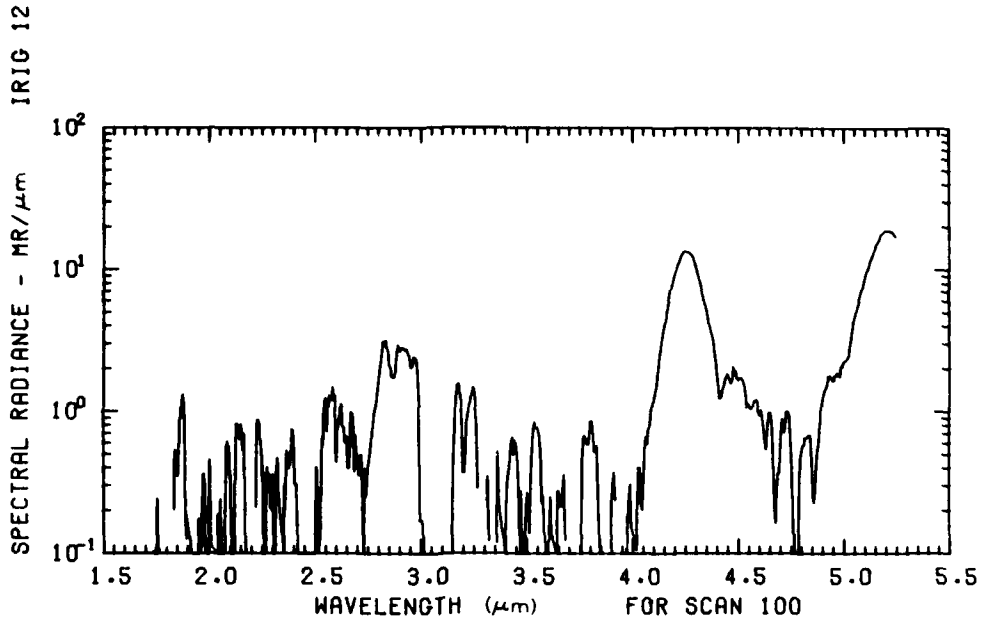

Figure B49. A10.205-2, Ascent, High Gain – 105.64 km

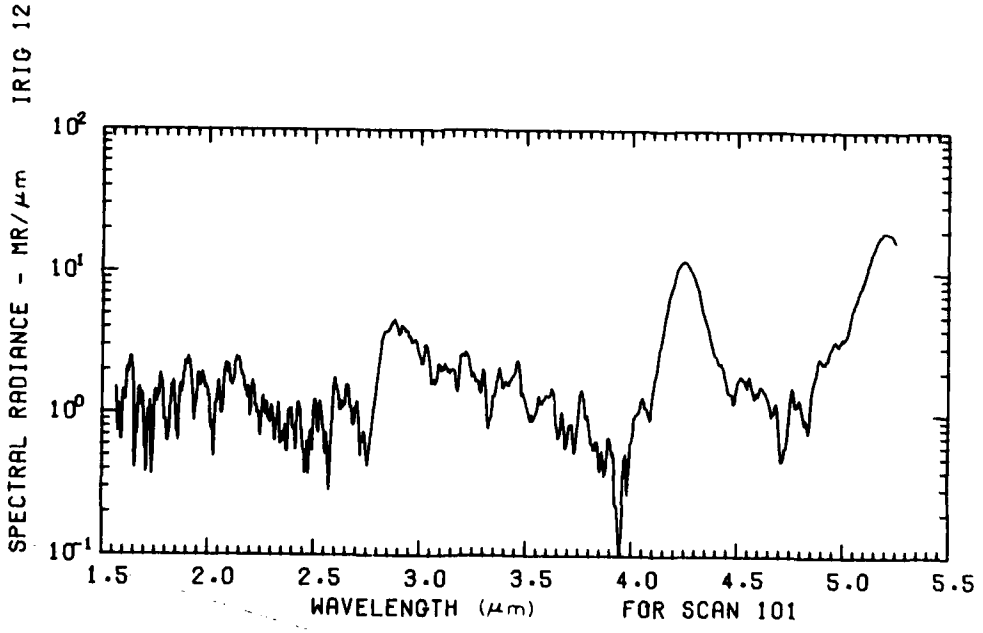

Figure B50. A10.205-2, Ascent, High Gain – 106.33 km

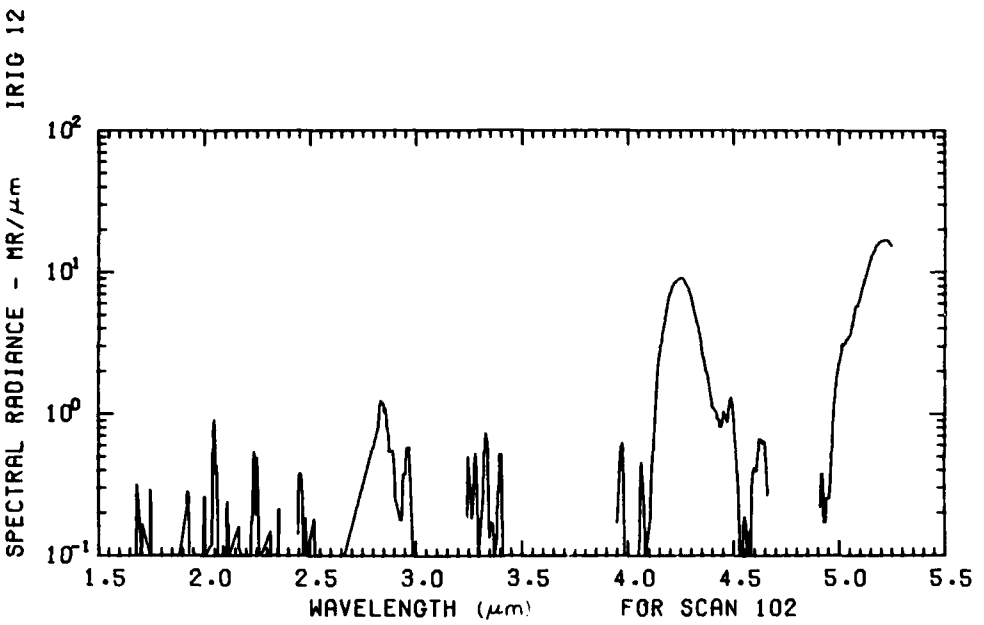

Figure B51. A10.205-2, Ascent, High Gain – 107.01 km

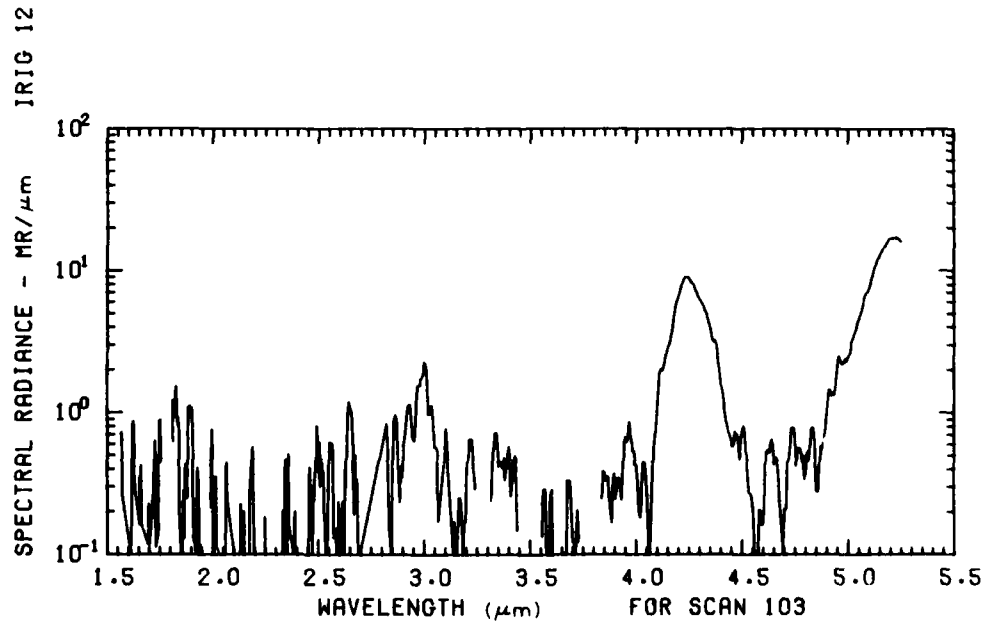

Figure B52. A10.205-2, Ascent, High Gain – 107.69 km

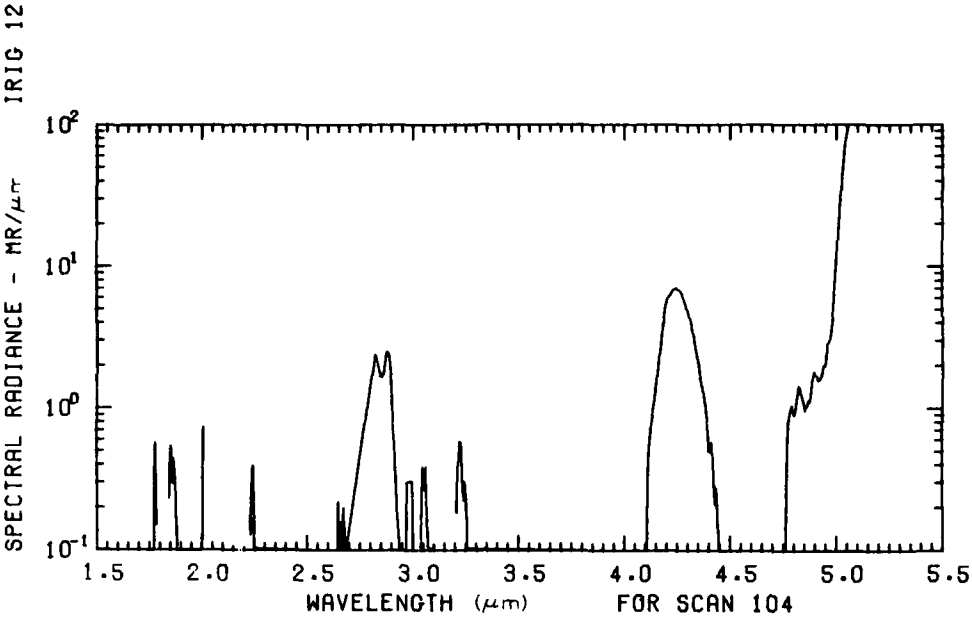

Figure B53. A10.205-2, Ascent, High Gain – 108.37 km

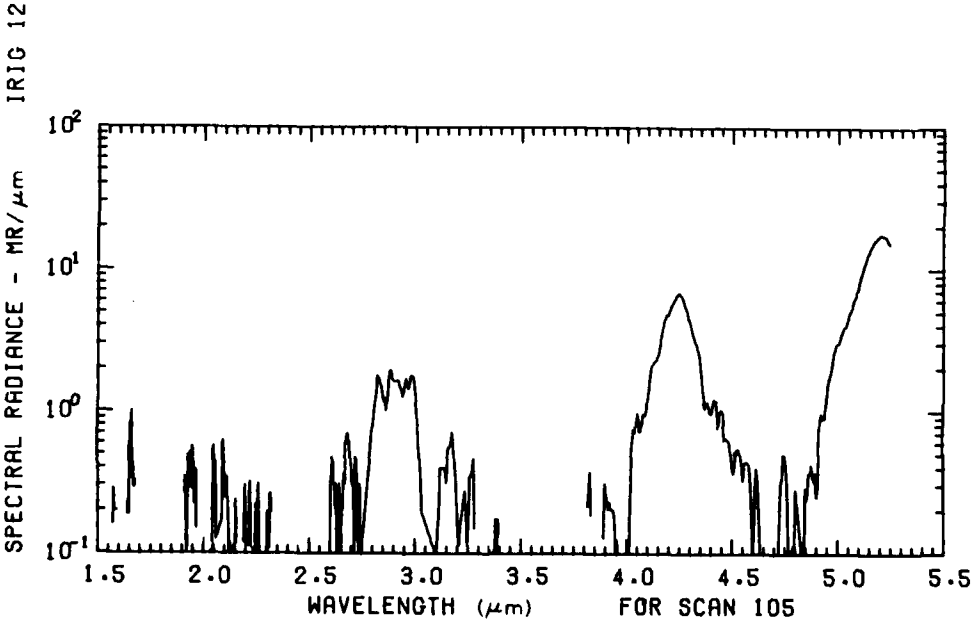

Figure B54. A10.205-2, Ascent, High Gain – 109.04 km

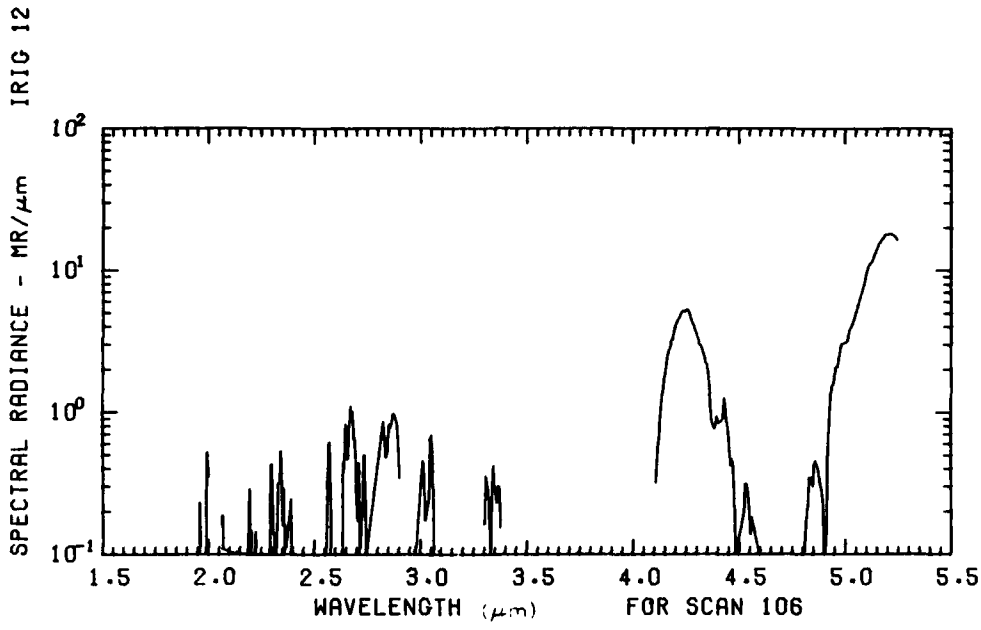

Figure B55. A10.205-2, Ascent, High Gain – 109.71 km

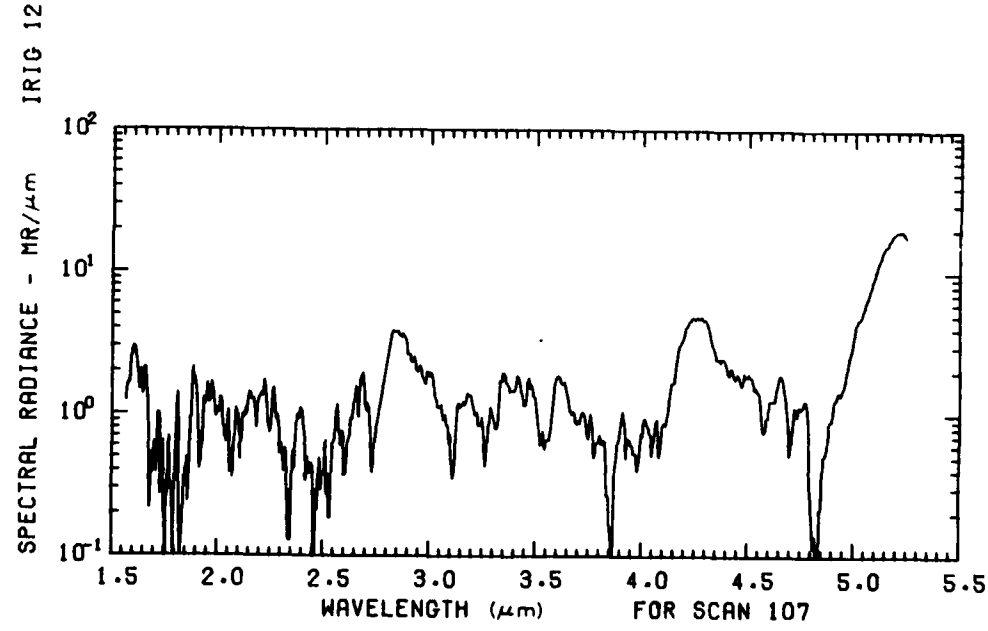

Figure B56. A10.205-2, Ascent, High Gain – 110.38 km

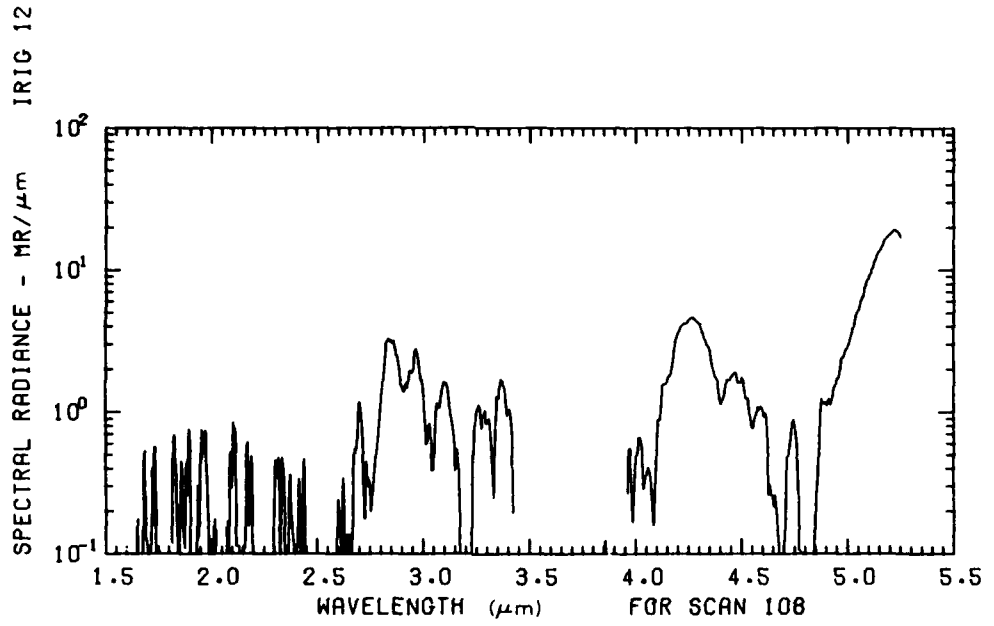

Figure B57. A10.205-2, Ascent, High Gain – 111.05 km

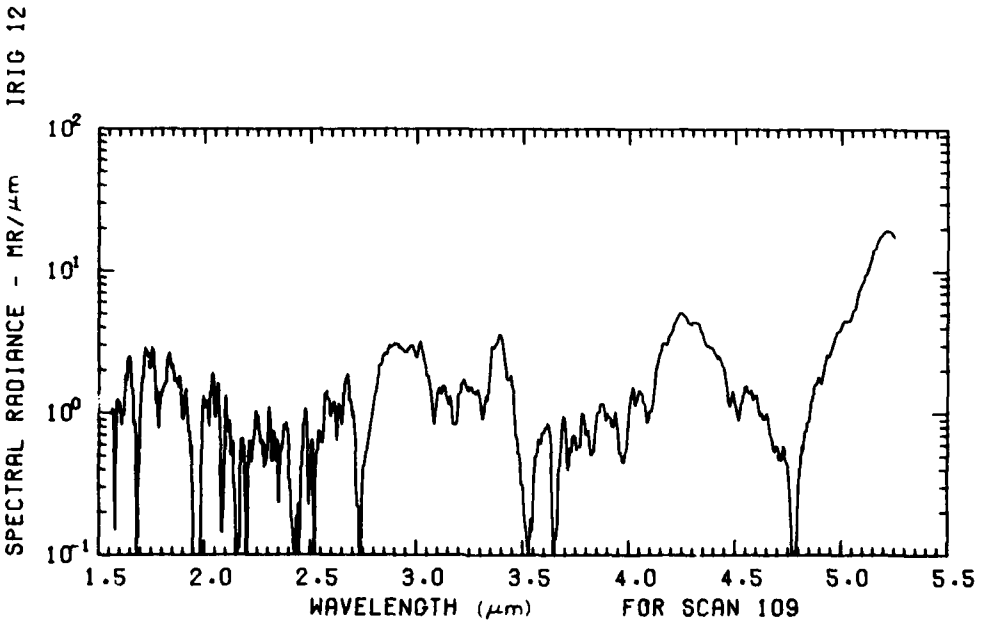

Figure B58. A10.205-2, Ascent, High Gain – 111.72 km

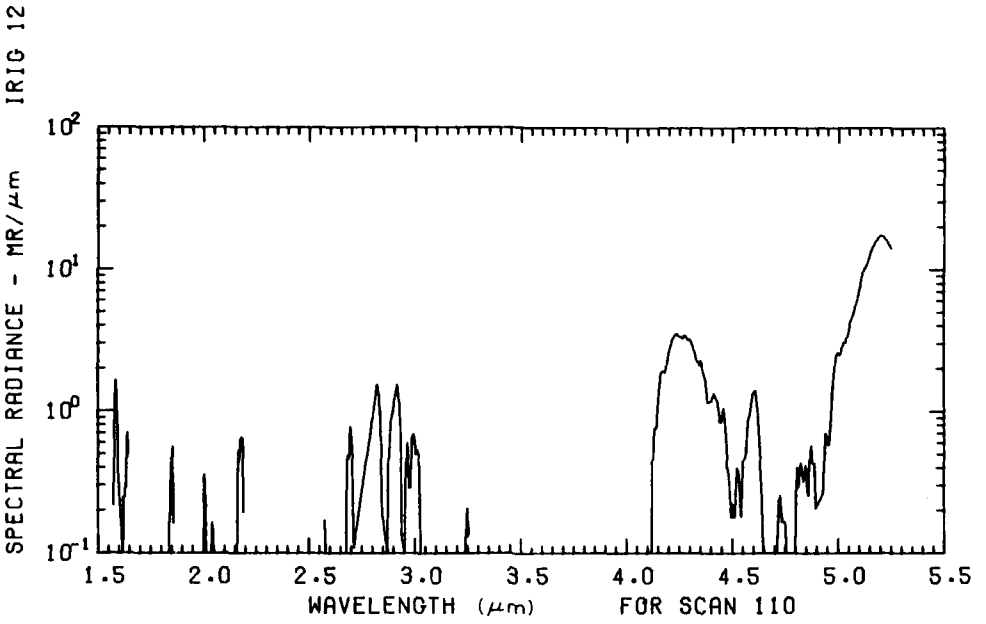

Figure B59. A10.205-2, Ascent, High Gain – 112.38 km

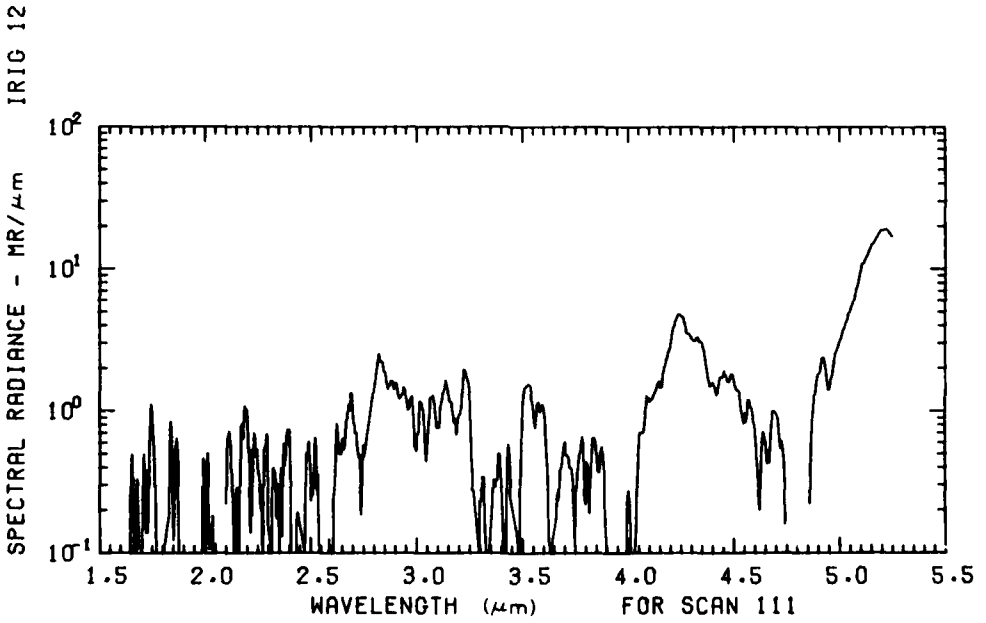

Figure B60. A10.205-2, Ascent, High Gain – 113.05 km

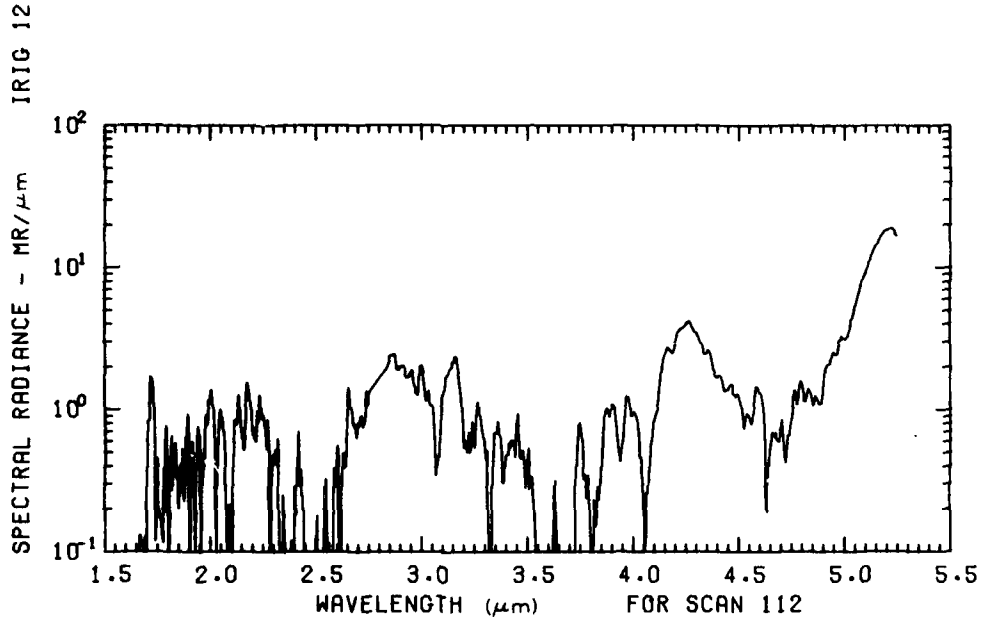

Figure B61. A10.205-2, Ascent, High Gain – 113.71 km

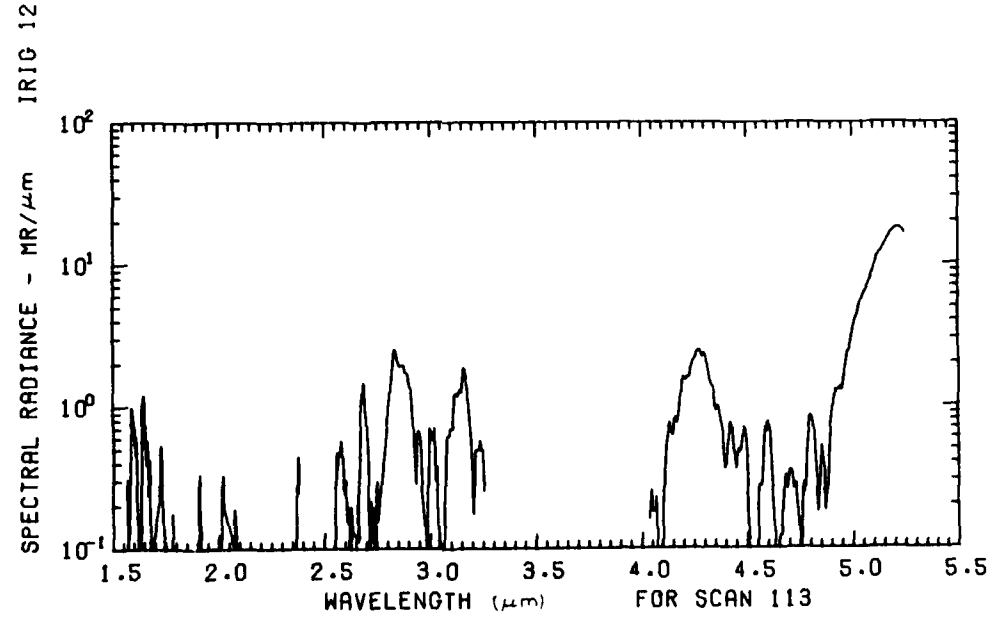

Figure B62. A10.205-2, Ascent, High Gain – 114.36 km

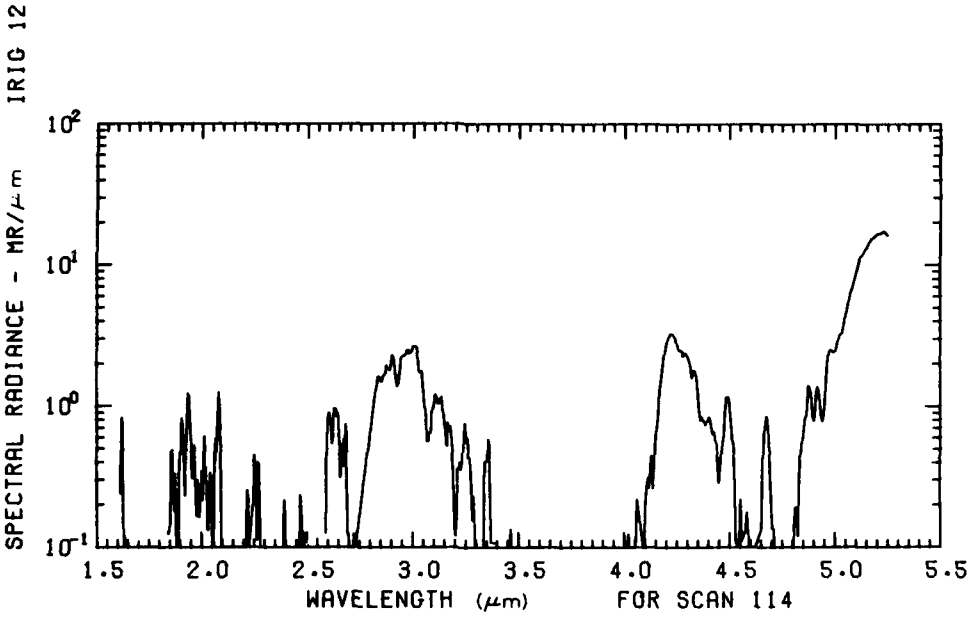

Figure B63. A10.205-2, Ascent, High Gain – 115.02 km

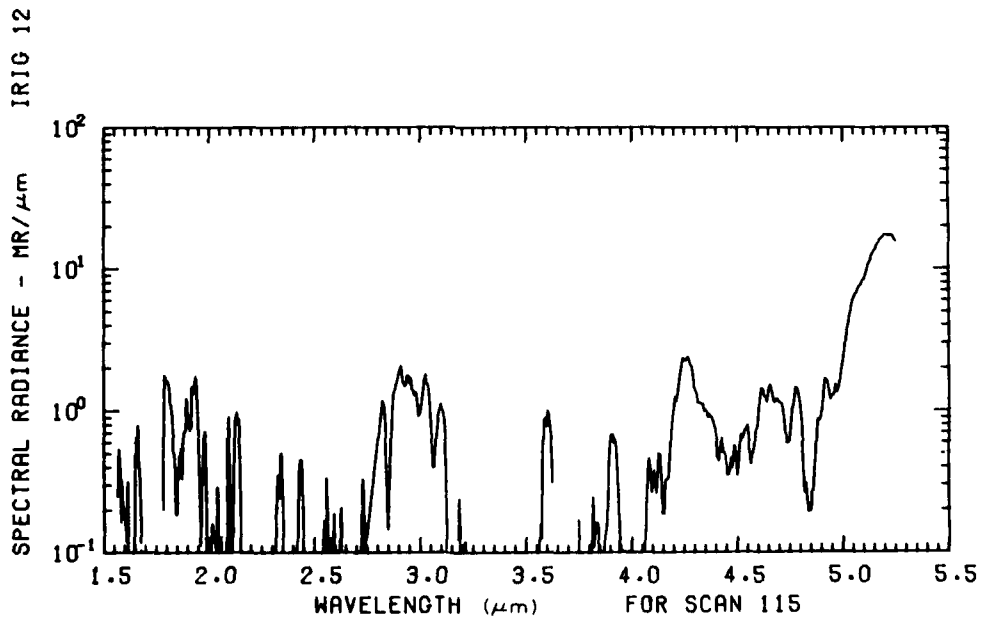

Figure B64. A10.205-2, Ascent, High Gain – 115.67 km

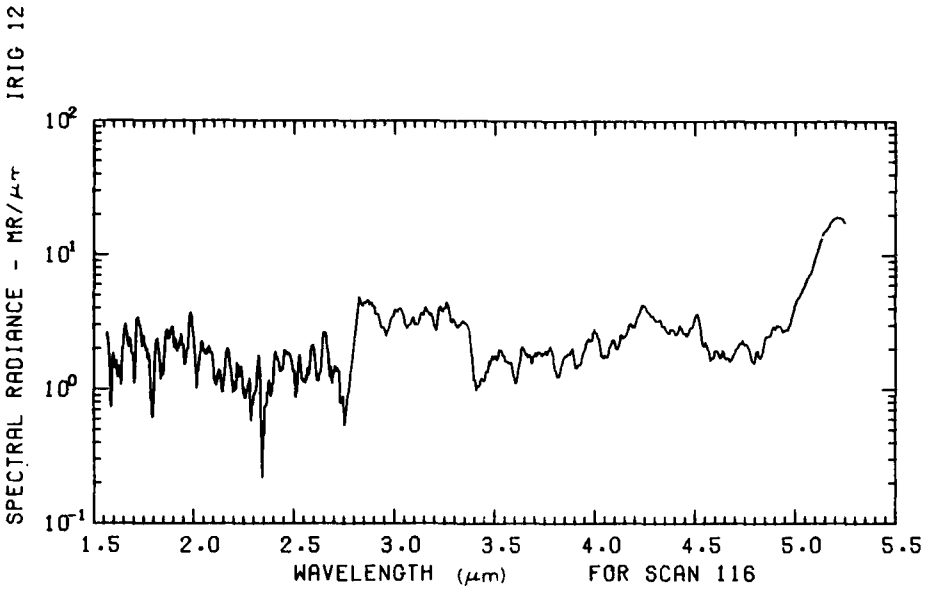

Figure B65. A10.205-2, Ascent, High Gain – 116.32 km

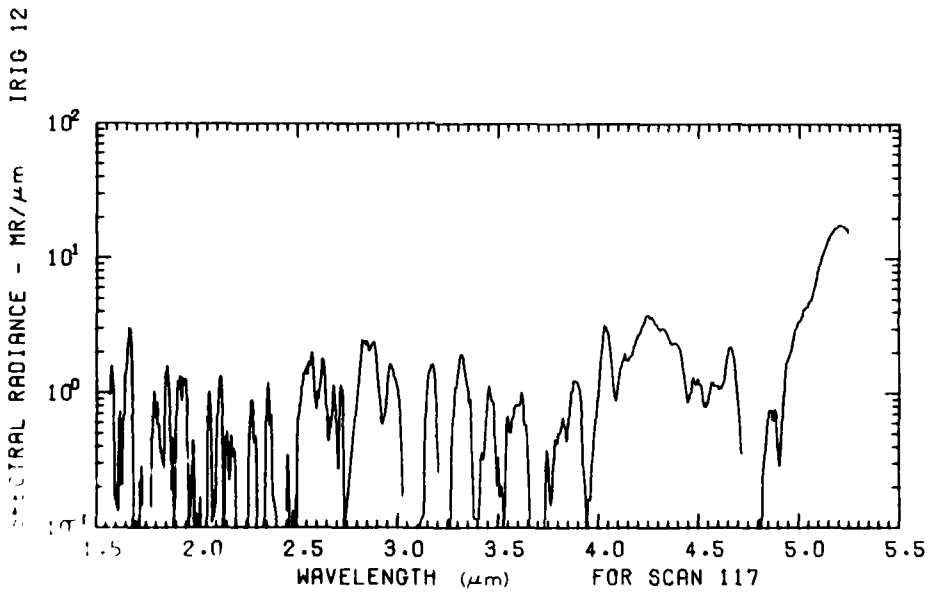

Figure B66. A10.205-2, Ascent, High Gain – 116.97 km

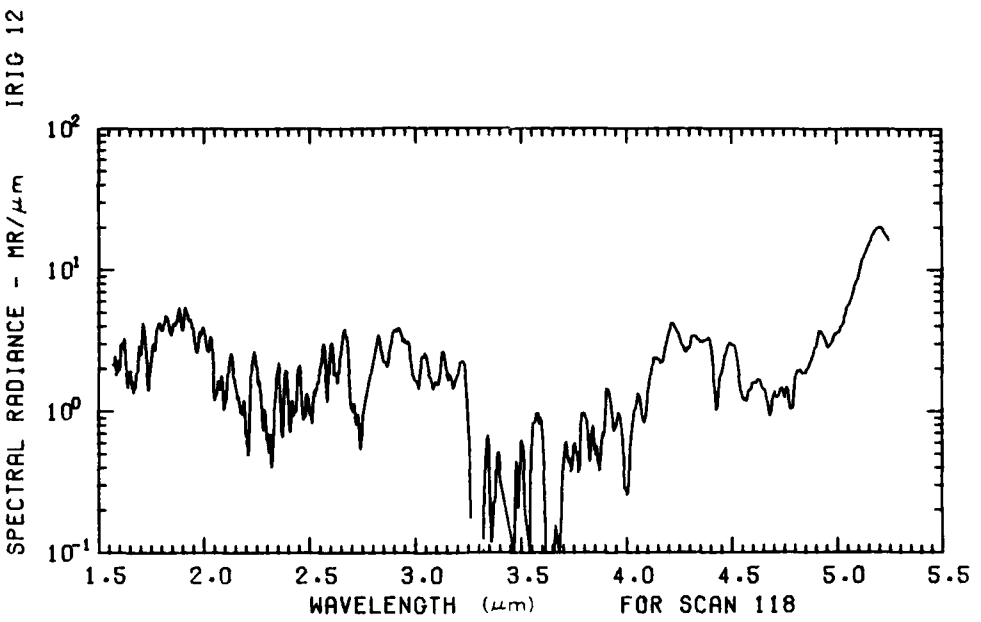

Figure B67. A10.205-2, Ascent, High Gain – 117.62 km

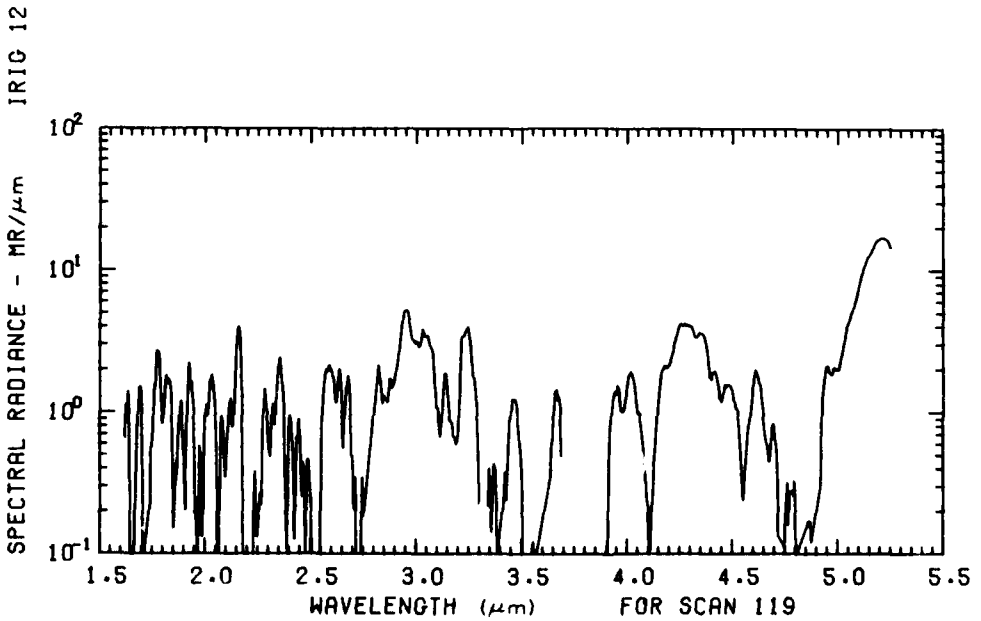

Figure B68. A10.205-2, Ascent, High Gain – 118.26 km

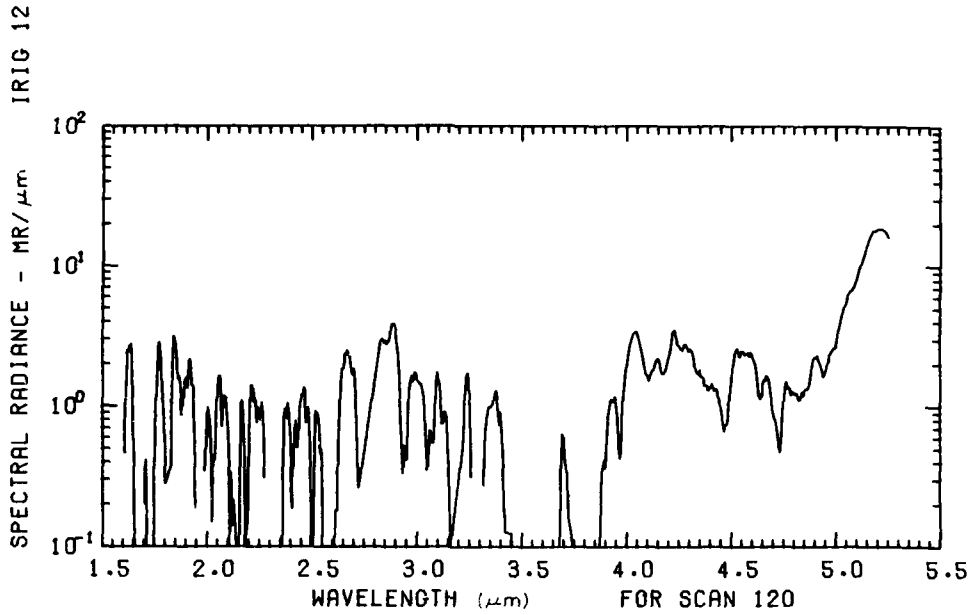

Figure B69. A10.205-2, Ascent, High Gain – 118.80 km

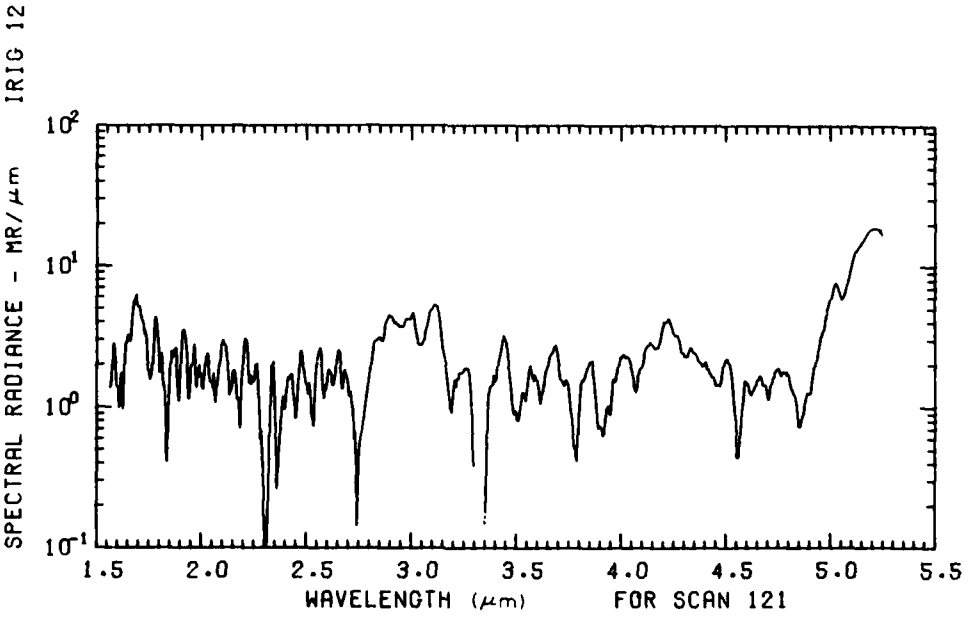

Figure B70. A10.205-2, Ascent, High Gain – 119.54 km

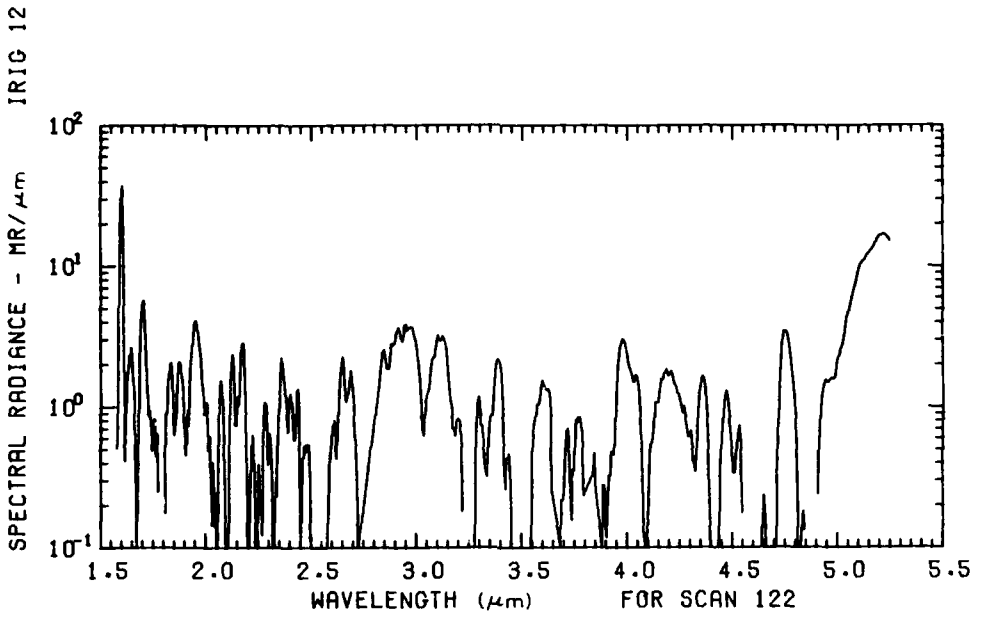

Figure B71. A10.205-2, Ascent, High Gain – 120.18 km

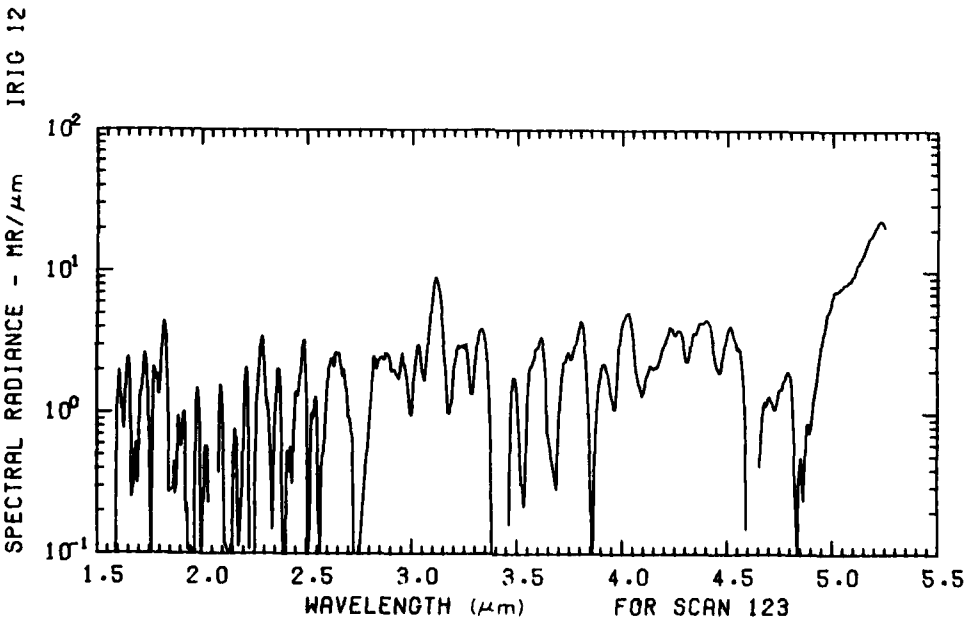

Figure B72. A10.205-2, Ascent, High Gain – 120.82 km

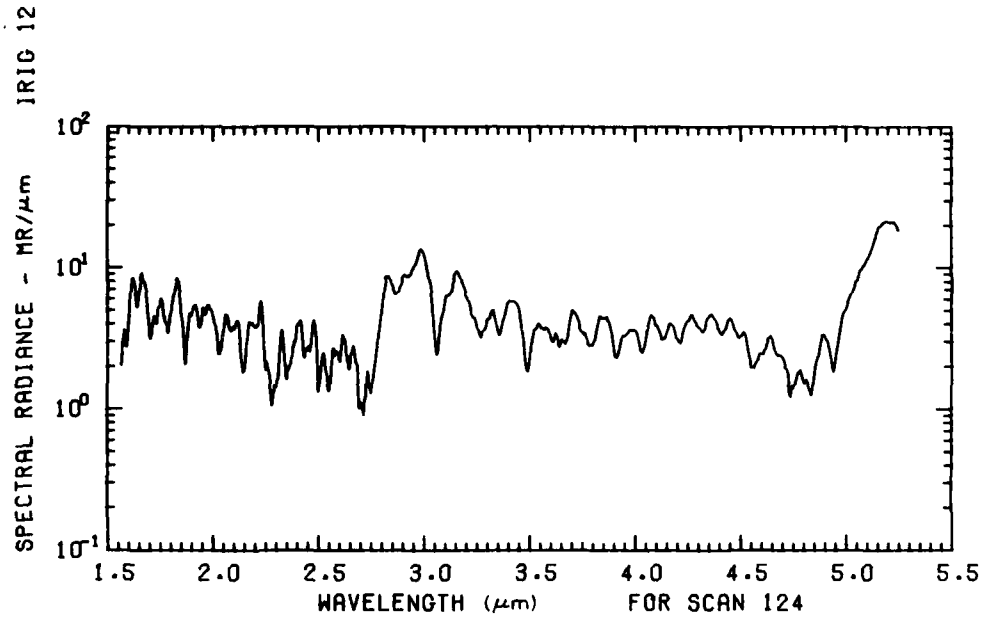

Figure B73. A10.205-2, Ascent, High Gain – 121.45 km

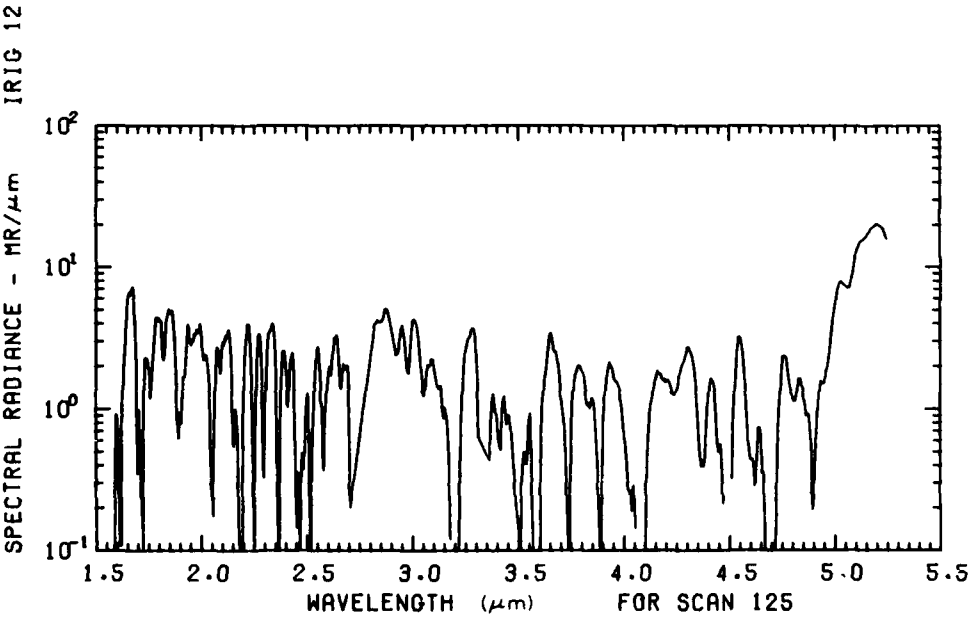

Figure B74. A10.205-2, Ascent, High Gain – 122.08 km

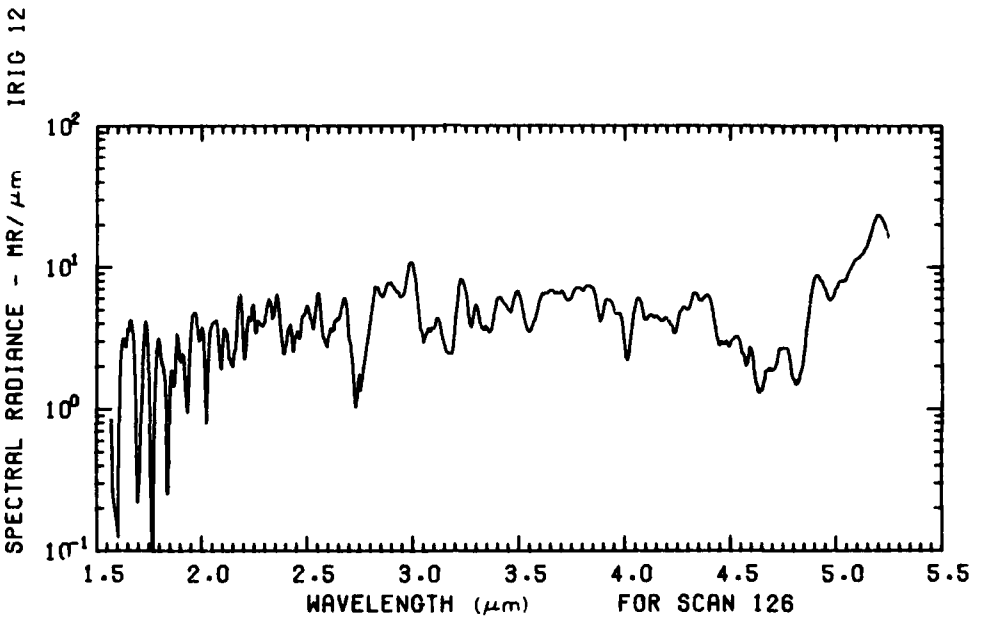

Figure B75. A10.205-2, Ascent, High Gain – 122.71 km

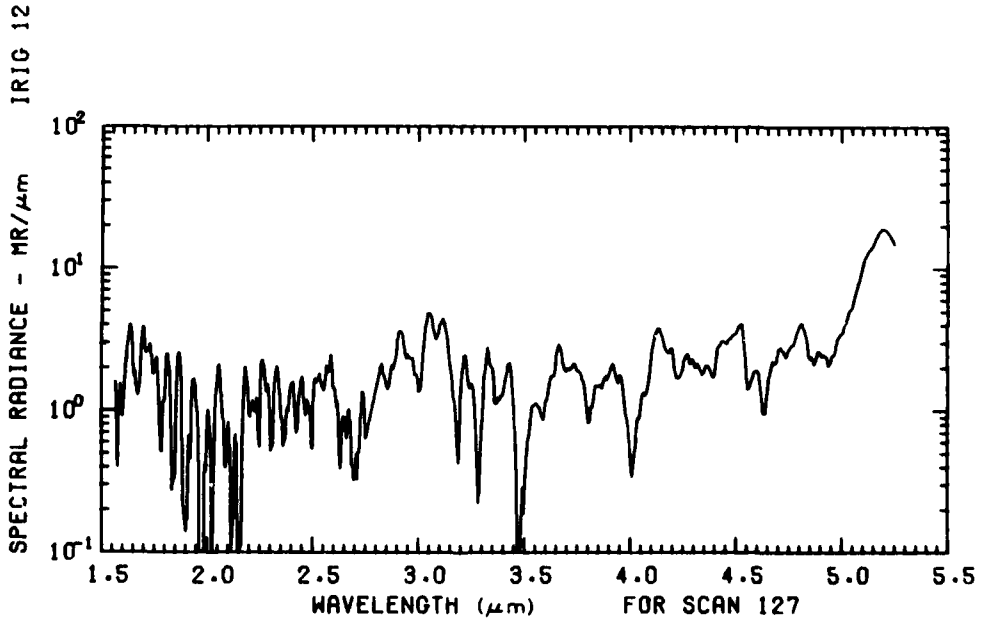

Figure B76. A10.205-2, Ascent, High Gain – 123.34 km

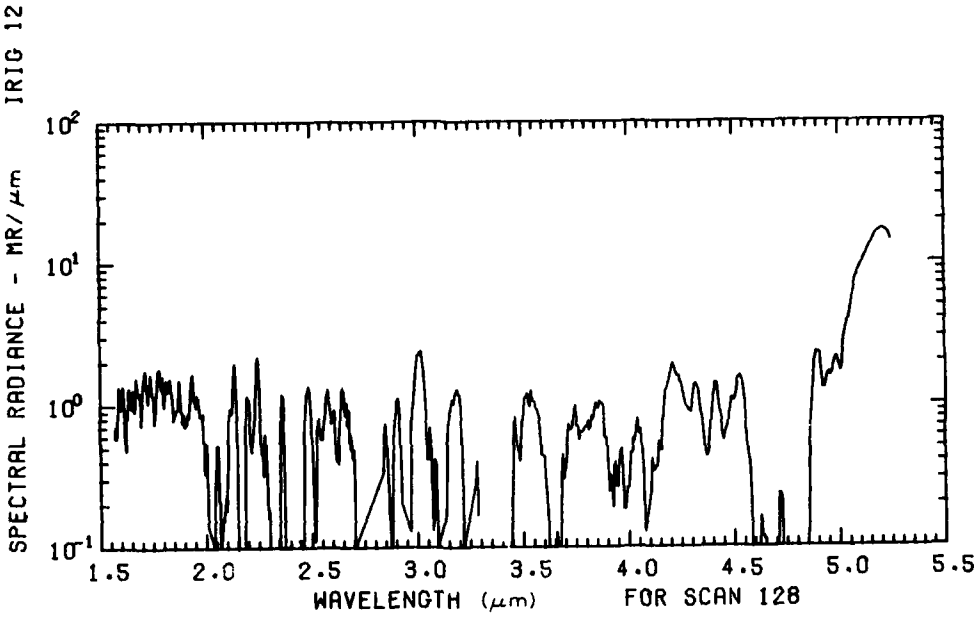

Figure B77. A10.205-2, Ascent, High Gain – 123.96 km

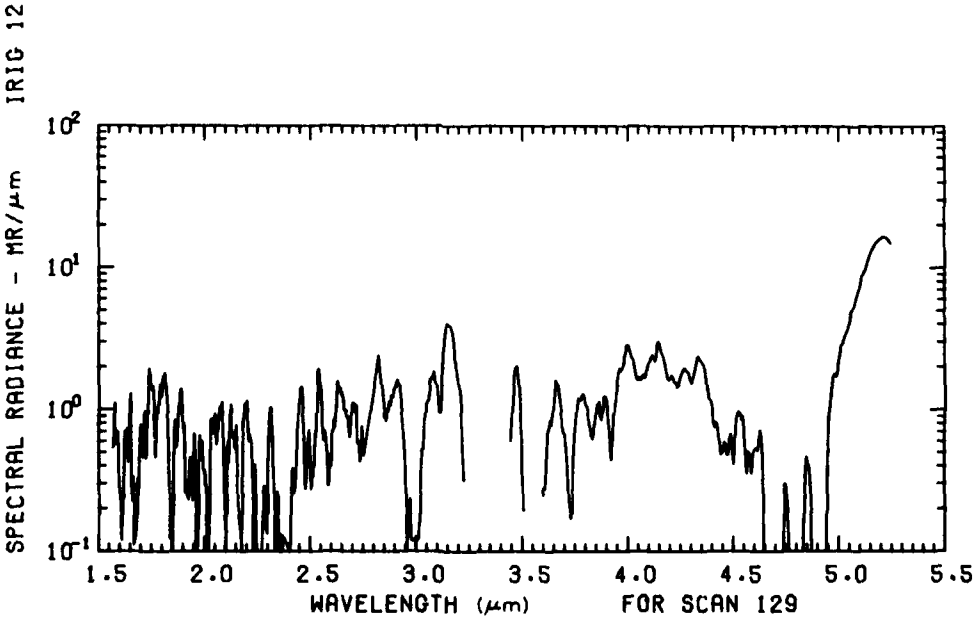

Figure B78. A10.205-2, Ascent, High Gain – 124.58 km

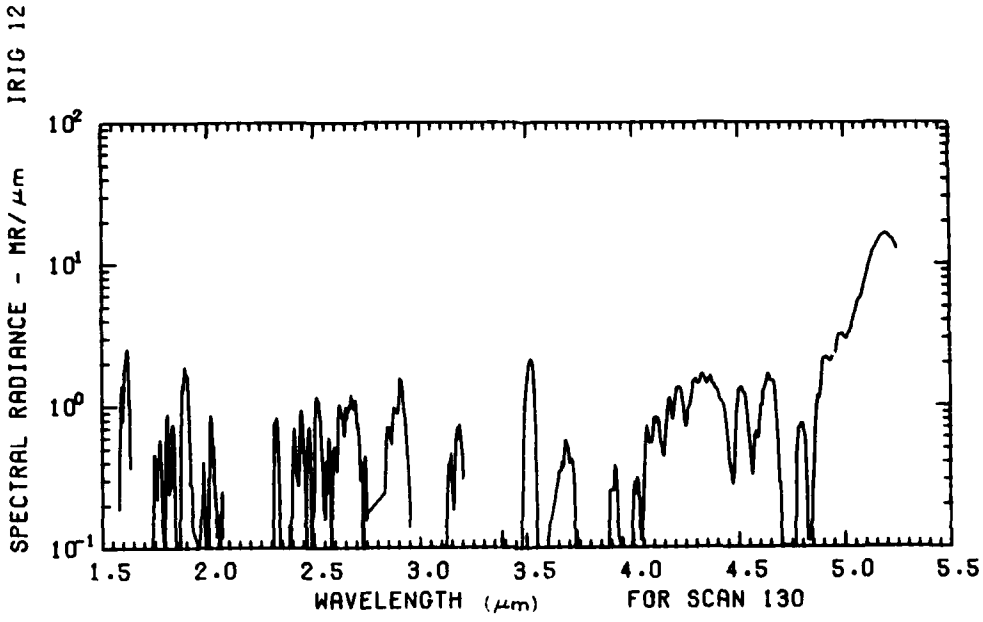

Figure B79. A10.205-2, Ascent, High Gain – 125.20 km

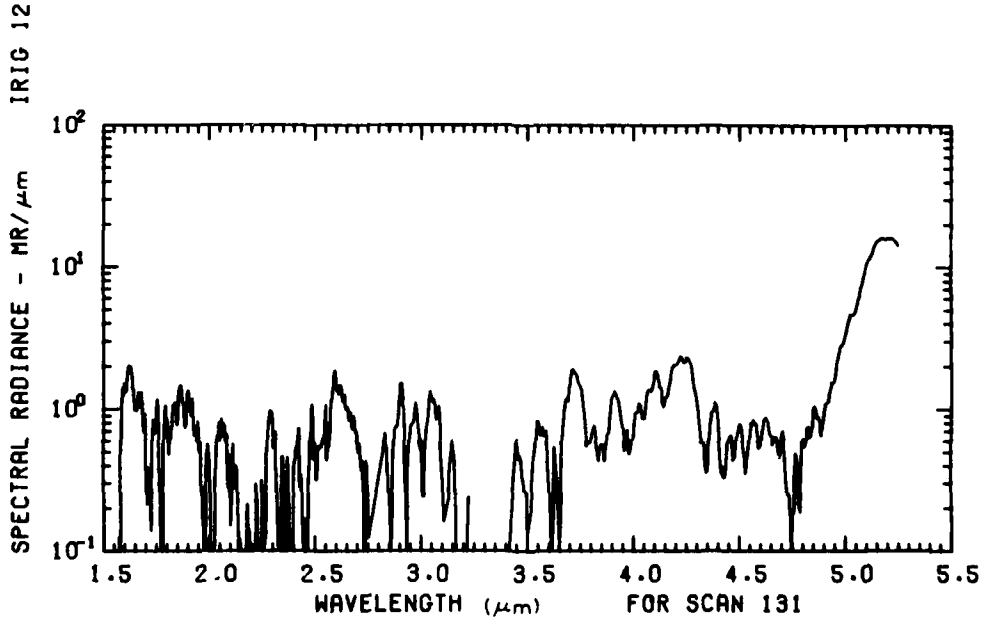

Figure B80. A10.205-2, Ascent, High Gain – 125.82 km

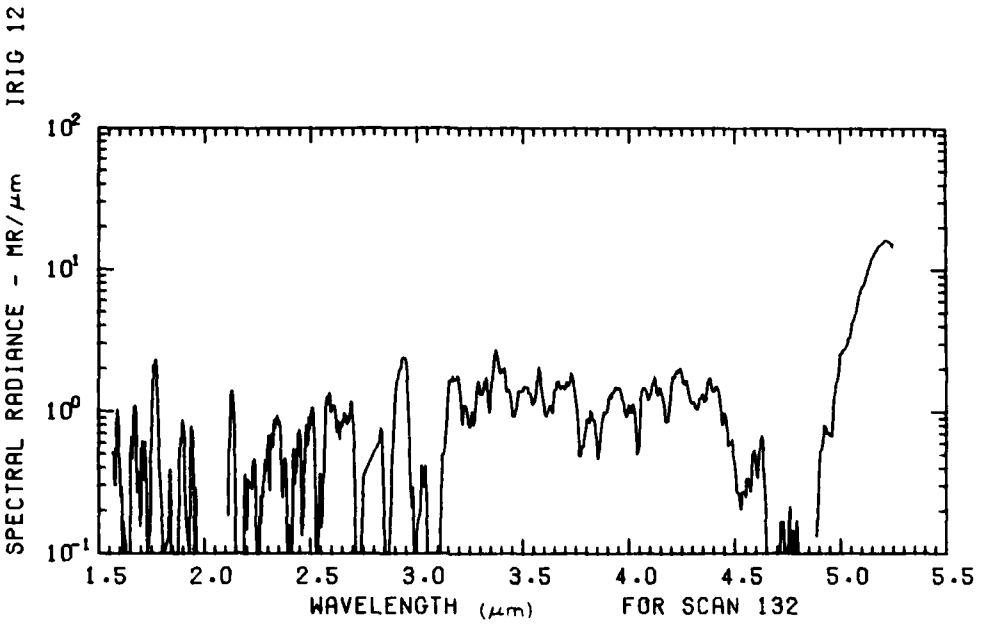

Figure B81. A10.205-2, Ascent, High Gain – 126.44 km

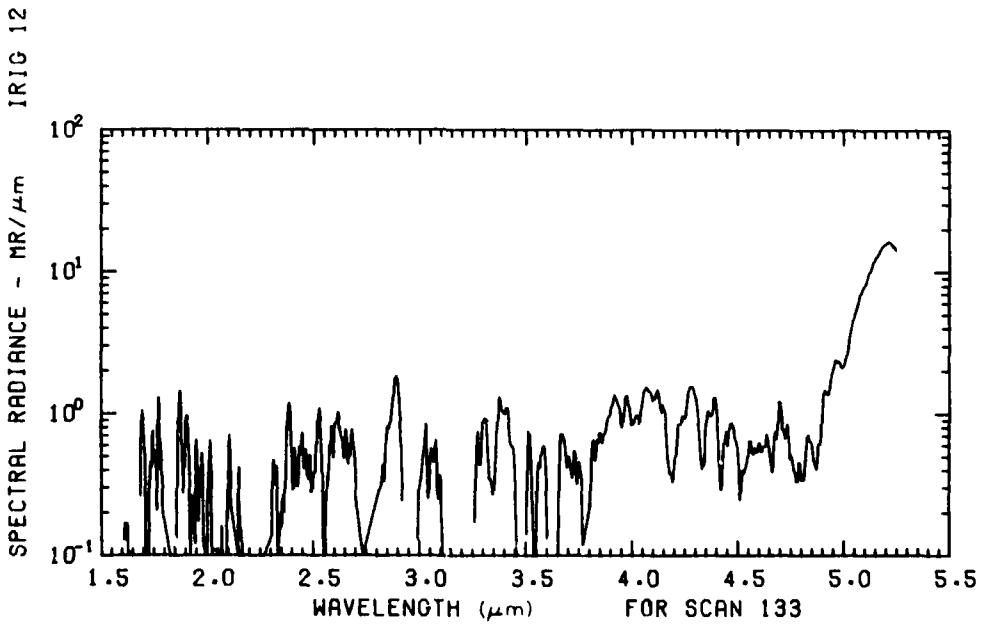

Figure B82. A10.205-2, Ascent, High Gain – 127.05 km

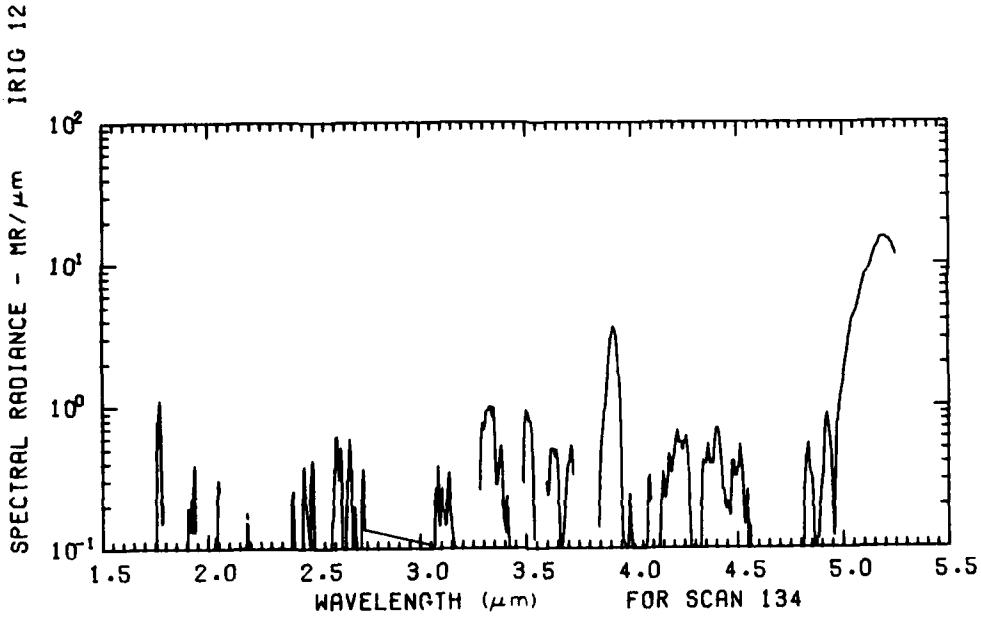

Figure B83. A10.205-2, Ascent, High Gain – 127.66 km

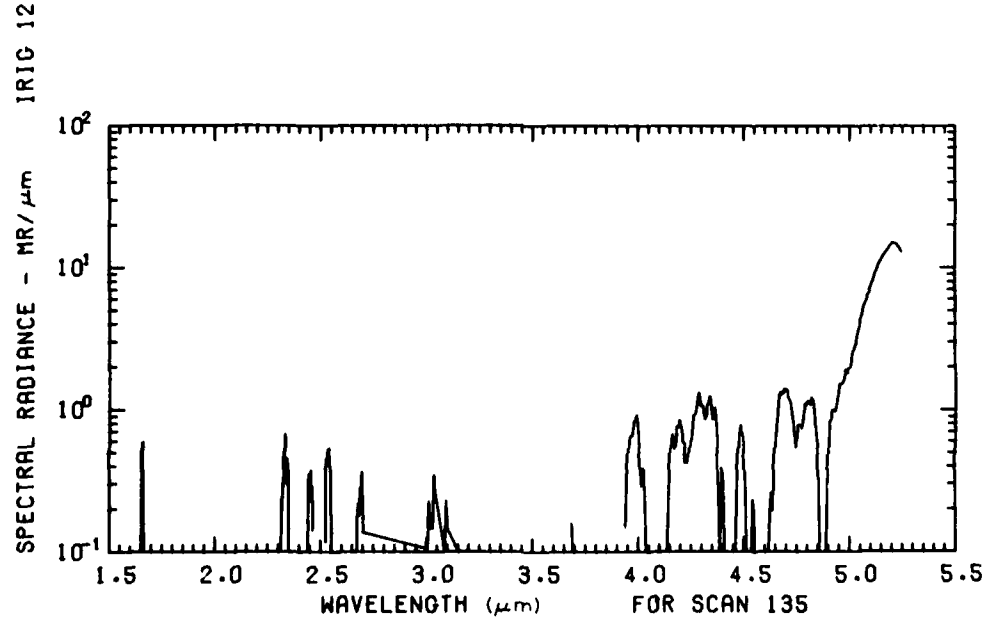

Figure B84. A10.205-2, Ascent, High Gain – 128.27 km

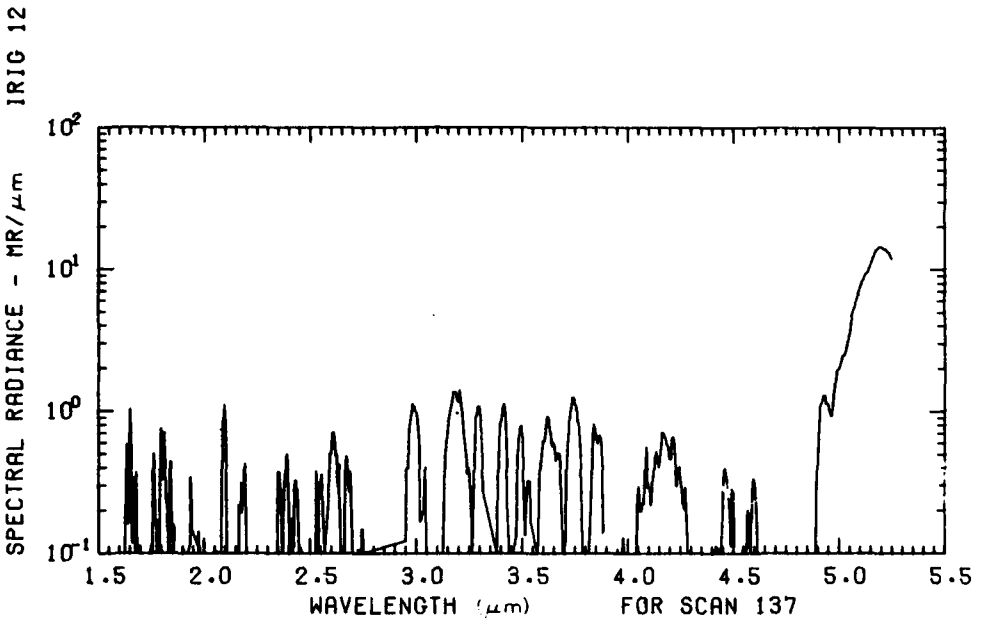

Figure B85. A10.205-2, Ascent, High Gain – 129.48 km

☆ U. S. GOVERNMENT PRINTING OFFICE: 1977--700-031--130

Distribution List

DEPARTMENT OF DEFENSE

Director
Defense Advanced Rsch Proj Agency
Architect Building
1400 Wilson Blvd.
Arlington, VA 22209

01 CY Attn: LTC W.A. Whitaker
01 CY Attn: STO J. Jenney
01 CY Attn: Maj. Gregory Canavan

Defense Documentation Center
Cameron Station
Alexandria, VA 22314

(12 copies if open publication, otherwise 2 copies)
12 CY Attn: TC

Director
Defense Nuclear Agency
Washington, DC 20305

03 CY Attn: STTL Tech Library
01 CY Attn: STST Archives
03 CY Attn: RAAE Charles A. Blank
01 CY Attn: RAAE Gordon Sopar
01 CY Attn: RAAE Maj. John Clark

DEPARTMENT OF DEFENSE (Continued)

Director of Defense RSCH & Engineering
Department of Defense
Washington, DC 20301

01 CY Attn: DD/S&SS Daniel Brockway
01 CY Attn: DDS&SS Richard S. Ruffine

Commander
Field Command
Defense Nuclear Agency
Kirtland AFB, NM 87115

01 CY Attn: FCPR

Chief
Livermore Division Fld Command DNA
Lawrence Livermore Laboratory
P.O. Box 808
Livermore, CA 94550

01 CY Attn: FCPRL

DEPARTMENT OF ARMY

Commander/Director
Atmospheric Sciences Laboratory
U.S. Army Electronics Command
White Sands Missile Range, NM 88002

01 CY Attn: DRSEL-BL-SY-S F.E. Niles
01 CY Attn: E. Butterfield DRSEL-BL-SY-R

Commander
Harry Diamond Laboratories
2800 Powder Mill Road
Adelphi, MD 20783
(CNWDI-INNER Envelope: Attn: DRXDO-RBH)

02 CY Attn: DRXDO-NP

Commander
U.S. Army Nuclear Agency
Fort Bliss, TX 79916

01 CY Attn: ATCA-NAW J. Berberet

DEPARTMENT OF NAVY

Chief of Naval Research
Navy Department
Arlington, VA 22217

01 CY Attn: Code 427 CDR Ronald J. Oberle

DEPARTMENT OF NAVY (Continued)

Commander
Naval Electronics Laboratory Center
San Diego, CA 92152

01 CY Attn: Code 2200 1 Verne E. Hildebrand
01 CY Attn: Code 2200 Ilan Rothmuller

Director
Naval Research Laboratory
Washington, DC 20375

01 CY Attn: Douglas P. McNutt
01 CY Attn: Code 7127 Charles Y. Johnson
01 CY Attn: Code 2027 Tech Lib
01 CY Attn: Code 7700 Timothy P. Coffey
01 CY Attn: Code 7701 Jack D. Brown
01 CY Attn: Code 7750 Darrell F. Strobel
01 CY Attn: Code 7750 Paul Juluenne

Commander
Naval Surface Weapons Center
White Oak, Silver Spring, MD 20910

01 CY Attn: Code WA501 Navy Nuc Prgms Off

DEPARTMENT OF THE AIR FORCE

AF Geophysics Laboratory, AFSC
Hanscom AFB, MA 01731

01 CY Attn: LKB Kenneth S. W. Champion
01 CY Attn: OP John S. Garing
01 CY Attn: OPR Alva T. Stair
01 CY Attn: OPR James C. Ulwick

AF Weapons Laboratory, AFSC
Kirtland AFB, NM 87117

01 CY Attn: DYT Capt David W. Goetz
01 CY Attn: SUL
01 CY Attn: DYT LtC Don Mitchell

Commander
ASD
WPAFB, OH 45433

01 CY Attn: ASD-YH-EX LtC Robert Leverette

SAMSO/SZ
Post Office Box 92960
Worldway Postal Center
Los Angeles, CA 90009
(Space Defense Systems)

01 CY Attn: SZJ Maj. Lawrence Doan

U. S. ENERGY RSCH AND DEV ADMIN

Division of Military Application
U. S. Energy Rsch & Dev Admin
Washington, DC 20545

01 CY Attn: DOC Con for Maj. D.A. Haycock

Los Alamos Scientific Laboratory
P.O. Box 1663
Los Alamos, NM 87545

01 CY Attn: DDC CON for R.A. Jeffries

OTHER GOVERNMENT

Department of Commerce
Office of Telecommunications
Institute for Telecom Science
Boulder, CO 80302

01 CY Attn: William F. Utlaut
01 CY Attn: Glenn Falcon

DEPARTMENT OF DEFENSE CONTRACTORS

Aerodyne Research, Inc.
Bedford Research Park
Crosby Drive
Bedford, MA 01730

01 CY Attn: F. Bien
01 CY Attn: M. Camac

Aerospace Corporation
P.O. Box 92957
Los Angeles, CA 90009

01 CY Attn: T. Taylor
01 CY Attn: R.D. Rawcliffe
01 CY Attn: Harris Mayer
01 CY Attn: R. Grove

Denver, University of
Colorado Seminary
Denver Research Institute
P.O. Box 10127
Denver, CO 80210

(only 1 copy of class rpts)
01 CY Attn: Sec Officer for Mr. Van Zyl
01 CY Attn: Sec Officer for David Murcray

DEPARTMENT OF DEFENSE CONTRACTORS (Continued)

General Electric Company
Tempo-Center for Advanced Studies
816 State Street (P.O. Drawer QQ)
Santa Barbara, CA 93102

05 CY Attn: DASIAC Art Feryok
01 CY Attn: Warren S. Knapp

General Research Corporation
P.O. Box 3587
Santa Barbara, CA 93105

01 CY Attn: John ISe Jr.

Geophysical Institute
University of Alaska
Fairbanks, AK 99701
(All Class Attn: Security Officer)

01 CY Attn: T.N. Davis (Uncl Only)
03 CY Attn: Neal Brown (Uncl Only)

Honeywell Incorporated
Radiation Center
2 Forbes Road
Lexington, MA 02173

01 CY Attn: Jerry Bates

Institute for Defense Analyses
400 Army-Navy Drive
Arlington, VA 22202

01 CY Attn: Ernest Bauer
01 CY Attn: Hans Wolfhard

Lockheed Missiles and Space Company
3251 Hanover Street
Palo Alto, CA 94304

01 CY Attn: John B. Cladis, Dept 52-12
01 CY Attn: J.B. Reagan D/52-12
01 CY Attn: Billy M. McCormac Dept 52-54
01 CY Attn: Tom James
01 CY Attn: Robert D. Sears Dept 52-14
01 CY Attn: John Kumer
01 CY Attn: Martin Walt Dept 52-10
01 CY Attn: Richard G. Johnson Dept 52-12

Mission Research Corporation
735 State Street
Santa Barbara, CA 93101

01 CY Attn: P. Fischer
01 CY Attn: D. Archer

DEPARTMENT OF DEFENSE CONTRACTORS (Continued)

Photometrics, Inc.
442 Marrett Road
Lexington, MA 02173

01 CY Attn: Irving L. Kofsky

Physical Dynamics Inc.
P.O. Box 1069
Berkeley, CA 94701

01 CY Attn: Joseph B. Workman

Physical Sciences, Inc.
30 Commerce Way
Woburn, MA 01801

01 CY Attn: Kurt Wray

R&D Associates
P.O. Box 9695
Marina Del Rey, CA 90291

01 CY Attn: Forrest Gilmore
01 CY Attn: Robert E. Lelevier

R&D Associates
1815 N. Ft. Myer Drive
11th Floor
Arlington, VA 22209

01 CY Attn: Herbert J. Mitchell

Rand Corporation, The
1700 Main Street
Santa Monica, CA 90406

01 CY Attn: James Oakley

Science Applications, Inc.
P.O. Box 2351
La Jolla, CA 92038

01 CY Attn: Daniel A. Hamlin

Space Data Corporation
1331 South 26th Street
Phoenix, AZ 85034

01 CY Attn: Edward F. Allen

Stanford Research Institute
333 Ravenswood Avenue
Menlo Park, CA 94025

01 CY Attn: Walter G. Chestnut
01 CY Attn: M. Baron
01 CY Attn: Ray L. Leadabrand

DEPARTMENT OF DEFENSE CONTRACTORS (Continued)

Stanford Research Institute
1611 North Kent Street
Arlington, VA 22209

01 CY Attn: Warren W. Berning

Technology International Corporation
75 Wiggins Avenue
Bedford, MA 01730

01 CY Attn: W. P. Boquist

Utah State University
Logan, UT 84321

01 CY Attn: Doran Baker
01 CY Attn: Kay Baker
01 CY Attn: D. Burt
01 CY Attn: C. Wyatt

Visidyne, Inc.
19 Third Avenue
North West Industrial Park
Burlington, MA 01803

01 CY Attn: William Reidy
01 CY Attn: J. W. Carpenter
01 CY Attn: T. C. Degges